STRUCTURE-FUNCTION STUDIES OF ELECTRON TRANSFER COMPLEXES IN BOVINE HEART MITOCHONDRIA

\

BY

JIAN ZHU

Bachelor of Biochemistry
ZHONGSHAN (SUN YAT-SEN) UNIVERSITY
Guangzhou, P. R. China
1994

Submitted to the Faculty of the
Graduate College of the
OKLAHOMA STATE UNIVERSITY
in partial fulfillment of
the requirements for
the Degree of
DOCTOR OF PHILOSOPHY
December, 2004

STRUCTURE-FUNCTION STUDIES OF

ELECTRON TRANSFER

COMPLEXES IN BOVINE

HEART MITOCHONDRIA

Dissertation Approved:

Chang-An Yu

Thesis Adviser

Linda Yu

H. Olin Spivey

Ulrich Melcher

Robert Burnap

A. Gordon Emslie

Dean of the Graduate College

ACKNOWLEDGEMENTS

I wish to express my sincere appreciation to my major advisor, Dr. Chang-An Yu for his intelligent supervision, constructive guidance, and inspiration. I am also equally grateful to Dr. Linda Yu for her encouragement and guidance during my study. I want to express my thanks to them and the Department of Biochemistry and Molecular Biology for providing financial support and research opportunity.

My sincere appreciation also extends to my committee members, Dr. Ulrich Melcher, Dr. Olin Spivey, and Dr. Robert Burnap for their advice and guidance.

I am greatly indebted to my parents, Lingping Shen and Weiwen Zhu, for their love, patience, guidance through out the years. I wish to offer this thesis to them. Finally I want to thank my fiancé, Jieya Shao, for her love and encouragement.

TABLE OF CONTENTS

Chapter Page

LIST OF FIGURES

Figure Page

LIST OF TABLES

Table Page

LIST OF ABBREVIATIONS

ATP	adenosine triphosphate
Azido-Q	3-azido-2-methyl-5-methoxy-6-geranyl-1, 4-benzoquinone
BSA	bovine serum albumin
CcO	cytochrome *c* oxidase
DCPIP	dichlorophenolindophenol
DMSO	dimethylsulfoxide
DNA	deoxyribonucleic acid
EPR	electron paramagnetic resonance
FAD	flavin adenine dinucleotide
FP	flavoprotein
FPLC	fast protein (peptide) liquid chromatography
GST	glutathione S-transferase
[3H]azido-Q	3-azido-2- methyl-5-methoxy-6-(3,7-dimethyl-octyl)-1, 4-benzoquinone
HPLC	high performance liquid chromatography
HRP	horseradish peroxidase
IP	iron-sulfur protein
β-ME	β-mercaptoethanol

IPTG	isopropyl-β-D-thiogalactopyranoside
NAD^+	nicotinamide adenine dinucleotide
NADH	reduced form of nicotinamide adenine dinucleotide
PAGE	polyacrylamide gel electrophoresis
PBS	20 mM sodium/sodium phosphate buffer, pH 7.3, containing 150 mM NaCl
PMSF	phenylmethylsulfonylfluoride
PVDF	polyvinylidene difluoride
Q	ubiquinone
Q·	radical of ubiquinone
QH·	protonated form of ubiquinone radical
QH_2	ubiquinol
Q_0C_{10}	2,3-dimethoxy-5-methyl-6-decyl-1,4-benzoquinone
QCR	quinol-cytochrome *c* reductase
QFR	quinolfumarate reductase
QPs	ubiquinone-binding proteins in SQR
SCR	succinate-cytochrome *c* reductase
SDH	succinate dehydrogenase
SDS	sodium dodecylsulfate
SQR	succinate-ubiquinone (Q) reductase
TBS	20 mM Tris-HCl buffer, pH 7.4, 500 mM NaCl

TTBS	20 mM Tris-HCl buffer, pH 7.4, 500 mM NaCl, 0.05% Tween-20
TTFA	2-Thenoyltrifluoroacetone
UV	ultra-violet
X-gal	5-bromo-4-chloro-3-indolyl-β-galactopyranoside

CHAPTER I

INTRODUCTION

The mitochondrion is the cell's "power plant" as it produces most of the energy in cells through oxidative phosphorylation. Electrons are passed through a series of respiratory enzyme complexes located in the inner mitochondrial membrane. The energy released by this electron transfer is used to pump protons across the membrane. This results in the formation of an electrochemical gradient, which enables adenosine 5-triphosphate (ATP) synthase to synthesize the energy carrier ATP (Figure 1).

A series of four enzyme complexes forms the electron-transport chain. Electrons are passed through these complexes from lower to higher standard reduction potentials. Complex I (NADH:Ubiquinone Reductase) catalyzes the oxidation of nicotinamide adenine dinucleotide (NADH) by Coenzyme Q (CoQ). Complex II (Succinate:Ubiquinone Reductase) catalyzes the oxidation of flavin adenine dinucleotide ($FADH_2$) by CoQ. Because this redox reaction does not release sufficient free energy to synthesize ATP, Complex II functions only to extract the electrons from $FADH_2$ and transfer them into the electron-transport chain. CoQ then carries electrons to Complex III (Ubiquinol:Cytochrome *c* Reductase or bc_1 complex), which catalyzes oxidation of reduced CoQ by cytochrome *c*. Complex IV (Cytochrome *c* Oxidase) catalyzes the oxidation of reduced cytochrome *c* by O_2, the terminal electron acceptor of the electron-transport process (Figure 2). The free energy released by electron transport is utilized by Complex V (ATP synthase) to synthesize ATP. Peter Mitchell first proposed the chemiosmotic theory (the general mechanistic principle of oxidative and phosphorylation) in 1961, this theory explains the coupling between respiration and ATP

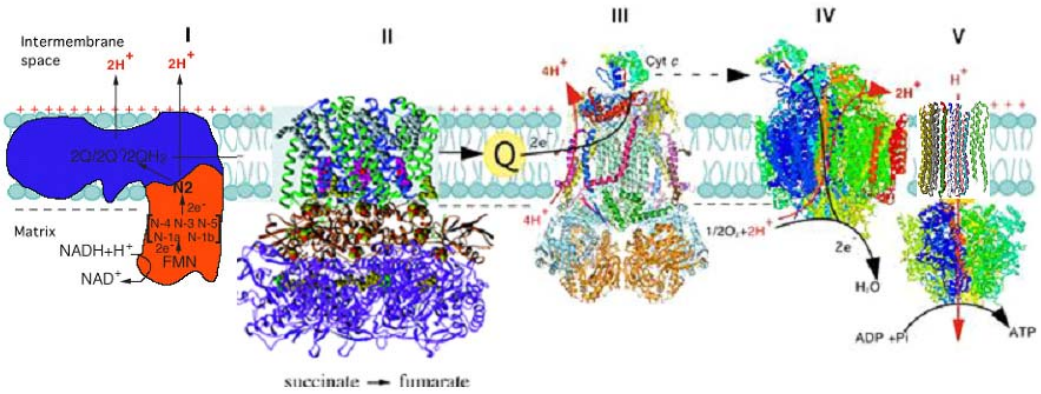

Figure 1. Mitochondrial electron-transport chain.

synthesis in mitochondria. It has become a paradigm in the intellectual framework of bioenergetics since the mid-1970.

During the past 20 years, study in mitochondrial bioenergetics has shifted from experiments with crude organelle preparations to direct molecular approaches. Atomic resolution structures are now available for several complexes of the electron transport chain. They are cytochrome bc_1 (1,2), cytochrome c oxidase (3,4), and F_1 of ATP synthase (5) from bovine, F_1c_{10} complex from *Saccharomyces cerevisiae* (6), succinate:ubiquinone oxidoreductase from *Escherichia coli* (*E. coli*) (7), and fumarate reductase, which some believe is the homologous enzyme of Complex II, from *E. coli* (8) and *Wolinella succinogenes* (9).

The structural information of electron transfer complexes not only has substantiated earlier biophysical and biochemical experimental data about enzyme mechanisms, but also stimulated discussions about possible alternative mechanisms. For example, the crystal structure of the F_1-ATPase reveals the intrinsic asymmetry of the enzyme, and supports the proposal of Boyer (10) that the three active sites within the F_1 head function in a rotating manner. The histidine cycle hypothesis of cytochrome c oxidase was favored before the structure information was available. It proposes that two protons are simultaneously carried through the barrier by a moving histidine (11). Recent crystallographic studies refute the histidine cycle hypothesis, as the metal coordination does not appear to change upon reduction of the enzyme. Based on the crystallographic data, two putative channels, D (D91) and K (K319) channels, for delivery of protons to the dioxygen reduction site and for pumping of protons across the membrane were

proposed (4). This led to a new search for a possible proton-pumping mechanism in cytochrome *c* oxidase. The mechanism remains unclear, and the debate continues (12,13).

Complex I, NADH:Ubiquinone Oxidoreductase

This complex is the entry point for electrons from NADH into the respiratory chain of mitochondria. It is the largest, most complicated, and least understood among the complexes. It catalyzes the electron transfer from NADH through a series of enzyme bound redox centers (flavin mononucleotide (FMN) and Fe-S clusters) to ubiquinone, which is reduced to ubiquinol. An electrochemical proton potential gradient across the membrane of the mitochondrion is formed by converting the redox energy during this process. It is generally considered that for every two electrons that pass through the enzyme, four protons are translocated out of the mitochondrial matrix (14).

Bovine complex I contains at least 45 different subunits in an unknown stoichiometry and has a molecular weight over 1,000 kilo Daltons (kDa). There are at least 35 subunits in *Neurospora crassa*, another eukaryote that has been extensively studied, and with a total molecular weight over 700 kDa (15-17). Even in *Paracoccus denitrificans*, a Gram-negative soil bacterium, this complex contains at least 14 subunits, which is considered the minimum requirement of this complex (18).

In bovine complex I, there are seven hydrophobic intrinsic membrane subunits, known as ND1-ND6 and ND4L (19). They are encoded by the mitochondrial genome, and have been sequenced in a wide range of eukaryotes. These include mammals (20-22), birds (23), fish (24), insects (25,26), amphibians (27), invertebrates including sea urchins

(28), nematode worms (29) and brine shrimps (30), protozoans (31), algae (32), and fungi (33-35). Homologues of these subunits are also encoded in the chloroplast genomes of higher plants (36,37). The homologues of part or all of the mitochondrial genes among these species prove the presence of complex I in a wide variety of species. The yeast *Saccharomyces cerevisiae* has no ND genes in its mitochondrial DNA and is a notable exception. The rest of the constituent polypeptides of this complex, thirty-five so far, are nuclear gene products that are imported into the organelle from the cytoplasm of the cell (38). The monomeric enzyme complex from bovine heart mitochondria contains one FMN, at least six different iron-sulfur centers (two [2Fe-2S], N1a and N1b; four [4Fe-4S], N2 to N5), and at least three bound quinol molecules (one ubiquinone, and two EPR-detectable semiquinone species) (16,39,40). By using an azido-ubiquinone derivative, our group rececntly identified the ubiquinone-binding site in *E. coli* complex I, which locates in the helix 4 of NuoM subunit (41). A comparison of mammalian and bacterial complex I shows the presence of 32 strictly conserved cysteine residues, which allows the binding of eight iron-sulfur centers (42).

There are several ways to subfractionate the bovine complex I (43-45). The most commonly used is to treat the isolated enzyme with the chaotropic anion, perchlorate (see Figure 2). This process separates the complex into two fractions, a soluble fraction and a precipitate hydrophobic protein fraction, HP. The soluble fraction can be further resolved into two parts, a flavoprotein containing fraction (FP) and an iron-protein containing fragment (IP). The FP fraction contains one molecule of each of the 51 ([4Fe-4S] and FMN), 24 ([2Fe-2S]), and 10 kDa protein subunits, one molecule of FMN and six atoms of bound iron (46). As found in complex I (47,48), it has the same kinetic parameters of

NADH and NAD^+ binding, and ferricyanide and other artificial substrates can act as electron acceptors. The 51 kDa subunit has been identified as the NADH-binding site by photoaffinity labeling (49). In the fraction IP, its flavin content is low, and it contains 48 nmol Fe mg^{-1} of protein, which corresponds to 9-10 of the iron atoms in complex I (50). The IP fragment is not a homogeneous stoichiometric complex, and its polypeptides composition seems to differ from one to the other preparations. But it appears the 75, 49, 30, 18, 15 and 13 kDa subunits are considered invariant (51).

The HP fraction is the precipitate from the perchlorate treatment with all the rest of the subunits, and it doesn't show any structural integrity. It contains not only the hydrophobic components of complex I, for example, ND1 (51), but also globular water-soluble subunits of complex I, for example, PSST ((38), also see Figure 2).

Another common way to disrupt the bovine complex I is to use detergent (*N*,*N*-dimethyldodecylamine *N*-oxide) treatment to split the enzyme into two subcomplexes, named Iα and Iβ (52). Iα contains 22 subunits, and represents the majority of the extrinsic membrane domain of complex I. It has all of the subunits of IP and FP fractions, as well as many other subunits that are indicated to be globular by their sequences. However, it also contains some of the hydrophobic subunits, ND2, MLRQ, B9, MWFE, and the 42 kDa subunits. Subcomplex Iα can transfer electrons from NADH to ferricyanide or ubiquinone-I, and contains all of the iron-sulfur clusters that have been detected by electron paramagnetic resonance (EPR) spectroscopy in intact complex I. Subcomplex Iβ consists of about 13 different polypeptides. They include the hydrophobic mitochondrial gene products ND4 and ND5, and 11 nuclear coded proteins. It didn't

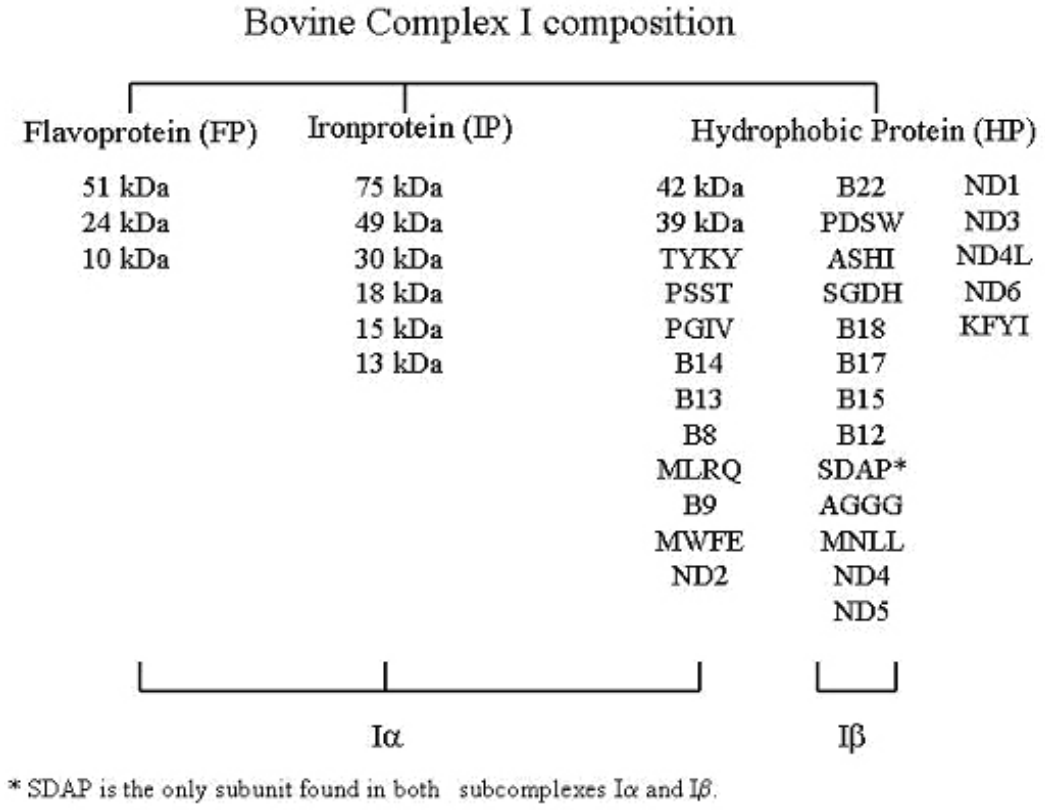

Figure 2. Subfractionation of bovine Complex I.

show any known redox centers (52), and no biochemical functions have been detected (38). Table I shows all of the nuclear-coded subunits in bovine complex I and their properties (modified from (38)).

Photoaffinity analogues of NAD^+ react with the 51 kDa subunit in the FP fragment (49). Therefore, it is believed that the NADH binding site is within the 51 kDa subunit. By sequence comparison with other NADH-binding sites of known structure, Walker suggested a possible location of this binding site in the 51 kDa subunit (38). But the exact location of the NADH binding site remains unknown. FMN, which is usually considered as the most likely immediate oxidant of NADH, is also thought to bind with the 51 kDa subunit (38). The standard reduction potential of FMN is between those of NADH and the most electronegative of the EPR visible iron-sulfur clusters. It can take up two electrons at a time and release one at a time to the one electron acceptor Fe-S cluster, and still maintain a stable structure. Since the substrate NADH is bound at the 51 kDa subunit, one may predict that the FMN might be bound to the same polypeptide. There is no evidence that shows the other two subunits of the FP fraction, 24 kDa and 10 kDa, bind with FMN. There was a prediction, also suggested by Walker, of the possible binding site for FMN in the 51 kDa subunit, but the exact location will be revealed once the structure information becomes available (38).

The Iα subcomplex of complex I, which includes both FP and IP fragments, contains all of the iron-sulfur clusters that have been detected by EPR spectroscopy in intact complex I. In an effort to localize the subunits that host these Fe-S clusters of bovine complex I, EPR spectra were determined for the FP and IP fragments, and simpler

fragments were derived from them by further purification. Thus, clusters N-1b and N-3 were localized in the 24 kDa subunit and 51 kDa subunit, respectively (53). The other clusters were found or predicted to be housed in 75 kDa, TYKY (23 kDa), and PSST (20 kDa) subunits, as show in Table I (15,37,54,55).

Due to the extreme structural complexity, the difficulty of applying optical spectroscopy to analyze the redox state of intrinsic chromophores within the membrane, and the absence of inhibitors that block the pathway at specific intermediate sites, the study of the electron pathway of complex I is extremely difficult (38,56). However, the L-shape (57), two arms structure with a water soluble peripheral part that contains all known prosthetic groups and a membrane part that carries the binding site for ubiquinone provides a framework to constrain the proton-translocating machinery.

The FP fragment of bovine complex I, also called NADH dehydrogenase, is considered as the entry point of electron translocation of this complex. Its FMN and NADH binding ability, the presence of Fe-S clusters N-1b and N-3, and simplicity to prepare in comparison with the whole enzyme complex, make it an attractive candidate to be the first fully understood subcomplex of this complicated complex. Its structural information through crystallography will greatly facilitate the studies of the electron transport pathway within complex I, and shed light on the involvement of mitochondria in aging and cell death, Parkinson's disease and Huntington's disease, which are related to deficiencies of complex I in human mitochondria (38).

Table I Properties of nuclear-coded subunits of bovine complex I

Subunit	Molecular weight by gel (kDa)	Molecular weight from sequence	No. amino acids	Post-translational modifications
75 kDa (IP)	75	76960.2	704	[4Fe-4S] (N-1a); [4Fe-4S] (?); [2Fe-2S]
51 kD (FP)	51	48416.1	444	NADH-binding; FMN; [4Fe-4S] (N-3)
49 kDa (IP)	49	49174.4	430	
42 kDa	42	36692.8	320	
39 kDa	39	39115.1	345	
30 kDa (IP)	30	26431.8	228	
24 kDa (FP)	24	23814.4	217	[2Fe-2S] (N-1b)
B22	22	21700.6	178	N-acetyl
TYKY	23	20195.9	176	2x[4Fe-4S]
PDSW	22	20833.6	175	
PSST	20	20077.5	178	1x[4Fe-4S]
PGIV	19	19959.9	171	Fe-S protein?
ASHI	19	18737	158	
SGDH	16	16726.3	143	
B18	18	16476.5	136	Nα-myristyl
18 kDa (IP)	18	15337.2	133	
B17	16.5	15434.9	127	Nα-acetyl
B15	15	15095.1	128	Nα-acetyl
B14	14	14964.3	127	Nα-acetyl
B13	13	13226.4	115	Nα-acetyl
15 kDa (IP)	15	12536.4	105	
B8	8	10990.6	98	Nα-acetyl
B12	12	11009.4	97	Modified
13 kDa (IP)	13	10535.7	96	
SDAP	8	10109.5	88	Pantethenic acid
B9	9	9217.7	83	
MLRQ	9	9324.7	82	
10 kDa (FP)	10	8437.3	75	
AGGG	7.9	8493.3	72	
MWFE	7.5	8135.4	70	
MNLL	7	6966.1	57	
KFYI	6	5828.7	49	
B17.2	17.2	17131.6	145	Nα-acetyl

Complex II, Succinate–Ubiquinone Oxidoreductase

Succinate-ubiquinone oxidoreductase (SQR), which catalyzes electron transfer from succinate to ubiquinone (Q), has been isolated and characterized (58-60). The reductase is composed of two parts: soluble succinate dehydrogenase and a membrane anchoring protein fraction. Purified reductase has five protein subunits in a high resolution sodium dodecylsulfate-polyacrylamide gel electrophoresis (SDS-PAGE) system with apparent molecular weights of 70, 27, 15, 13, and 11 kDa (61). The two largest subunits are succinate dehydrogenase and the three smaller ones comprise the membrane anchoring protein fraction. The isolated complex contains six prosthetic groups: one FAD, three iron–sulfur clusters ([2Fe–2S], [3Fe–4S], and [4Fe–4S]), cytochrome *b*-560, and Q. The FAD is covalently bound to the 70 kDa subunit (Fp) and all three iron–sulfur clusters are in the 27 kDa subunit (Ip) of succinate dehydrogenase (62,63). Cytochrome *b*-560 and Q are found in the membrane anchoring protein fraction (64). While studies of succinate dehydrogenase have been extensive and a wealth of information has been obtained (62), knowledge of the membrane anchoring protein fraction is relatively limited (65).

The membrane anchoring protein fraction has been isolated in several laboratories under different names, such as $CII_{3,\,4}$ (66), cytochrome b_{560} fraction (67), or QPs (68). The term, QPs (Quinone-binding Protein in SQR), was named by our group (Table II). QPs provides membrane anchoring for succinate dehydrogenase and is responsible for the Q-binding in succinate–ubiquinone reductase. The ubisemiquinone radicals, which do not show power saturation, even at 200 mW, are detected in intact and reconstituted

Table II Subunit composition of bovine heart SQR

Molecular Mass (kDa)	Name	Prothetic Group (content in SQR)	Midpoint Poteintial (mV)
70	Flavin Protein (FP)	His-FAD (5.8 nmol/mg)	-79
27	Iron Sulfur Protein (IP)	[2Fe-2S] (S-1) [4Fe-4S] (S-2) [3Fe-4S] (S-3) (48 ngatom)	0 -260 +60
15	Q-binding Protein (QPs1)	Heme (1.2 nmol/mg)	-185
13	Q-binding Protein (QPs2)		
11	Q-binding Protein (QPs3)	Quinone (2 nmol/mg)	+84

succinate–ubiquinone reductases in the presence of exogenous Q (69). When quinone derivatives are used as the electron acceptor for succinate–ubiquinone reductase, a 5 carbon side chain is required for maximum activity (70) and the methyl group at the 5-position is less important than are the methoxy groups at the 2- and 3-positions (71). Replacing the 5-methyl group with hydrogen causes a slight increase in activity. However, replacing one or both of the 2- and 3-methoxy groups with a methyl completely abolishes electron-acceptor activity.

When succinate–ubiquinone reductase is subjected to photoaffinity labeling with an [^{3}H]azido-Q derivative, most of the radioactivity was found in the QPs1 subunit, indicating that QPs1 is involved in Q-binding (61). The Q-binding domain in QPs1, using a structure for QPs1 based on the deduced amino acid sequence (72,73), is located in the stretch connecting transmembrane helices 2 and 3, which extrudes from the surface of the M side of the mitochondrial inner membrane (61) (Figure 3).

In addition to participating in Q-binding, QPs1 is believed to be cytochrome b_{560}. The involvement of cytochrome b_{560} in catalysis by succinate–ubiquinone reductase is controversial. The presence of substoichiometric amounts of cytochrome b_{560}, with respect to FAD, in isolated beef succinate–cytochrome *c* and succinate–ubiquinone reductases, together with its non-reducibility by succinate has led some investigators to rule out a catalytic function for cytochrome b_{560}. On the other hand, it has been proposed that cytochrome b_{560} functions as a mediator between low potential F1/F· and Q/Q· couples in a dual pathway model (74) of electron flow through cardiac Complex II. Despite its uncertain catalytic role, cytochrome *b*-560 is involved in the binding of

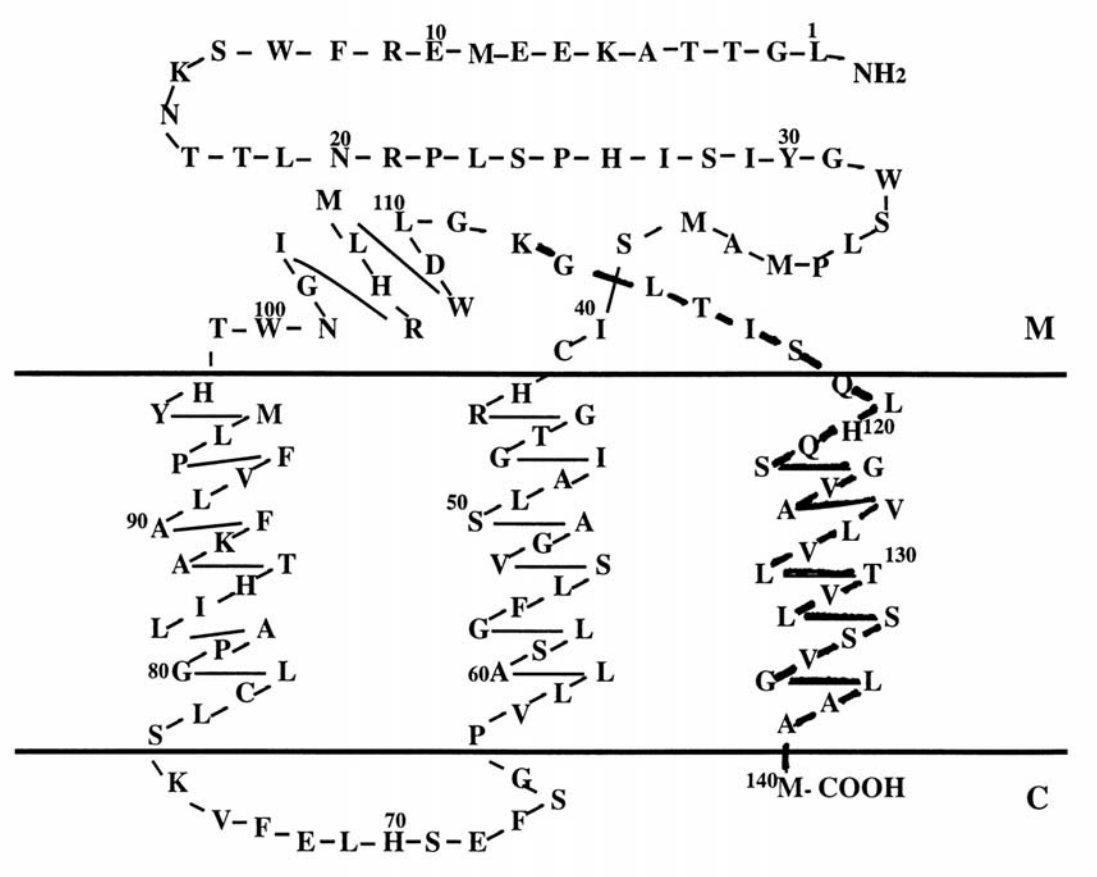

Figure 3. Proposed structure of QPs1. Bold line indicates the tryptic peptide involved in Q-binding of QPs1.

succinate dehydrogenase to QPs as indicated by the restoration of its absorption properties, redox potential, and EPR characteristics, upon reconstitution of succinate–ubiquinone reductase from QPs and succinate dehydrogenase (64).

The ligands of cytochrome b_{560} in *E. coli* and beef succinate–ubiquinone reductases have been identified as bis-histidine (75,76). H42 and H98 of QPs1 are thought to be involved in heme ligation of cytochrome b_{560} in the beef enzyme (72) because these two histidines are conserved in *sdh* C peptides of *E. coli* and *Bacillus subtilis* and are located on the matrix side of the membrane. However, the report of Nakamura et al. (77), using a gene deletion approach, indicates that both *sdh*C and *sdh*D peptides of the *E. coli* enzyme are required for heme ligation of cytochrome b_{556}. Precise localization of these bis-histidine ligands will facilitate our understanding of electron transfer in this segment of the mitochondrial respiratory chain.

The 3-D structure of *E. coli* SQR was reported in 2003 (7). Comparison of the transmembrane domain subunits (SdhC and SdhD) between *E. coli* SQR and *E. coli* and *W. succinogenes* fumarate reductase (QFR) shows some major differences (Figure 4): 1) number of subunits. *E. coli* SQR and QFR have two subunits (three transmembrane helices for each), whereas *W. succinogenes* QFR has only one subunit, with five transmembrane helices; 2) number of heme *b* molecules. *E. coli* SQR has only one heme *b*; however, *W. succinogenes* QFR has two heme *b* molecules and *E. coli* QFR has none. The histidine ligands for heme *b* were identified as H84 of SdhC, and H71 of SdhD in *E. coli* SQR.

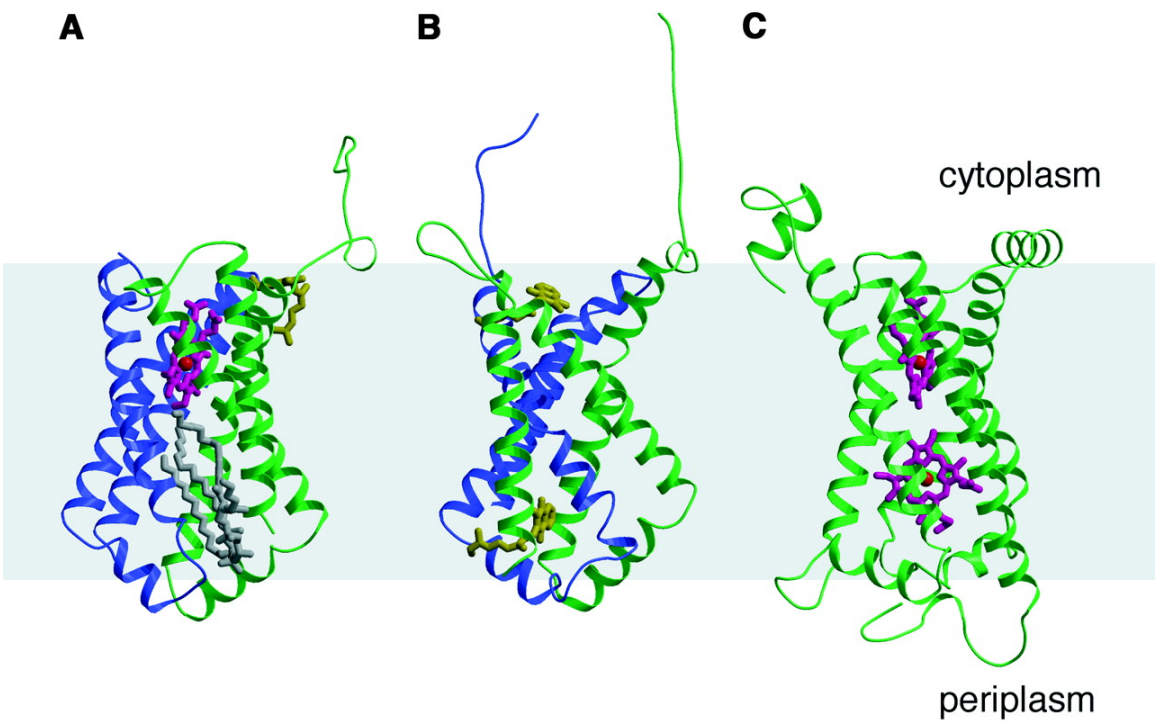

Figure 4. Comparison of the transmembrane domain structures of (**A**) *E. coli* SQR, (**B**) *E. coli* QFR, and (**C**) *W. succinogenes* QFR. All three are viewed parallel to the membrane from the same direction. SdhC and SdhD subunits are shown in green and blue, respectively. The equivalent subunits in *E. coli* QFR are shown in the same colors. *W. succinogenes* QFR has a single transmembrane subunit. Ubiquinone and menaquinone are shown in brownish yellow in (A) and (B). Heme *b* and cardiolipin are shown in purple and gray, respectively. Gray shading represents the position of the membrane (7). Figure is taken from reference 7.

Complex III, Ubiquinol:Cytochrome *c* Oxidoreductase

Ubiquinol:cytochrome *c* oxidoreductase catalyzes the transfer of electrons from ubiquinol to cytochrome *c*, both oxidation of ubiquinol (QH_2) and reduction of ubiquinone (Q) occur during the reaction cycle as part of the proton-translocating apparatus (78).

Bovine mitochondrial cytochrome bc_1 contains 11 protein subunits with four redox prosthetic groups: cytochromes b_{566} (b_L) and b_{562} (b_H) cytochrome *c*1, and a high-potential iron–sulfur cluster [(2Fe–2S)]. The three (subunits III, IV, and V), which house *b*-type cytochromes, cytochrome *c*1, and the iron–sulfur cluster, respectively, are essential subunits, while the eight (subunits I, II, VI–XI) containing no redox prosthetic groups are termed supernumerary subunits. The complex consists of 2165 amino acid residues with a total molecular mass of 248 kDa, not including approximately forty molecules of bound phospholipids (79).

The three-dimensional (3-D) structure of bovine mitochondrial *bc*1 complex was first available in 1997 by collaboration between our group and Dr. Deisenhofer's group. The structure information not only established the location of the redox centers and inhibitor binding sites but also suggested some unexpected features of the complex, which are: movement of the head domain of the iron-sulfur protein (ISP) during *bc*1 catalysis (1,2,80,81); close interaction between two symmetrically related monomers (1); and inhibition of the mitochondrial-processing peptidase (MPP) activity by the binding of subunit IX at the active site of MPP, located in interface of the subunits I and II (82).

As shown in Figure 5 (83), the cytochrome bc_1 complex can be divided into three regions: matrix, transmembrane helix, and intermembrane space. The enzyme projects 75 Å into the matrix space, spans 42 Å within the inner mitochondrial membrane, and extends 38 Å into the intermembrane space. The core 1 and core 2 subunits, along with subunits VI and IX, position entirely in the matrix space. Cytochrome *b*, cytochrome c_1, the iron-sulfur protein, and subunits VII, X, and XI span the membrane, while subunit VIII lies solely in the intermembrane space.

The transmembrane helix region consists of 13 helices in each monomer, eight from cytochrome *b* (A-H), and the remaining five belonging to cytochrome c_1, ISP, and subunits VII, X, and XI. Four helixes (A-D) of cytochrome *b* form a bundle, which both heme b_L and b_H are bound to. Heme b_L is liganded by residues H83 and H182 from helices B and D, respectively; while heme b_H is liganded by H97 and H196 from helices B and D. The Q_i site of the protein has been defined by structures of the enzyme in the presence and absence of the Q_i site inhibitor antimycin. Residues from helices A, D, and E, and a short helix near the N terminus of the peptide chain form the binding pocket. The electron density for antimycin suggests that this inhibitor binds within 4 Å of heme b_H. By analogy, ubiquinone should bind in a similar fashion at this site. The Q_o site of the protein positions within cytochrome *b* near the iron-sulfur protein. It consists mainly of residues from helix C, helix F, the loop region connecting helices C and D, and the loop connecting helices E and F (42).

Cytochrome c_1 consists of an extramembranous domain in the intermembrane space along with a single transmembrane helix. Heme c_1 is liganded with residues C37

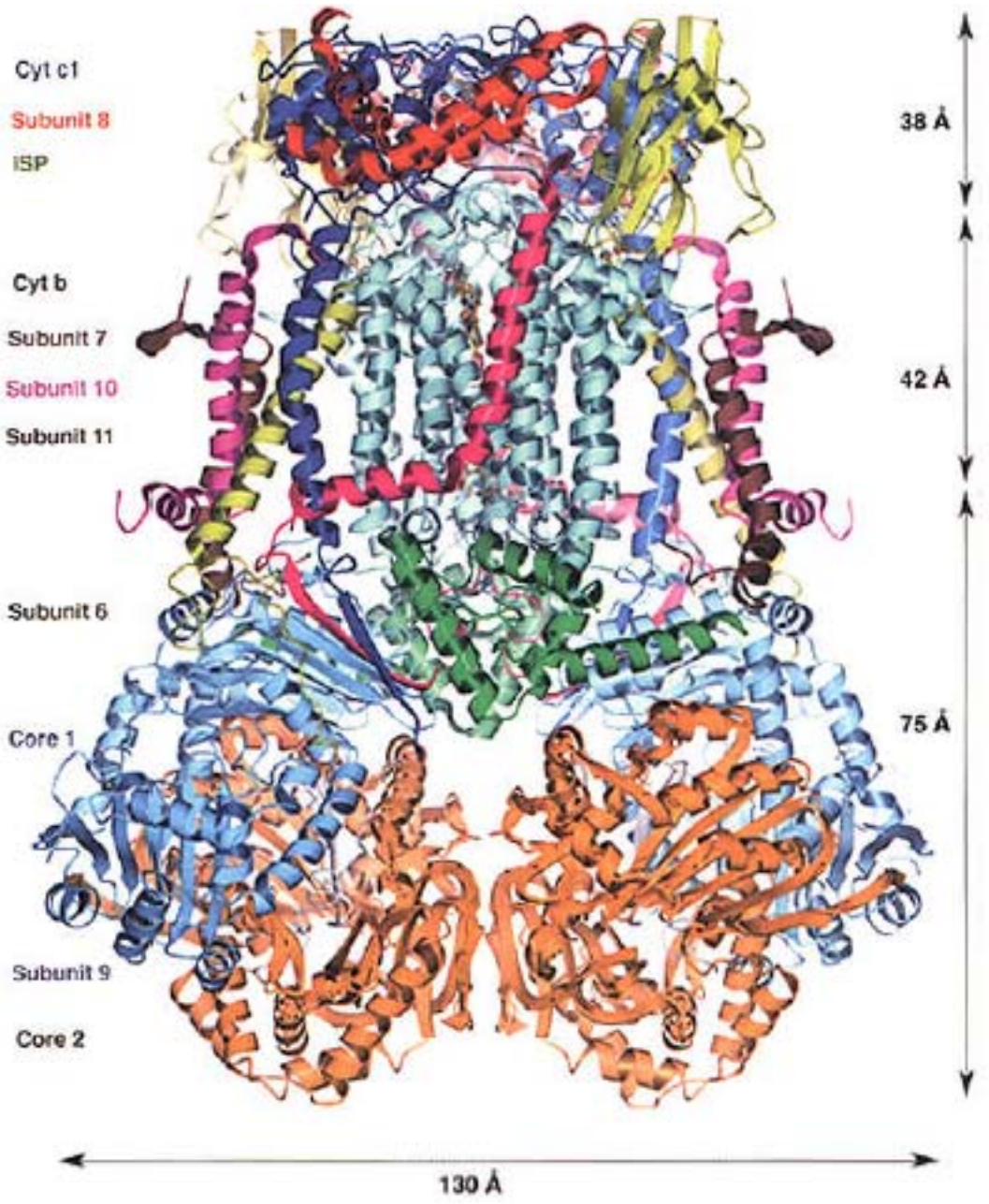

Figure 5. Structural model of the dimeric bovine mitochondrial cytochrome *bc*1 complex. The polypeptides are drawn as ribbons and heme moieties as ball-and-stick models. The top of the diagram is in the mitochondrial intermembrane space; the bottom is in the mitochondrial matrix space. Figure is taken from reference 83.

and C40. The carboxy group of one of the propionates of heme c_1 forms a salt bridge with R120, while the other propionate of the heme extends toward the iron-sulfur protein. A methyl group on the porphyrin ring is solvent-exposed, likely near the binding site for cytochrome *c* (42,83).

The iron-sulfur protein (ISP) contains a transmembrane helix and a hydrophilic domain in the intermembrane space. ISP extends across the interface between the two monomers, with the transmembrane helix in one monomer and the extramembranous domain within the other. This intertwining structure of the two monomers implies that the functional enzyme complex exists as a dimer. In ISP, the [2Fe-2S] cluster positions near the edge of the extramembranous domain, bound by C139, H141, C158, and H161. A comparison of reported crystal structures has shown that the position of [2Fe-2S] changes during the binding of different Q_o site inhibitors (1,2,81), suggesting that domain movement is part of the reaction mechanism of the enzyme. Further more, molecular genetic manipulation of the flexibility of the ISP neck region in the bacterial cytochrome bc_1 complex has shown greatly reduced electron transfer activity with decreased flexibility of the neck region (84,85).

Binding of inhibitors at the Q_o site has revealed two overlapping substrate binding pockets. In the presence of inhibitor stigmatellin, the iron-sulfur cluster is in contact with the Q_o site (78,84). The electron density for stigmatellin suggests a possible hydrogen bond with H161 of the iron-sulfur protein. The distance between the stigmatellin and heme b_L is 12 Å. In the presence of inhibitors myxothiazole or methoxyacrylate-stilbene reveal that the distance from the ring structures of these two inhibitors are approximately

5.5 Å toward heme b_L, relative to the position of stigmatellin (86). Also, the iron-sulfur cluster was oriented toward the c_1 heme in these crystals and was not interacting directly with the inhibitors. In the presence of inhibitor 5-undecyl-6-hydroxy-4,7-dioxobenzothiazol (UHDBT), it appears to bind in a position intermediate between those of stigmatellin and myxothiazole, with a weak interaction between the inhibitor and the ISP (81).

In 1976, Mitchell proposed the Q-cycle mechanism for turnover of cytochrome bc_1 to explain the phenomenon of oxidant-induced reduction. The reduction level of the *b* hemes in anaerobic, succinate-reduced mitochondria increased upon exposure of the mitochondria to dioxygen, particularly in the presence of the inhibitor antimycin (87). As shown in Figure 6, the key features of this mechanism for electron transfer and proton translocation are the bifurcation of quinol oxidation at the Q_o site and quinone reduction at a separate Q_i site (87,88). After one full reaction cycle, two molecules of ubiquinol are oxidized, with the associated release of four protons to the cytoplasmic side of the membrane, one molecule of ubiquinone is reduced, coupled to the uptake of two protons from the matrix space, and two molecules of cytochrome *c* are reduced. Overall, four protons are released for every two molecules of cytochrome *c* reduced, giving a $2H^+/1e^-$ proton translocation stoichiometry (Equation 1).

$$2QH_2 + 2cytc^{3+} + Q + 2H^+(matrix) \rightarrow 2Q + 2cytc^{2+} + QH_2 + 4H^+(cytosol) \quad (1)$$

The most important point of this mechanism is that the branched electron transfer in the bc_1 complex is under kinetic control, not thermodynamic control. The

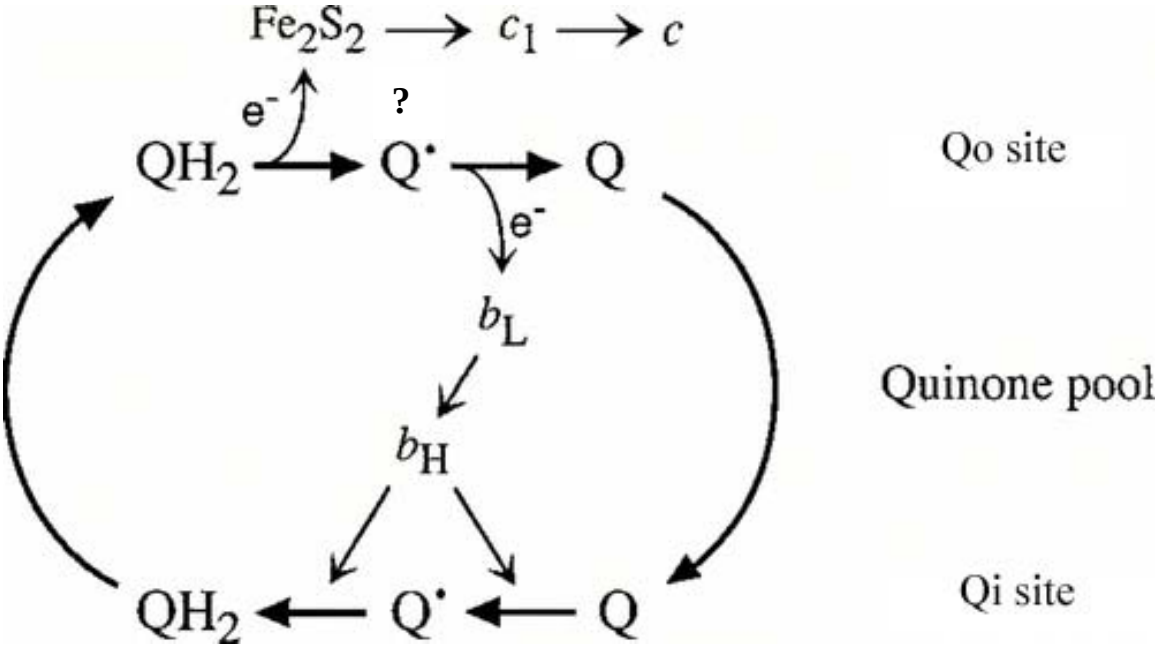

Figure 6. Schematic diagram of the Q-cycle mechanism of cytochrome bc_1. Thick arrows denote substrate transformation or movement. Thin arrows denote electron transfer. Q: ubiquinone; $Q^{\bullet}$: ubisemiquinone; QH_2: ubiquinol.

thermodynamically favored reaction is the transfer of both electrons from ubiquinol through ISP to cytochrome *c*, bypassing the *b* hemes altogether. Thus, the key to proton pumping in this enzyme is directing the second electron from the oxidation of ubiquinol into cytochrome *b* instead of the iron-sulfur cluster. There are two hypotheses for this scheme. First, the mobile ISP extramembrane domain, reduced by the first electron from quinol, can only donate the electron to cytochrome c_1 after the second electron from semiquinone reduces heme b_L due to a 31 Å distance between ISP and cytochrome c_1 (89). This is in accord with single-turnover experiments of quinol with cytochrome bc_1, in which heme *b* reduction is more rapid than that of heme c_1 (90-92). The electron transfer from semiquinone to heme b_L is faster than the diffusion motion of the ISP which is necessary for the cytochrome c_1 reduction.

Second, after the reoxidation of ISP, which is close to heme c_1 at the time, is unable to return to its original position, to be reduced, until the second electron from semiquinone reduces heme b_L (93). The fact that there are different sites for inhibitor binding in the Q_o site seems to support this hypothesis. There are two possible binding modes for the quinol oxidation, one is specific for quinol, which is similar to that observed for stigmatellin, while the other is for semiquinone, which is similar to that observed for myxathiazole (42).

Both hypotheses lead to a speculation that the change of the quinol-binding site to a semiquinone binding site, along with the reduction of heme b_L, result in a conformational change in cytochrome *b* which facilitates the electron transfer between

ISP and cytochrome c_1 by allowing ISP to move close to heme c_1 (89,93). However, the lack of detectable ubisemiquinone during catalysis does not support this hypothesis (94).

In 1998, Yu *et al.* proposed that the electron donor for the ISP is a quinol heme b_L complex, rather than quinol itself (89). Once the first electron of quinol within the complex is transfered to ISP, the second electron immediately transfers to heme b_L and then to heme b_H. Thus, no semiquinone is generated. The structure information revealing the close proximity of the two b_L from each of the monomer suggests the possibility that this might facilitate the transfer of the second electron to heme b_L. Thus the second electron of quinol may reach heme b_H or Q at the Q_i site around the same time as the first electron reaches heme c_1. While the exact nature of quinol binding in the Q_o site is unknown, it is the major remaining issue in understanding the fundamental electron transfer and proton translocation process in this enzyme.

Structural evidence of quinone binding at the Q_i site (1) is in line with the Q-cycle mechanism. Quinone is closely bound to heme b_H, within 5 Å of the edge of the heme tetrapyrrole, allowing a rapid electron transfer between Q and heme b_H and vice versa. An aspartate residue (D228), which is very close to one of the carbonyl groups of quinone, may play a role in protonations, after quinone is reduced (83). The potential energy of the cytochrome *b* increases due to the introduction of a negative charge at the Q_i site, which results from electron transfer from semiquinone to heme b_H and quinone at the Q_i site. Compensation of the negative charge through proton uptake, and reduction of quinone or semiquinone at the Q_i site complete the electron transfer through the enzyme.

The crystal structures of cytochrome bc_1 have provided not only a structural basis for the Q-cycle mechnism, but also insight into the details of the branched electron transfer mechanism. As a result of substrate binding, electrostatic interactions, and intrinsic domain movements, significant changes in the structure of the protein take place during the reaction cycle. The mechanism of cytochrome bc_1 can serve as a basis for understanding the requirements for proton pumping on a molecular level.

Because of the difficulty of following the reduction of ISP optically and the relative long mixing dead time of conventional stopped-flow apparatus, direct evidence of the early involvement of ISP in ubiquinol oxidation is not available. To be able to observe the reduction of ISP and its relation to heme *b* reduction by quinol at the Qo site will greatly facilitate the study of the electron transfer in complex III.

REFRENCES

1. Xia, D., Yu, C. A., Kim, H., Xia, J. Z., Kachurin, A. M., Zhang, L., Yu, L., and Deisenhofer, J. (1997) *Science* **277**, 60-66
2. Iwata, S., Lee, J. W., Okada, K., Lee, J. K., Iwata, M., Rasmussen, B., Link, T. A., Ramaswamy, S., and Jap, B. K. (1998) *Science* **281**, 64-71
3. Tsukihara, T., Aoyama, H., Yamashita, E., Tomizaki, T., Yamaguchi, H., Shinzawa-Itoh, K., Nakashima, R., Yaono, R., and Yoshikawa, S. (1995) *Science* **269**, 1069-1074
4. Tsukihara, T., Aoyama, H., Yamashita, E., Tomizaki, T., Yamaguchi, H., Shinzawa-Itoh, K., Nakashima, R., Yaono, R., and Yoshikawa, S. (1996) *Science* **272**, 1136-1144
5. Abrahams, J. P., Leslie, A. G., Lutter, R., and Walker, J. E. (1994) *Nature* **370**, 621-628
6. Stock, D., Leslie, A. G., and Walker, J. E. (1999) *Science* **286**, 1700-1705
7. Yankovskaya, V., Horsefield, R., Tornroth, S., Luna-Chavez, C., Miyoshi, H., Leger, C., Byrne, B., Cecchini, G., and Iwata, S. (2003) *Science* **299**, 700-704
8. Iverson, T. M., Luna-Chavez, C., Cecchini, G., and Rees, D. C. (1999) *Science* **284**, 1961-1966
9. Lancaster, C. R., Kroger, A., Auer, M., and Michel, H. (1999) *Nature* **402**, 377-385
10. Boyer, P. D. (1993) *Biochim Biophys Acta* **1140**, 215-250
11. Wikstrom, M., Bogachev, A., Finel, M., Morgan, J. E., Puustinen, A., Raitio, M., Verkhovskaya, M., and Verkhovsky, M. I. (1994) *Biochim Biophys Acta* **1187**, 106-111
12. Michel, H. (1998) *Proc Natl Acad Sci U S A* **95**, 12819-12824
13. Wikstrom, M. (2000) *Biochim Biophys Acta* **1458**, 188-198
14. Weiss, H., Friedrich, F., Paulmichl, M., Woll, E., Lang, F., Friedrich, T., Waldegger, S., Hofhaus, G., and Preis, D. (1991) *Biochim Biophys Acta* **1069**, 165-170
15. Friedrich, T., Weidner, U., Nehls, U., Fecke, W., Schneider, R., and Weiss, H. (1993) *J Bioenerg Biomembr* **25**, 331-337
16. Skehel, J. M., Fearnley, I. M., and Walker, J. E. (1998) *FEBS Lett* **438**, 301-305
17. Videira, A. (1998) *Biochim Biophys Acta* **1364**, 89-100
18. Leif, H., Sled, V. D., Ohnishi, T., Weiss, H., and Friedrich, T. (1995) *Eur J Biochem* **230**, 538-548
19. Chomyn, A., Cleeter, M. W., Ragan, C. I., Riley, M., Doolittle, R. F., and Attardi, G. (1986) *Science* **234**, 614-618
20. Anderson, S., de Bruijn, M. H., Coulson, A. R., Eperon, I. C., Sanger, F., and Young, I. G. (1982) *J Mol Biol* **156**, 683-717
21. Bibb, M. J., Van Etten, R. A., Wright, C. T., Walberg, M. W., and Clayton, D. A. (1981) *Cell* **26**, 167-180
22. Arnason, U., Gullberg, A., and Widegren, B. (1991) *J Mol Evol* **33**, 556-568
23. Desjardins, P., and Morais, R. (1990) *J Mol Biol* **212**, 599-634

24. Johansen, S., Guddal, P. H., and Johansen, T. (1990) *Nucleic Acids Res* **18**, 411-419
25. Clary, D. O., and Wolstenholme, D. R. (1985) *J Mol Evol* **22**, 252-271
26. Garesse, R. (1988) *Genetics* **118**, 649-663
27. Roe, B. A., Ma, D. P., Wilson, R. K., and Wong, J. F. (1985) *J Biol Chem* **260**, 9759-9774
28. Cantatore, P., Roberti, M., Rainaldi, G., Gadaleta, M. N., and Saccone, C. (1989) *J Biol Chem* **264**, 10965-10975
29. Okimoto, R., Macfarlane, J. L., Clary, D. O., and Wolstenholme, D. R. (1992) *Genetics* **130**, 471-498
30. Batuecas, B., Garesse, R., Calleja, M., Valverde, J. R., and Marco, R. (1988) *Nucleic Acids Res* **16**, 6515-6529
31. Pritchard, A. E., Seilhamer, J. J., Mahalingam, R., Sable, C. L., Venuti, S. E., and Cummings, D. J. (1990) *Nucleic Acids Res* **18**, 173-180
32. Denovan-Wright, E. M., and Lee, R. W. (1992) *Curr Genet* **21**, 197-202
33. Burger, G., and Werner, S. (1985) *J Mol Biol* **186**, 231-242
34. Nelson, M. A., and Macino, G. (1987) *Mol Gen Genet* **206**, 307-317
35. Cummings, D. J., McNally, K. L., Domenico, J. M., and Matsuura, E. T. (1990) *Curr Genet* **17**, 375-402
36. Stern, D. B., Bang, A. G., and Thompson, W. F. (1986) *Curr Genet* **10**, 857-869
37. Oda, K., Yamato, K., Ohta, E., Nakamura, Y., Takemura, M., Nozato, N., Akashi, K., Kanegae, T., Ogura, Y., Kohchi, T., and et al. (1992) *J Mol Biol* **223**, 1-7
38. Walker, J. E. (1992) *Q Rev Biophys* **25**, 253-324
39. Vinogradov, A. D., Sled, V. D., Burbaev, D. S., Grivennikova, V. G., Moroz, I. A., and Ohnishi, T. (1995) *FEBS Lett* **370**, 83-87
40. Brandt, U. (1997) *Biochim Biophys Acta* **1318**, 79-91
41. Gong, X., Xie, T., Yu, L., Hesterberg, M., Scheide, D., Friedrich, T., and Yu, C. A. (2003) *J Biol Chem* **278**, 25731-25737 Epub 22003 May 25702
42. Schultz, B. E., and Chan, S. I. (2001) *Annu Rev Biophys Biomol Struct* **30**, 23-65
43. Hatefi, Y. (1985) *Annu Rev Biochem* **54**, 1015-1069
44. Ragan, C. I. (1987) *Curr. Topics Bioenerget.* **15**, 1
45. Ramsay, T. P. S. a. R. R. (1992) *Molecular Mechanisms in Bioenergetics*, Elsevier, Amsterdam
46. Ragan, C. I., Galante, Y. M., Hatefi, Y., and Ohnishi, T. (1982) *Biochemistry* **21**, 590-594
47. Dooijewaard, G., and Slater, E. C. (1976) *Biochim Biophys Acta* **440**, 1-15
48. Dooijewaard, G., and Slater, E. C. (1976) *Biochim Biophys Acta* **440**, 16-35
49. Deng, P. S., Hatefi, Y., and Chen, S. (1990) *Biochemistry* **29**, 1094-1098
50. Ragan, C. I., Galante, Y. M., and Hatefi, Y. (1982) *Biochemistry* **21**, 2518-2524
51. Walker, J. E., Arizmendi, J. M., Dupuis, A., Fearnley, I. M., Finel, M., Medd, S. M., Pilkington, S. J., Runswick, M. J., and Skehel, J. M. (1992) *J Mol Biol* **226**, 1051-1072

52. Finel, M., Skehel, J. M., Albracht, S. P., Fearnley, I. M., and Walker, J. E. (1992) *Biochemistry* **31**, 11425-11434
53. Ohnishi, T., Ragan, C. I., and Hatefi, Y. (1985) *J Biol Chem* **260**, 2782-2788
54. Runswick, M. J., Gennis, R. B., Fearnley, I. M., and Walker, J. E. (1989) *Biochemistry* **28**, 9452-9459
55. Dupuis, A., Skehel, J. M., and Walker, J. E. (1991) *Biochemistry* **30**, 2954-2960
56. Ohnishi, T. (1993) *J Bioenerg Biomembr* **25**, 325-329
57. Guenebaut, V., Schlitt, A., Weiss, H., Leonard, K., and Friedrich, T. (1998) *J Mol Biol* **276**, 105-112
58. Doeg, D. M. Z. a. K. A. (1962) *Arch. Biochem. Biophys.* **97**, 41
59. R. A. Capaldi, J. S., and A. Merli. (1977) *Biochemistry* **10**, 2509
60. Yu, L., and Yu, C. A. (1982) *J Biol Chem* **257**, 2016-2021
61. Lee, G. Y., He, D. Y., Yu, L., and Yu, C. A. (1995) *J Biol Chem* **270**, 6193-6198
62. Ohnishi, L. H. a. T. (1992). Molecular Mechanisms in Bioenergetics (Ernster, L., Ed.), Elsevier Science, New York
63. B. A. C. Ackrell, M. J., R. P. Gunsalus, and G. Cecchini. (1992). Chemistry and Biochemistry of Flavoenzymes (Muller, F., Ed.), 3, CRC Press, London
64. Yu, L., Xu, J. X., Haley, P. E., and Yu, C. A. (1987) *J Biol Chem* **262**, 1137-1143
65. Hagerhall, C., and Hederstedt, L. (1996) *FEBS Lett* **389**, 25-31
66. Ackrell, B. A., Ball, M. B., and Kearney, E. B. (1980) *J Biol Chem* **255**, 2761-2769
67. Hatefi, Y., and Galante, Y. M. (1980) *J Biol Chem* **255**, 5530-5537
68. Yu, C. A., and Yu, L. (1980) *Biochemistry* **19**, 3579-3585
69. Miki, T., Yu, L., and Yu, C. A. (1992) *Arch Biochem Biophys* **293**, 61-66
70. Yu, C. A., Gu, L. Q., Lin, Y. Z., and Yu, L. (1985) *Biochemistry* **24**, 3897-3902
71. Gu, L. Q., Yu, L., and Yu, C. A. (1990) *Biochim Biophys Acta* **1015**, 482-492
72. Yu, L., Wei, Y. Y., Usui, S., and Yu, C. A. (1992) *J Biol Chem* **267**, 24508-24515
73. Cochran, B., Capaldi, R. A., and Ackrell, B. A. (1994) *Biochim Biophys Acta* **1188**, 162-166
74. Cammack, R. (1986). Iron-Sulfur Protein Research (H. Matsubara, T. K., and K. Wada, Ed.), Japan Sci. Soc. Press, Tokyo
75. Peterson, J., Vibat, C., and Gennis, R. B. (1994) *FEBS Lett* **355**, 155-156
76. Crouse, B. R., Yu, C. A., Yu, L., and Johnson, M. K. (1995) *FEBS Lett* **367**, 1-4
77. Nakamura, K., Yamaki, M., Sarada, M., Nakayama, S., Vibat, C. R., Gennis, R. B., Nakayashiki, T., Inokuchi, H., Kojima, S., and Kita, K. (1996) *J Biol Chem* **271**, 521-527
78. Trumpower, B. L., and Gennis, R. B. (1994) *Annu Rev Biochem* **63**, 675-716
79. Yue, W. H., Zou, Y. P., Yu, L., and Yu, C. A. (1991) *Biochemistry* **30**, 2303-2306

80. Zhang, Z., Huang, L., Shulmeister, V. M., Chi, Y. I., Kim, K. K., Hung, L. W., Crofts, A. R., Berry, E. A., and Kim, S. H. (1998) *Nature* **392**, 677-684
81. Kim, H., Xia, D., Yu, C. A., Xia, J. Z., Kachurin, A. M., Zhang, L., Yu, L., and Deisenhofer, J. (1998) *Proc Natl Acad Sci U S A* **95**, 8026-8033
82. Deng, K., Zhang, L., Kachurin, A. M., Yu, L., Xia, D., Kim, H., Deisenhofer, J., and Yu, C. A. (1998) *J Biol Chem* **273**, 20752-20757
83. Yu, C. A., Tian, H., Zhang, L., Deng, K. P., Shenoy, S. K., Yu, L., Xia, D., Kim, H., and Deisenhofer, J. (1999) *J Bioenerg Biomembr* **31**, 191-199
84. Tian, H., Yu, L., Mather, M. W., and Yu, C. A. (1998) *J Biol Chem* **273**, 27953-27959
85. Tian, H., White, S., Yu, L., and Yu, C. A. (1999) *J Biol Chem* **274**, 7146-7152
86. Crofts, A. R., Barquera, B., Gennis, R. B., Kuras, R., Guergova-Kuras, M., and Berry, E. A. (1999) *Biochemistry* **38**, 15807-15826
87. Mitchell, P. (1976) *J Theor Biol* **62**, 327-367
88. Trumpower, B. L. (1990) *J Biol Chem* **265**, 11409-11412
89. Yu, C. A., Xia, D., Kim, H., Deisenhofer, J., Zhang, L., Kachurin, A. M., and Yu, L. (1998) *Biochim Biophys Acta* **1365**, 151-158
90. De Vries, S., Albracht, S. P., Berden, J. A., and Slater, E. C. (1982) *Biochim Biophys Acta* **681**, 41-53
91. Snyder, C., and Trumpower, B. L. (1998) *Biochim Biophys Acta* **1365**, 125-134
92. Hansen, K. C., Schultz, B. E., Wang, G., and Chan, S. I. (2000) *Biochim Biophys Acta* **1456**, 121-137
93. Brandt, U. (1996) *Biochim Biophys Acta* **1275**, 41-46
94. Junemann, S., Heathcote, P., and Rich, P. R. (1998) *J Biol Chem* **273**, 21603-21607

CHAPTER II

RECONSTITUTION OF CYTOCHROME b_{560} AND IDENTIFICATION OF HEME-LIGATING RESIDUES OF THE LARGEST MEMBRANE-ANCHORING SUBUNIT (QPs1) OF BOVINE HEART MITOCHONDRIAL SUCCINATE–UBIQUINONE REDUCTASE

Gyesoon Yoon Lee, Jian Zhu, Linda Yu, and Chang-An Yu

Biochimica et Biophysica Acta (BBA) – Bioenergetics, 1636, 35-36 (1998)

Jian Zhu, Chang-An Yu, and Linda Yu

Biophysical Journal, 45th Annual Meeting Abstracts, 80, 43a (2001)

ABSTRACT

The QPs1 subunit of bovine heart mitochondrial succinate–ubiquinone reductase was over-expressed in *Escherichia coli* DH5α cells as a glutathione S-transferase fusion protein (GST–QPs1) using the expression vector, pGEX/QPs1. QPs1 is released from the fusion protein by proteolytic cleavage with thrombin. Isolated recombinant QPs1 shows one protein band in SDS-polyacrylamide gel electrophoresis corresponding to the subunit III of mitochondrial succinate–ubiquinone reductase. Although isolated recombinant QPs1 is dispersed in 0.01% dodecyl maltoside, it is in a highly aggregated form, with an apparent molecular mass of over 1 million. Recombinant QPs1 contains little cytochrome b_{560} heme. However, addition of hemin chloride reconstitutes the spectral characteristics of cytochrome b_{560}. Reconstituted cytochrome b_{560} in recombinant QPs1 shows an EPR signal at g=2.91. Histidine residues at positions 98 and 120 are responsible for heme ligation because the H98N or H120N-reconstituted QPs1 fail to restore cytochrome b_{560} upon addition of hemin chloride.

INTRODUCTION

A better understanding the structural and functional relationship of SQR, especially of the amino acid residues involved in Q-binding, succinate dehydrogenase docking, and heme b_{560} ligation, requires functionally active QPs subunits. Three subunits, denoted as QPs1, QPs2, and QPs3, with apparent molecular masses of 15, 13 and 11 kDa, respectively, are found in the purified, reconstitutively active QPs. QPs1 has been thought as cytochrome b_{560}. Thus it is necessary to obtain purified QPs1 for heme-ligating studies. There are two ways to obtain purified QPs1: one is by biochemical resolution of QPs; the other is by gene expression to generate recombinant QPs1 protein. The availability of the cDNA for QPs1 in our laboratory together with our past experience in over-expressing the subunit VII and subunit IV of the cytochrome bc_1 complexes from beef heart mitochondria and *Rhodobacter sphaeroides* encouraged us to obtain purfied QPs1 by the gene expression approach. The pGEX expression system was used because it allows one step purification of recombinant fusion protein with glutathione-agarose gel (1). Herein we report the construction of the expression vector, pGEX/QPs1, growth conditions for over-expression of the active soluble form of GST-QPs1 fusion protein in E. coli DH5a and properties of recombinant QPs1. The heme *b*-560 ligating property of recombinant QPs1 is established by its ability to restore the spectra properties of cytochrome b_{560} upon addition of hemin chloride. The amino acid residues of QPs1 involved in heme ligation were identified by site-directed mutagenesis.

EXPEIMENTAL PROCEDURES

Materials

Restriction endonucleases, T4 DNA ligase, T4 DNA polymerase and T4 polynucleotide kinase were obtained from either Promega Corporation or Bethesda Research Laboratories. DNase I (Type IV), RNase A, isopropyl-β-D-thiogalactopyranoside (IPTG), gelatin, ampicillin, tetracycline, D-aminolevulinic acid, ferrous sulfate, hemin chloride, sorbitol, betaine, glutathione (reduced form), glutathione–agarose beads, thrombin, leupeptin, 2,6-dichlorophenol indophenol (DCPIP) and phenylmethylsulfonylfloride (PMSF) were from Sigma. Nitrocellulose membrane was from MSI. Agarose, acrylamide, bis-acrylamide, Horseradish Peroxidase (HRP) color development reagents 4CN, and protein A horseradish peroxidase conjugate were from Bio-Rad. LB agar, LB broth base, Select Peptone-140, and Select Yeast Extract were from GIBCO BRL. Oligonucleotides were synthesized by the DNA/Protein Core Facility at Oklahoma State University. Antibodies against QPs1 were generated in rabbits and purified by the method previously reported (2). Other chemicals were obtained commercially in the highest purity available.

Bacterial Strains and Plasmids

E. coli JM109 [*rec*A1, *end*A1, *gyr*A96, *thi*-, *hsd*R17 (r^-_k, m^-_k), *sup*E44, *rel*A1, λ^-, Δ(*lac, pro*), F', *tra*D36, *pro*AB *lac*I^qZ ΔM15] was used as host for pSelect (Promega), and pGEX-2TH (Pharmacia) plasmids. *E. coli* DH5α[F^-, ϕ80d, *lac*ZΔM15, *end*A1,

*rec*A1, *hsd*R17 (r^-_k, m^+_k), *sup*E44, *thi*-1, λ^-, *gyr*A96, Δ(*lac*ZYA-*arg*F), U169] was used as host for pGEX-2TH/QPs1. *E. coli* strains were grown in LB medium (3). *E. coli* strain INVαF'[–F', *end*A1, *rec*A1, *hsd*R17, (r_k^-, m_k^+), *sup*E44, *thi-1, gyr*A96, *rel*A1, ϕ80d, *lac*ZΔM15, Δ(*lac*ZYA-*arg*F), U169, λ^-] was used as host for pCR2.1 vector (Invitrogen) and single strand DNA preparation. When necessary, ampicillin (100 μg/ml) or tetracycline (15 μg/ml) was added.

DNA Manipulation and DNA Sequencing

Restriction enzyme digestion, large-scale isolation and minipreparation of plasmid DNA, were performed according to reported methods (3). DNA sequencing was performed with an Applied Biosystems model 373 automatic DNA sequencer at the Recombinant DNA/Protein Resource Facility at Oklahoma State University.

Construction of *E. coli* Strains Expressing Wild-type and Mutant QPs1

QPs1 DNA mutations were generated by site-directed mutagenesis using the Altered Sites™ Mutagenesis system from Promega. A 432 bp *Bam*HI–*Hin*dIII fragment from pSelect$_{amp}^r$/QPs1$_{BΔBH}$ was cloned into *Bam*HI and *Hin*dIII sites of pGEX-2TH to generate pGEX/QPs1 expression plasmid. The single-stranded pSelect/QPs1 was used as the template in the mutagenesis reactions. The mutagenic oligonucleotides used were as follows:

```
H26D 5′-TTGTCTCCCGATATCAGCAT; H42D 5′-GTCCATTTGCGACCGTGGCAC;
H70D 5′-CTTTGAGTCTGATTTGGAATT; H85D 5′-AGCACTGATCGACACAGCCAA;
H98D 5′-TCTCATGTATGACACCTGGAA; H105D 5′-TGGGATCCGAGACTTGATGTG;
```

H120D 5′-TTTCCCAGCTAGACCAGTCTG;

H26N 5′-TTGTCTCCCAATATCAGC; H42N 5′-GTCCATTTGCAACCGTGGCACTGGT;

H70N 5′-CTTTGAGTCTAATTTGGA; H85N 5′-AGCACTGATCAACACAGCC;

H98N 5′-CTCATGTATAACACCTGG; H105N 5′-GGGATTCGAAACTTGATG;

H120N 5′-TCCCAGCTAAACCAGTCT.

The single mutant of QPs1: H26D, H42D, H70D, H85D, H98D, H105D, H120D, H26N, H42N, H70N, H85N, H98N, H105N, and H120N were constructed by using each of these oligonucleotides, in combination with an ampicillin repair oligonucleotide, and annealed to the single-stranded pSELECT/QPs1. The double mutants, QPs1 (H26D & H69D), QPs1 (H42D & H120D), and QPs1 (H42D & H98D) were constructed by annealing each of the two mutated oligonucleotides with an ampicillin repair oligonucleotide to the single-stranded pSelect/QPs1. The triple mutant, QPs1 (H42D, H105D, H120D) was constructed by annealing each of the three mutated oligonucleotides with an ampicillin repair oligonucleotide to the single-stranded pSelect/QPs1. The hexad mutant (except H26) and septenary mutant were constructed by annealing H26D, H70D, H85D, H98D-mutated oligonucleotides with an ampicillin repair oligonucleotide to the single-stranded pSELECT/QPs1 (H42, 105, 120D).

A 432 bp *Bam*HI–*Hin*dIII fragment containing mutated QPs1 was excised from pSelect/QPs1$_m$ and cloned into *Bam*HI and *Hin*dIII of pGEX2TH vector to generate pGEX2TH/QPs1$_m$, which was then transformed into JM109 cells. Mutations were confirmed by DNA sequencing of both pSelect/QPs1$_m$ and pGEX2TH/QPs1$_m$. pGEX2TH/QPs1$_m$ plasmids were further transformed into host *E. coli* DH5α cells.

Transformants expressing the GST-QPs1$_m$ protein were identified by immunological screening of colonies with antibodies against the QPs1.

Production and Purification of Recombinant Wild-type and Mutant QPs1.

250 ml of an overnight grown culture of *E. coli* DH5α/pGEX/QPs1 was used to inoculate 12 liters of enriched medium (2% Selected peptone 140, 0.2% Na_2HPO4, 0.1% KH_2PO4, 0.8% NaCl, 1.5% Select yeast extract, and 0.2% glucose) containing 2.5 mM betaine, 440 mM sorbitol, and 100 μg/ml ampicillin, and incubated at 37°C with vigorous shaking until the $OD_{660\,nm}$ reached 0.7. The culture was cooled to 27°C and IPTG was added to a final concentration of 0.5 mM to induce the synthesis of the GST–QPs1 fusion protein. Cells were grown at 27°C for 3 hours before they were harvested by centrifugation at 8000x*g* for 15 min. The cell paste (43 g) was suspended in 80 ml of PBS buffer (20 mM sodium/potassium phosphate, pH 7.3, containing 150 mM NaCl) and sonicated at 30 milliwatts at 0 °C with four 20-s pulses at 3 to 4 min intervals. During sonication, protease inhibitor, PMSF (phenylmethylsulfonyl fluoride), 100 mM in absolute alcohol, was added to a final concentration of 1 mM. Triton X-100 was added to the broken cell suspension to a final concentration of 1% (w/v). This mixture was stirred gently on ice for 1 h before being centrifuged at 30,000 x *g* for 20 min. The supernatant obtained was mixed with an equal volume of glutathione–agarose gel equilibrated with PBS. The mixture was gently shaken for 2 h at 4 °C and packed into a 2.5x13 cm column. The column was washed with 800 ml of 50 mM Tris–Cl buffer, pH 7.5, then with 100 ml of 50 mM Tris–Cl, pH 8.0, containing 0.1 mM glutathione and 0.25 M sucrose, and finally eluted with 50 mM Tris–HCl, pH 8.0, containing 5 mM glutathione and 0.25 M

sucrose. Fractions containing the GST-QPs1 fusion protein were pooled and dialyzed against 50 mM Tris–Cl, pH 8.0, containing 0.25 M sucrose, overnight, with two changes of buffer. The dialyzed sample was concentrated with a Centricon-10 to a protein concentration of 10 mg/ml, mixed with glycerol to a final concentration of 10%, and frozen at -80°C until use. QPs1 protein was released from GST-QPs1 fusion protein by thrombin digestion (1 μg/500 μg of protein) and recovered by gel filtration using a FPLC superose-12 column. Recombinant QPs1 mutants were obtained in the same manner as the wild type protein.

Enzyme Preparations and Assays

Succinate-Q reductase (4), succinate dehydrogenase (5), and QPs (6) were prepared and assayed as previously reported. Succinate–ubiquinone reductase was assayed for its ability to catalyze the Q-mediated DCPIP reduction by succinate. One ml assay mixture contains 100 mmoles of sodium/potassium phosphate buffer, pH 7.4, 50 nmoles of DCPIP, 20 mmoles of succinate, 10 nmoles of EDTA, 16 nmoles of Q_2 and 0.1 mg of Triton X-100. The reduction of DCPIP was followed by an absorption decrease at 600 nm using a millimolar extinction coefficient of 21 cm^{-1} mM^{-1}.

Absorption spectra and spectrophotometric activity assays were performed at room temperature in a Shimadzu UV-2101PC spectrometer. Protein concentration was determined by the Lowry method (7) using bovine serum albumin as standard. The heme content was determined from the reduced pyridine hemochromogen spectra using a millimolar extinction coefficient of 34.6 cm^{-1} mM^{-1} for the absorbance difference between 557 nm and 600 nm (8). Analytical SDS-PAGE was performed in a Bio-Rad

Mini-Protein dual slab cell using the gel system of Schägger et al. (9), with modifications (10). Western blots were performed as previously described (11). The EPR measurements were made with a Bruker ER-200D equipped with an Air Product Heli-Tran System. EPR settings are detailed in figure legends.

RESULTS AND DISCUSSION

Purity and Properties of Purified Recombinant QPs1

When purified recombinant GST-QPs1 fusion protein preparation was subjected to SDS-PAGE (lane 3 of Figure 7 (A)), three major protein bands were observed: one with an apparent molecular weight of 41 kDa which accounted for 65% of the total protein, one with a molecular weight of about 68 kDa that accounted for 5% of the total protein and one smear band with the molecular weight span from 26.5 to 27 kDa that accounted for 30% of the total protein. The 41 kDa protein was GST–QPs1 fusion protein, the 26.5–27 kDa smear band contained incomplete GST–QPs1 fusion proteins, and the 68 kDa band was a contaminant protein. These assignments were based on the observation that both 41 kDa and 26.5–27 kDa proteins reacted with antibodies against QPs1 (lane 3 of Figure 7 (B)) and produced GST (M_r=26000 Da) upon thrombin digestion (see lane 4 of Figure 7 (A)). To date, we have been unable to obtain a GST–QPs1 preparation free of incomplete GST–QPs1 proteins, with a reasonable yield. However, the introduction of a 0.1 mM glutathione washing of the GST–QPs1 bound

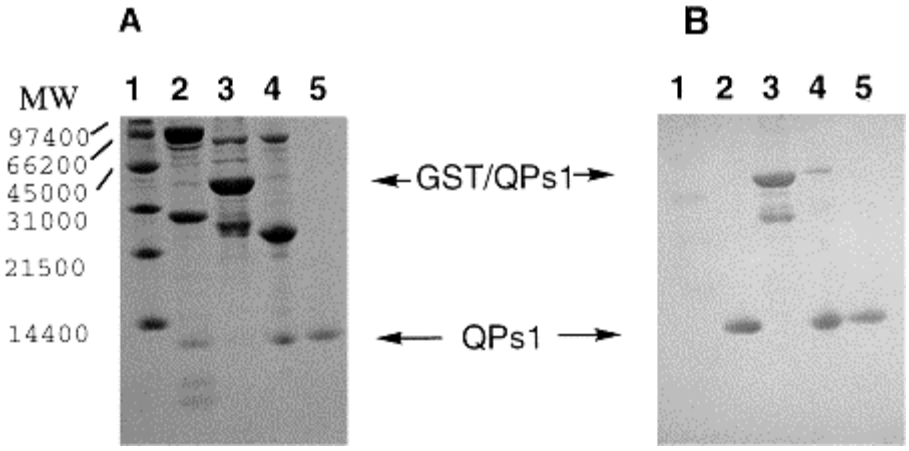

Figure 7. Identity of recombinant QPs1. (A) SDS-PAGE of isolated recombinant QPs1. Lane 1, molecular weight standard; lane 2, bovine heart mitochondrial succinate–ubiquinone reductase; lane 3, glutathione–agarose gel purified recombinant GST–QPs1; lane 4, thrombin digested recombinant GST–QPs1; and lane 5, purified recombinant QPs1. The high resolution SDS-PAGE gel of Schägger et al. (9) was used. (B) The proteins on the gel of (A) were electrophoretically transferred to a nitrocellulose membrane, without staining, and reacted with anti-QPs1 antibodies. Protein A horseradish peroxidase conjugate was used as the second antibody.

glutathione–agarose gel prior to elution of GST–QPs1 with 5 mM glutathione decreased the amount of incomplete GST–QPs1 proteins in the final preparation.

QPs1 was progressively released from GST–QPs1 fusion protein by treatment with thrombin (0.5 unit/mg protein) at room temperature. The reaction was completed after 30 min of incubation at room temperature. Recombinant QPs1 released from GST becomes highly aggregated and was recovered as a precipitate. The aggregation of QPs1 in aqueous solution was apparently due to the presence of hydrophobic domains, the three transmembrane helices, in the protein (10). Inclusion of 0.01% of dodecyl maltoside during thrombin digestion did not affect thrombin activity and permited recovery of QPs1 in a soluble (detergent dispersed) form. When this thrombin digested fusion protein was applied to a Superose-12 FPLC column equilibrated with 50 mM Tris–Cl, pH 7.8, containing 0.01% dodecyl maltoside, purified recombinant QPs1 was recovered in the void volume, indicating that purified QPs1, in 0.01% dodecyl maltoside, was still highly aggregated, with apparent molecular mass of over 1 million. The Superose-12 column chromatography separated uncleaved GST–QPs1 fusion protein, released GST, and thrombin, from QPs1. When the QPs1 containing fraction recovered from the Superose-12 column was subjected to SDS-PAGE, a single band, corresponding to the third subunit (QPs1) of purified succinate–ubiquinone reductase, was observed (lane 5 of Figure 7 (A)). However, when this purified recombinant QPs1 was subjected to partial N-terminal amino acid sequencing, two extra residues, glycine and threonine, were observed. The addition of these two extra residues was due to the recombinant manipulation.

Reconstitution of Cytochrome b_{560} from Recombinant QPs1 and Hemin Chloride

Although QPs1 was believed to be cytochrome b_{560} with bis-histidine ligands (12), isolated recombinant QPs1, obtained from cultures with or without aminolevulinic acid, contained little cytochrome b_{560} heme. Probably the lack of cytochrome b_{560} heme in recombinant QPs1 resulted from the inability of *E. coli* DH5α/pGEX-QPs1 cells to either incorporate heme into apoprotein or to produce enough heme. In other words, the expressed GST–QPs1 fusion protein had the correct structure for heme ligation and cytochrome b_{560} could be formed if heme was available. One way to test these possibilities is to reconstitute recombinant QPs1 *in vitro* with heme chloride to form cytochrome b_{560}. Reconstitution was first attempted with the fusion protein because it is soluble in aqueous solution.

When hemin chloride in DMSO was added to GST-QPs1, the maximum absorption peak (Soret band) of the oxidized form of heme progressively shifted from 398 nm to 411 nm, with increasing absorption intensity, during the incubation (see Panel A of Figure 8). It took 2 h to complete the spectral red shift and to reach maximum absorption. When heme-reconstituted sample was reduced with dithionite, it had symmetrical α-absorption at 559.5 nm, a broad β-absorption peak at 530 nm, and Soret absorption at 425 nm. These absorption characteristics were identical to those of cytochrome b_{560} in an isolated, reconstitutively active QPs preparation (6). Thus, cytochrome b_{560} was restored to GST–QPs1 fusion protein by heme addition.

Since GST from *Scistosoma japonicum* in recombinant GST–QPs1 contains 6 histidines and was reported to have heme binding activity (13), it is important to establish

A

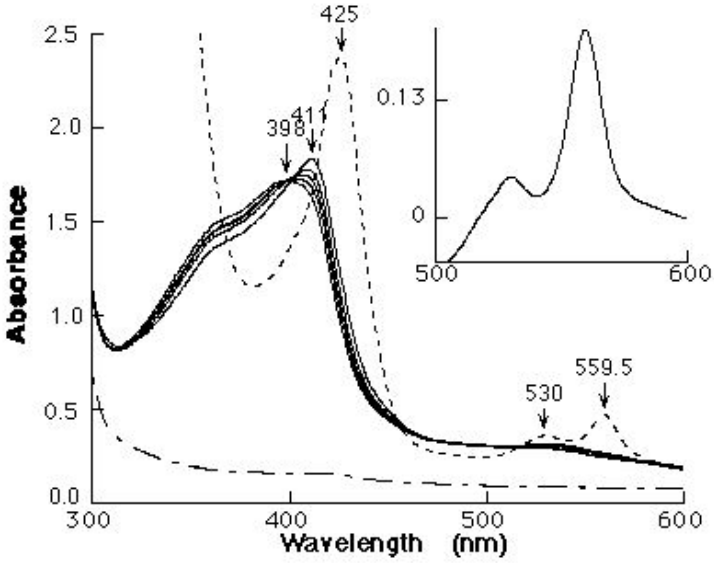
425
411
398
559.5
530
0.13
0
500
600
2.5
2.0
1.5
1.0
0.5
0.0
Absorbance
300
400
500
600
Wavelength (nm)

B

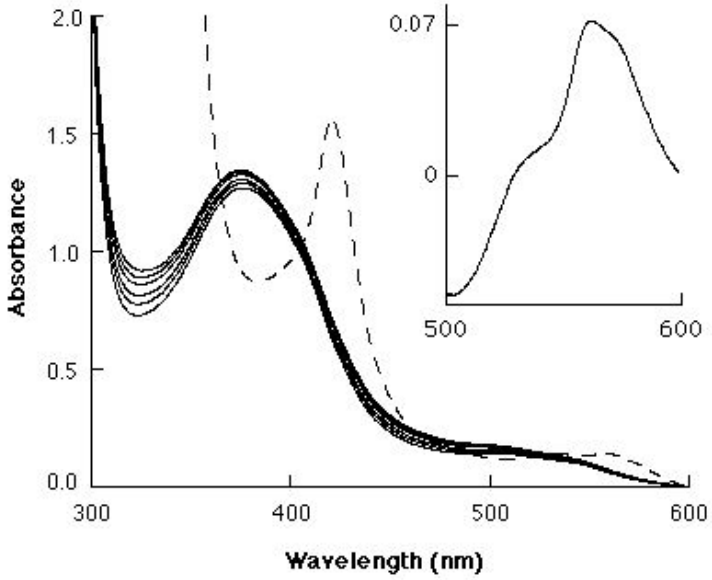
0.07
0
500
600
2.0
1.5
1.0
0.5
0.0
Absorbance
300
400
500
600
Wavelength (nm)

Figure 8. Restoration of cytochrome b_{560} to isolated recombinant GST–QPs1 fusion protein by heme. Three μl aliquots of hemin chloride (6.18 mM) in DMSO were added to 3 mg of purified recombinant GST–QPs1 fusion protein (panel A) and 3 mg of GST (panel B) in 1 ml, 50 mM Tris–Cl buffer, pH 8.0, containing 0.25 M sucrose. The mixtures were incubated at room temperature and absorption spectra were recorded from time to time during the incubation period. Total incubation time was about 2 hrs. When the oxidized Soret absorption peak no longer changed (——), a small amount of dithionite was added and spectra recorded (- - -). The inserts are the difference spectra of the dithionite-reduced vs. oxidized form at the α and β absorption regions.

that the bis-histidine ligands of reconstituted cytochrome b_{560} in GST–QPs1 were provided by the QPs1, and not by the GST moiety. This was achieved by comparing the absorption spectra and EPR characteristics of heme-ligated GST with those of heme-ligated GST–QPs1. Recombinant GST was produced in DH5α/pGEX cells and purified by glutathione–agarose gel. Since, after addition of heme to purified recombinant GST, under conditions identical with those for GST–QPs1, no cytochrome b_{560} spectrum was produced (panel B, Figure 8), the bis-histidine ligands of reconstituted cytochrome b_{560} were provided by the QPs1 moiety of the fusion protein. The heme-ligated GST had a very broad α-absorption at 540 nm in the dithionite-reduced form.

Reconstitution of cytochrome b_{560} into GST–QPs1 was heme concentration dependent. When GST–QPs1 was incubated with various amounts of hemin chloride, the peak height at 559.5 nm increased as the amount of heme added was increased (Figure 9). Maximum reconstitution was reached when the molar ratio of heme to fusion protein used in the system was 0.6. When the heme to protein ratio was higher than 0.6, the sample had an increased absorbance at 559.5 nm compared to that reconstituted with a 0.6 molar ratio of heme, but with a discernible broad shoulder at around 580 nm. This increased 559.5 nm absorbance was diminished when the sample was treated with thrombin (see Figure 9), indicating that excess heme cross ligated to a histidine residue in the GST moiety to form a cytochrome b_{560}-like spectra. No change in 559.5 nm absorbance was observed with reconstituted cytochrome b_{560}, formed with less than 0.6 molar ratio of heme, after thrombin digestion. A millimolar coefficient for reconstituted cytochrome b_{560} was calculated to be 9.9 cm^{-1} mM^{-1} for $A_{559.5\ nm}–A_{575\ nm}$ of the difference

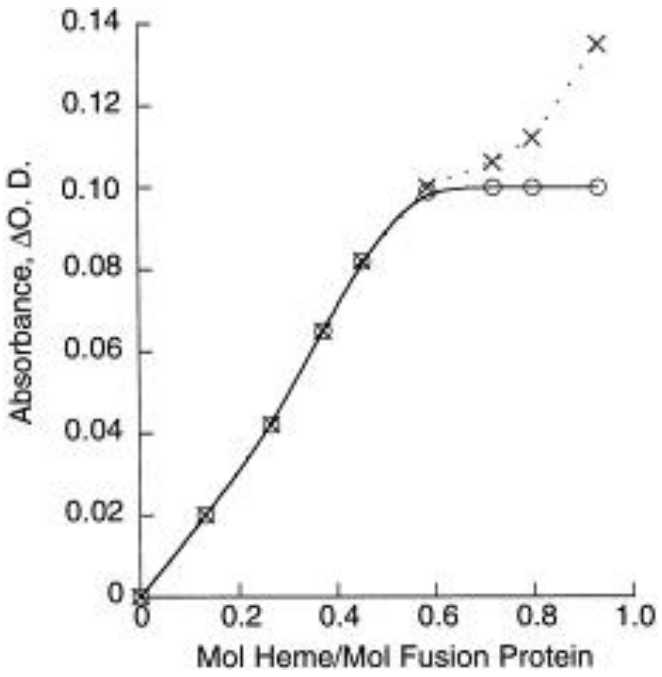

Figure 9. Effect of heme concentration on the reconstitution of cytochrome b_{560} in recombinant GST–QPs1 fusion protein. One ml aliquots of purified recombinant GST–QPs1 fusion protein, 0.7 mg/ml, in 50 mM Tris–Cl, pH 8.0, were added to 3 μl of DMSO containing indicated concentrations of hemin chloride. Mixtures were incubated at room temperature for 2 h and difference spectra between the oxidized and reduced forms of each sample were measured before (×) and after thrombin digestion (⊠). The thrombin digestion was carried out with 0.01 unit/μg protein at room temperature for 1 h.

spectra between the dithionite-reduced and the oxidized forms. This value is about half that determined for cytochrome b_{560} in isolated QPs.

The less than unit reconstitution can be explained by one or more of the following: (1) the presence of some incomplete GST–QPs1 proteins in the isolated fusion protein preparation; (2) partial availability of one of the histidine ligands in the QPs1 moiety resulting from the aggregation of isolated fusion protein in aqueous solution. When this partially available histidine residue is completely ligated by heme, excess heme is ligated to a histidine residue in the GST moiety to form a cytochrome b_{560}-like spectra which is diminished by thrombin digestion; (3) the two histidine ligands are from different QPs1 molecules. In this case, only one histidine residue of each QPs1 is involved. Results described in the next section seem to support the first possibility.

EPR Characteristics of Heme-Reconstituted Wild-type QPs1:

Figure 10 shows EPR characteristics of heme-ligated GST–QPs1, heme-ligated GST, and free heme. Reconstituted cytochrome b_{560} in GST–QPs1 showed an EPR peak at g=2.91 (trace A of Figure 10), which differed completely from the EPR characteristics of heme-treated GST (g=3.50 and g=3.86, trace C of Figure 10) and of free heme (a broad peak with g=3.80, trace D of Figure 10). When reconstituted cytochrome b_{560} in GST–QPs1 was treated with thrombin, no change in EPR characteristics was observed (see trace B of Figure 10). These supported the results obtained from absorption spectra which indicated that the bis-histidine ligands of cytochrome b_{560} were provided by the QPs1 moiety. The g=2.91 EPR signal observed for reconstituted cytochrome b_{560} in recombinant QPs1 corresponded to one of the two EPR signals (g=2.91 and g=3.07)

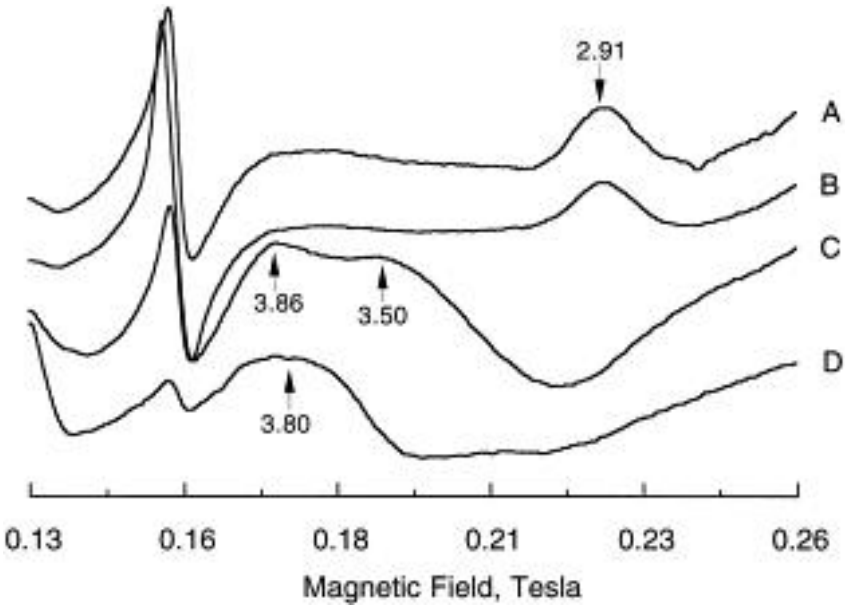

Figure 10. EPR spectra of reconstituted cytochrome b_{560}, thrombin-treated reconstituted cytochrome b_{560}, heme-added GST, and free heme. 18 μl aliquots of hemin chloride, 8.0 mM, in DMSO were added to 0.9 ml of 50 mM Tris–Cl buffer, pH 8.0, containing (A) GST–QPs1 fusion protein, 10 mg/ml; (C) purified recombinant GST, 10 mg/ml; (D) none. The mixtures were incubated at room temperature, with stirring, for 2 h prior to EPR measurement. Trace (B) was taken after treatment of (A) with thrombin (0.01 unit/μg protein) for 1 h at room temperature. The EPR instrument settings were: modulation frequency, 100 kHz; modulation amplitude, 20 G; time constant, 0.5 s; microwave frequency, 9.42 GHz; microwave power, 20 mW; scan rate, 200 G/s; and temperature, 11 K.

observed for cytochrome b_{560} in isolated QPs. This g=2.91 signal of cytochrome b_{560} in isolated QPs was not affected by the addition of succinate dehydrogenase to QPs to form succinate–ubiquinone reductase (6).

The incomplete GST–QPs1 (C-terminal truncated QPs1) proteins accounted for about 30% of the total protein in the isolated fusion protein preparation (see line 3 of Figure 7 (A)). These C-terminal truncated QPs1 proteins were probably missing one or both of the two histidine residues in QPs1 since the apparent molecular masses of these proteins were 500–1000 Da. If the bis-histidine ligands of reconstituted cytochrome b_{560} in GST–QPs1 were provided by the intact QPs1 moiety, 1 mol of heme ligated into 1 mol of intact QPs1–GST in the preparation would give maximum reconstitution with a 0.6 molar ratio of heme added. This idea was supported by the recovery of thrombin treated reconstituted cytochrome b_{560} in QPs1, which had a heme to protein ratio of 0.9, by a Sepharose-12 column chromatography, GST–QPs1 had only a heme to protein ratio of 0.57. Furthermore, the amount of cytochrome b_{560} restoration into GST–QPs1 correlates with the amount of intact QPs1 presented in the fusion protein preparation. Addition of heme to a GST–QPs1 preparation enriched with incomplete QPs1–GST proteins (to about 80%), gave maximum reconstitution (2 nmol/mg) when the heme to protein ratio in the system was 0.18. The incomplete GST–QPs1 enriched preparation was obtained in a 0.1 mM glutathione washing of GST–QPs1 adsorbed on glutathione–agarose gel during purification.

To date we have been unable to reconstitute cytochrome b_{560} reconstituted recombinant QPs1 with succinate dehydrogenase to form succinate-Q reductase. We

observed no change in the absorption spectra, EPR characteristics, and carbon monoxide reactivity of reconstituted cytochrome b_{560} in GST–QPs1 or in QPs1 upon addition of succinate dehydrogenase. This indicates that no specific interaction occurs between succinate dehydrogenase and recombinant QPs1. The failure of reconstituted cytochrome b_{560} in GST–QPs1 or in QPs1 to interact with succinate dehydrogenase to form succinate–ubiquinone reductase may be due to a requirement of QPs2 or QPs3 for this interaction.

Identification of Amino Acid Residues of QPs1 Involved in Ligation of Heme b_{560}

QPs1 contains seven histidine residues at positions 26, 42, 70, 85, 98, 105, and 120. To locate the heme-ligating residues, we altered each of these residues to aspartic acid and asparagine, by site-directed mutagenesis followed by spectral (absorption and EPR) characterization of heme-reconstituted recombinant QPs1 mutants. Figure 11 shows absorption spectra of heme-reconstituted recombinant QPs1 mutants. The absorption spectra of heme-reconstituted wild type QPs1 was included for comparison. The addition of hemin chloride to the H26D, H26N, H42D, H42N, H70D, H70N, H85D, H85N, H105D, or H105N mutant yielded absorption spectra similar to those of reconstituted wild type, indicating that H26, H42, H70, H85, and H105 were not involved in heme ligation. However, the Soret absorption peaks of heme-reconstituted mutants H98D, H98N, H120D and H120N were very different, with a 14 nm red shift of the peak maximum (from 424 nm to 438 nm) and a drastic decrease in absorbance (panel F, H, I, and J of Figure 11), indicating that His-98 and His-120 of QPs1 were involved in heme b560 ligation. As expected, when double mutants, H42D, H98D (panel L), and H98D,

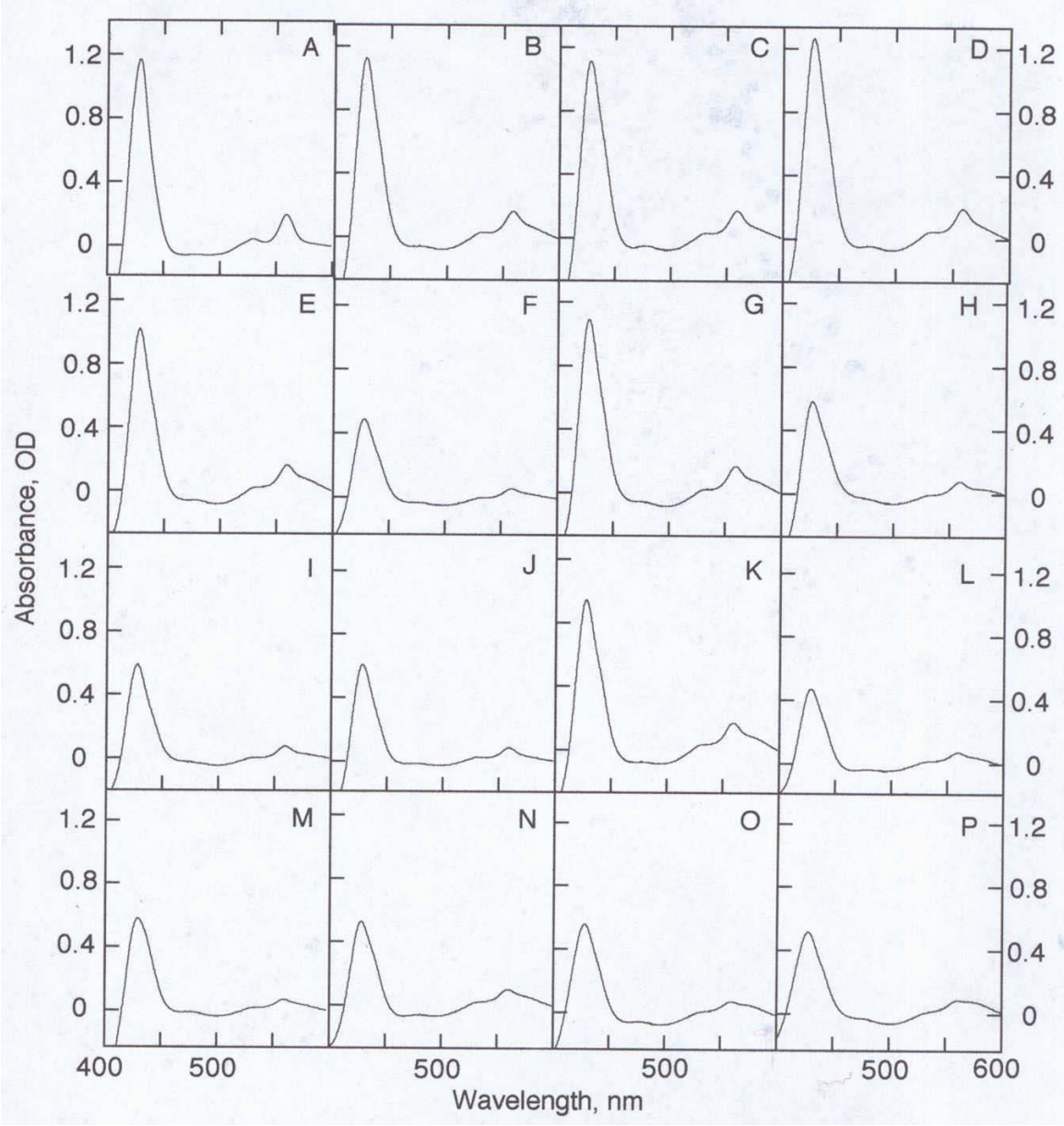

Figure 11. The dithionite-reduced minus –oxidized spectra of thrombin treated, heme-reconstituted mutant QPs1 fusion proteins. The *panels* are as follows: *A*, wild type; *B*, H26D; *C*, H42D; *D*, H70D; *E*, H85D; *F*, H98D; *G*, H105D; *H*, H120D; *I*, H98N; *J*, H120N; *K*, H26D, H70D; *L*, H42D, H98D; *M*, H42D, H105D, H120D; *N*, H98D, H120D; *O*, H42D, H70D, H85D, H98D, H105D, H120D; and *P*, H26D, H42D, H70D, H85D, H98D, H105D, H120D.

H120D (panel N), triple mutant, H42D, H105D, H120D (panel M), hexa mutant, H42D, H70D, H85D, H98D, H105D, H120D (panel O), and hepta mutant, H26D, H42D, H70D, H85D, H98D, H105D, H120D (panel P) were reconstituted with hemin chloride, no cytochrome b_{560} spectral characteristics were observed.

The crystal structure from *E. coli* SQR revealed the possible heme ligands for the cytochrome b_{560} (14). They were H84 from SdhC subunit and H71 from SdhD subunit. Unlike the FP and IP subunits, which have high sequence similarities through different species, the anchor polypeptides from different species show little apparent sequence similarity. In fact, the number of subunits and heme content are different between species, varying from one subunit containing two hemes like *Bacillus subtilis*, two subunits containing two hemes like *Thermoplasma acidophilum*, and two subunits containing no heme like *Saccharomyces cerevisiae* (15). So, the fact that we were able to demonstrate that the bis-histidine ligands were from QPs1 shows the variety of this anchoring protein among different spices. Another possibility could be unspecific ligand binding from other histidine residues in QPs1 under the current experimental conditions.

REFERNCES

1. Smith, D. B., and Johnson, K. S. (1988) *Gene* **67**, 31-40
2. Yu, L., Wei, Y. Y., Usui, S., and Yu, C. A. (1992) *J Biol Chem* **267**, 24508-24515
3. J. Sambrook, E. F. F., and T. Maniatis. (1989) *Appendix 1*, 2nd Ed. Molecular Cloning: A Laboratory Manual, Cold Spring Harbor Laboratory, Cold Spring Harbor, ny
4. Yu, L., and Yu, C. A. (1982) *J Biol Chem* **257**, 2016-2021
5. Yu, C. A., and Yu, L. (1980) *Biochim Biophys Acta* **591**, 409-420
6. Yu, L., Xu, J. X., Haley, P. E., and Yu, C. A. (1987) *J Biol Chem* **262**, 1137-1143
7. Lowry, O. H., Rosebrough, N. J., Farr, A. L., and Randall, R. J. (1951) *J Biol Chem* **193**, 265-275
8. K. G. Paul, H. T., and A. Akesson. (1955) *Acta Chem. Scand.* **7**, 1248
9. H. Schägger, T. A. L., W.D. Engel, and G. von Jagow. (1986). Methods Enzymol., 126
10. Lee, G. Y., He, D. Y., Yu, L., and Yu, C. A. (1995) *J Biol Chem* **270**, 6193-6198
11. Yu, L., Deng, K., and Yu, C. A. (1995) *J Biol Chem* **270**, 25634-25638
12. Crouse, B. R., Yu, C. A., Yu, L., and Johnson, M. K. (1995) *FEBS Lett* **367**, 1-4
13. Smith, D. B., Davern, K. M., Board, P. G., Tiu, W. U., Garcia, E. G., and Mitchell, G. F. (1986) *Proc Natl Acad Sci U S A* **83**, 8703-8707
14. Yankovskaya, V., Horsefield, R., Tornroth, S., Luna-Chavez, C., Miyoshi, H., Leger, C., Byrne, B., Cecchini, G., and Iwata, S. (2003) *Science* **299**, 700-704
15. Hagerhall, C. (1997) *Biochim Biophys Acta* **1320**, 107-141

CHAPTER III

PURIFICATION AND CRYSTALLIZATION OF NADH DEHYDROGENASE OF NADH-Q REDUCTASE

ABSTRACT

A purification procedure for NADH dehydrogenase was developed. This procedure involves acid extraction in the presence of organic solvent followed by ammonium sulfate fractionation, and DEAE Sepharose column chromatography. The purified NADH dehydrogenase contains 3 protein subunits with apparent molecular weight of 51, 24, and 10 kD. It catalyzed oxidation of NADH by artificial electron acceptor ferricyanide with specific activity of 471 μmol $Fe(CN)_6^{3-}$ reduced/(min mg) protein. The purified NADH dehydrogenase contained one FMN, five irons, and two EPR detectable iron sulfur clusters, one [4Fe-4S] and one [2Fe-2S]. Preliminary attempts of crystallization were discussed.

INTRODUCTION

Complex I serves as the entry point for electrons from NADH into the respiratory chain of mitochondria. Due to the extreme structural complexity, the difficulty of applying optical spectroscopy to analyze the redox state of intrinsic chromophores within the membrane, and the absence of inhibitors that block the pathway at specific intermediate sites, there is still uncertainty about the electron pathway of complex I.

The FP fragment of bovine complex I, also called NADH dehydrogenase, has been extensively studied, and is considered as the entry point of electron translocation of this complex. Its FMN and NADH binding ability, the presence of iron-sulfur clusters N-1b and N-3, and simplicity to prepare in comparison with the whole enzyme complex, make it an attractive candidate to be the first fully understood subcomplex of this complicated complex.

Since 1952, various forms of the mitochondrial NADH dehydrogenase have been isolated and studied (1,2). The schemes of these preparations are varied from one to another, but in general, they involve the following steps. First, solublizing agents such as ethanol, thiourea, snake venom, and $NaClO_4$ are used to extract the soluble part of proteins out of either various preparations of submitochondrial particles or complex I. Second, combining either several or all of the treatments such as changing the pH, alteing the temperature, fractionation by ammonium sulfate, dialysis, and column chromatography to further achieve the goal of purification.

We adopted and modified the NADH dehydrogenase purification method developed by Mackler (3), which uses ethanol as solublizing agent, and then further purify the enzyme through a series of steps. The specific activity from NADH to artificial electron acceptor ferricyanide was used to monitor the enzymic activity of this purification. The high resolution sodium dodecyl sulfate (SDS) polyacrylamide gel electrophoresis (PAGE) containing 8M urea was used to assess the purity of this purification.

EXPEIMENTAL PROCEDURES

Preparation of Submitochondrial Particles (SMP) from Bovine Heart

About 10 pounds of trimmed beef hearts, which were free of fat and connective tissues, were taken from a -20°C freezer, 12 hours prior to preparation and left at the room temperature for one hour, then moved to 4°C. Heart muscle was ground in a power-driven meat grinder and ground meat was divided into about 600 g per portion. Each portion of meat was placed into a blender, adding 1.8 L of 10 mM K_2HPO_4 and about 5.5 ml of 6 N NaOH, and blended for 30 seconds from low to high speed. 6 N NaOH was used to adjust the pH of the mixture to around 7.0~7.4 before blending for another 30 seconds. The blended mixture was centrifuged for 15 minutes at 2,800 rpm in a J-6 rotor (Beckman). The turbid supernatant was collected and poured through eight layers of cheese cloth. The precipitate was suspended with about 500 ml of 20 mM Na/K phosphate at pH 7.4, and centrifuged for 15 minutes at 2,800 rpm in a J-6 rotor. Again, the supernatant was collected and poured through eight layers of cheese cloth. For each 6 liters of combined filtrate, pH was adjusted to 5.5 with 2 N acetic acid, and then centrifuged for 25 minutes at 4,000 rpm in a J-6 rotor. The precipitate was homogenized in ~ 900 ml of 0.1 M phosphate borate buffer at pH 7.8. The mixture was centrifuged for 1 hour in a Ti45 rotor at 45,000 rpm. The precipitate was homogenized in water to a final volume approximately 1.8 L. The salt concentration at this step is still high.

Purification of NADH Dehydrogenase from SMP

In order to adjust the protein concentration and to further reduce the salt concentration, 600 ml of SMP were mixed with cold water to a final volume of 1.6 L. The pH was adjusted from around pH 7.0 to 5.5 with 2 N acetic acid. The mixture was centrifuged for 20 minutes at 4,000 rpm in a J-6 rotor. The precipitate was briefly suspended in cold water in the same centrifuge bottle to a final volume of about 800 ml, and centrifuged again for 20 minutes at 4,000 rpm. The precipitate was homogenized with cold water to give a final protein concentration of 40 mg/ml in about 400 ml. The sample was adjusted to pH 4.8 with 2 N acetic acid and 100% ethanol was added to give a final concentration of 9%. The mixture was placed into a water bath with a temperature of 55°C with constant stirring until the sample temperature reached 40°C. The sample was left at 40°C for 10 minutes with constant stirring. After that, the sample was immediately placed in an ice-salt water bath, with constant stirring, until it reached 4°C. The sample was centrifuged for 20 minutes at 45,000 rpm in a Ti45 rotor. A gold-light red colored supernatant, named S1, was collected.

Fine ammonium sulfate was slowly added to S1 with constant stirring to give a final 57% Am_2SO_4 saturation. After stirring for 10 minutes at 4°C, the mixture was centrifuged for 20 minutes at 45,000 rpm. The light yellow-brown color precipitate was collected and dissolved in about 3 ml of 5 mM K_2HPO_4/KH_2PO_4 (K/K phosphate) buffer, pH 6.5. The sample was then centrifuged for 10 minutes at 19,000 in a JA-20 rotor, in order to remove possible loose precipitates from the acid extraction.

Solution, named P2, was collected and applied to a G-25 column, which was equilibrated with 5 mM K/K phosphate at pH 6.5, with a sample volume to column volume ratio of about 5%. This reduces the sample salt concentration as is required for DEAE-Sepharose column chromatography. The G-25 effluent, with brownish color, named F3, was collected, and immediately applied to a DEAE-Sepharose CL-6B column equilibrated with 5 mM K/K phosphate at pH 6.5. The column was washed with equilibration buffer until no color was observed in the effluent. The NADH dehydrogenase was eluted with 5 mM K/K phosphate at pH 6.5 containing 25 mM NaCl. The sample was in red/brown color, named F4.

The protein concentration of F4 was determined by absorbance measurements at 278 nm with a specific absorptivity of 2.44 ml/(mg cm), which was determined by Bradford method, using Bovine Serum Albumin (BSA) as standard. F4 was then adjusted to protein concentration of ~1 mg/ml by the same eluting buffer. Fine ammonium sulfate was slowly added, with constant stirring, to give a final 60% saturation. The turbid solution was stirred at 0°C for10 minutes and centrifuged for 15 minutes at 19,000 rpm in a JA-20 rotor. The precipitate was collected and dissolved in 100 μl of 5 mM K/K phosphate at pH 6.5. This fraction was named P5. Normally a protein concentration of ~55 mg/ml, determined by the Bio-Rad protein assay, was obtained. If P5 was to be used for crystallization attempts or for storage (-80°C freezer), the following substances were added: dithiothreitol (DTT) (final concentration of 5 mM), cytochrome c oxidase (CcO) (0.002 mg/mg protein), cytochrome c (0.0005 mg/mg protein), and sodium ascorbate (NaAsc) (final concentration of 10 mM). Otherwise, P5 was used in the next purification step without any additions.

A 200 μl aliquot of P5 at protein concentration of ~20 mg/ml in 5 mM K/K phosphate, pH 6.5 was applied to a Superdex^{TM} 200 column (Pharmacia), equilibrated with 10 mM Na_2HPO_4/NaH_2PO_4 (pH 7.4) buffer containing 10 mM NaAc (pH 7.4), 10 mM DTT, 10 mM NaAsc, and 1 mM NaN_3. The flow rate was 0.5 ml/min, and the sample collecting size was 0.5 ml/tube. The collected sample, colored light brown, named F6, was concentrated by Centricon^{TM} 30 to ~20 mg/ml. Whether for crystallization attempts or for storage (-80°C freezer), the following substances were added: DTT (final concentration of 5 mM), CcO (0.002 mg/mg protein), cytochrome c (0.0005 mg/mg protein), and NaAsc (final concentration of 10 mM).

RESULTS AND DISCUSSION

Purification of NADH Dehydrogenase

Table III summarizes the purification data. Prior to acid extraction in ethanol, the salt concentration in preparation has to be lowed. Therefore, repeat dilution with water was needed to reduce the salt concentration. SMP was suspended in phosphate borate buffer with pH around 7.5. After diluted to three times with water, pH was adjusted to 5.5 instead of 4.8. This step was found necessary because it removes excess amount of blood remaining in the SMP, also it helps to further decrease the buffer capacity, which becomes critical later on when only small amount of acid would be needed to adjust the pH to 4.8 with protein concentration as high as 35 mg/mL.

It should be noted that when collecting the supernatant (S1) from acid/ethanol extraction, small amount of floating precipitates were found. These floating precipitates should be removed before proceeding to ammonium sulfate fractionation step. It's necessary to centrifuge S1 one more time in order to remove the precipitate.

The ammonium sulfate fractionation step, which was designed to concentrate and further purify the S1 fraction, caused 50% loss of total activity and 59% of total proteins, and therefore, should be modified. One possible reason for this loss could be the low pH from the previous step of acid extraction (pH 4.8). Without adjusting the pH back to neutral and proceeding to ammonium sulfate fractionation might cause the acid labile

Table III.

Summary of purification procedures, protein concentration and recovery, and specific activity at each step.

Purification Table for NADH Dehydrogenase									
Sample	Volume	[Protein]	Total Protein	%	Activity*	Total Activity**	%	Specific Activity	Fold
Acid Extraction (S1)	350ml	0.4 mg/ml	140 mg	100	66	23100	100	165	1
57% $AmSO_4$ ppt (P2)	3.5ml	12.5 mg/ml	43.8 mg	31	3300	11550	50	264	1.6
After G-25 (F3)	5.5ml	7 mg/ml	38.5 mg	28	1900	10450	45	271	1.6
After DEAE-Sepharose CL-6B (F4)	5ml	2.5 mg/ml	12.5 mg	9	1200	6000	26	480	2.9
60% $AmSO_4$ ppt (P5)	180µl	50 mg/ml	9 mg	6.5	24000	4320	19	480	2.9
Superdex 200 (F6)	375µl	20 mg/ml	7.5mg	5.4	9425	3535	15	471	2.9
*Activity is based on NADH to $Fe(CN)_6^{3-}$, monitor @ 420 nm, the reduction of $Fe(CN)_6^{3-}$.									
** Specific activity unit is µmol $Fe(CN)_6^{3-}$ reduced/min/mg protein.									

iron sulfur clusters to denature. Also considering other precipitant other than ammonium sulfate might prevent the loss of activity as well.

As shown in Table III, the F4 fraction, which was the eluted from the DEAE-Sepharose CL-6B column with 5 mM K/K phosphate at pH 6.5 containing 25 mM NaCl, recovered 60% of the total activity, but only 32% of the total protein, and 1.8 fold increase of specific activity. This was consistent with the observation that large portion of the protein, which couldn't be eluted out with 25 mM NaCl, bound tightly with the column. When eluting buffer containing 1 M NaCl was used, most of the protein was released from the column but with no detectable activity. This indicates that protein denaturation occurred. Currently, no solution to this problem has been found.

After Am_2SO_4 fractionation, P5, with 4 subunits as shown in panel A of Figure 12, was subjected to column chromatography by passing through a Superdex^{TM} 200 column. The effluent, named F6 (as shown in panel B of Figure 12), had only 3 subunits, didn't show any improvement of specific activity. Although the answer to this question wasn't clear, it's possible that denaturation of NADH dehydrogenase had occurred during the column chromatography, which results in the loss of activity, or the fourth subunit in P5 is actually critical for the activity.

Subunit Composition of P5 and F6 in NADH Dehydrogenase

Figure 12 shows SDS-PAGE of P5 and F6. P5 contains 4 subunits, with apparent molecular weight of 51, 24, 10, and 9 kD, and F6 contains 3 subunits, with apparent molecular weight of 51, 24, and 10 kD. N-terminal of each subunit was sequenced for 10

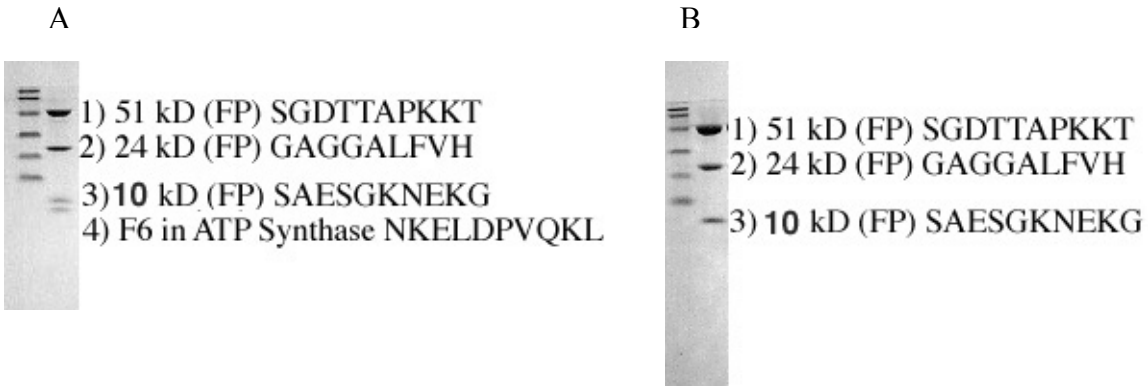

Figure 12. Protein composition and identification of NADH dehydrogenase. SDS-PAGE of fractions P5 (A) and F6 (B), right lane of each figure. The left lanes are molecular weight standards. Each band of P5 and F6 was sequenced, and the first 10 amino acids are indicated, along with its identity. The high resolution SDS-PAGE gel of Schägger et al. (5) was used.

amino acids. By comparing known protein sequences of SwissProt utilizing BLITZ, the identification and composition of the three and four subunits (fraction P5 and F6) were determined. In both P5 and F6, the compositions are 51, 24, and 10 kDa subunits of FP fragment in complex I. The fourth band of P5, however, is identified as Coupling Factor 6 of bovine complex V (ATP synthase).

Chemical Composition of NADH Dehydrogenase Preparation

a. FMN content of P5.

Acid-extractable flavin was determined fluorometrically using a Perkin-Elmer 650-40 Fluorescence Spectrophotometer and FMN (synthetic, from Sigma) as a standard. The concentration of the standard was calculated from the difference in absorption at 450 nm and 530 nm before and after addition of excess dithionite using an extinction coefficient of 10.3 mM^{-1} cm^{-1} (4). The molar ratio between FMN and P5 was found to be 1:1, which is consistent with the general consensus that there is one mole FMN per mole of complex I and that the FMN probably binds to the 51 kD subunit (5).

b. Non-heme iron content of P5 and F6.

By using the method developed by Doeg and Ziegler (6), iron was extracted from the sample by thioglycolic and acetic acids. Iron then was released into solution as the complex with 4,7-diphenyl-1,10-phenanthroline into isoamyl alcohol. The results show that the molar ratio between iron and P5, and iron and F6 were 5.13:1 and 4.98:1, respectively. The iron content was lower than expected since there are one [4Fe-4S] and one [2Fe-2S] within FP subcomplex, which should have given a 6:1 ratio between the

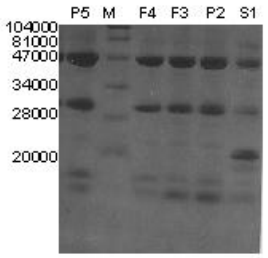

Figure 13. High resolution SDS-PAGE of protein samples from each purification steps. From left to right, fraction P5, (M) molecular-mass markers, fraction F4, F3, P2, and S1. Molecular weights of the marker are labeled at the left side of the figure.

iron and the FP, instead of about 5:1 in our preparation. The low iron content implies the loss in iron sulfur clusters, which results in drop of activities.

The specific activities based on NADH to ferricyanide of P5 and F6, as shown in Table I, are 480 and 471 μmol $Fe(CN)_6^{3-}$ reduced/(min mg protein). The specific activity is about the same as to the Mackler enzyme, which purified by similar procedure (7).

Absorption Spectra

As shown in Figure 14, the final absorption spectra of P5 and F6 shared similar features, with shoulders at about 350 nm (iron sulfur cluster) and 450 nm (flavin protein).

EPR Spectra of P5 and F6

Figure 15 shows EPR spectra of P5 and F6. In part A, both samples show the [4Fe-4S] (N3) clusters reducible by dithionite. In part B, both samples show the [2Fe-2S] (N1b) clusters reducible by dithionite, but with much lower content compared with part A. These results are consistent with previous reports that one [4Fe-4S] (N3) cluster is located in the 51 kD subunit of FP and one [2Fe-2S] (N1b) cluster is located in the 21 kD subunit of FP (8). The low content of N1b cluster was in concordance with our previous finding of lower than expected non-heme iron content, which suggests that there was loss of N1b cluster during preparation.

Stability of NADH Dehydrogenase

To test the stability of fraction P5, samples were stored in small microfuge tubes and tested for specific activity (μmol $Fe(CN)_6^{3-}$ reduced/(min mg protein)) from time to

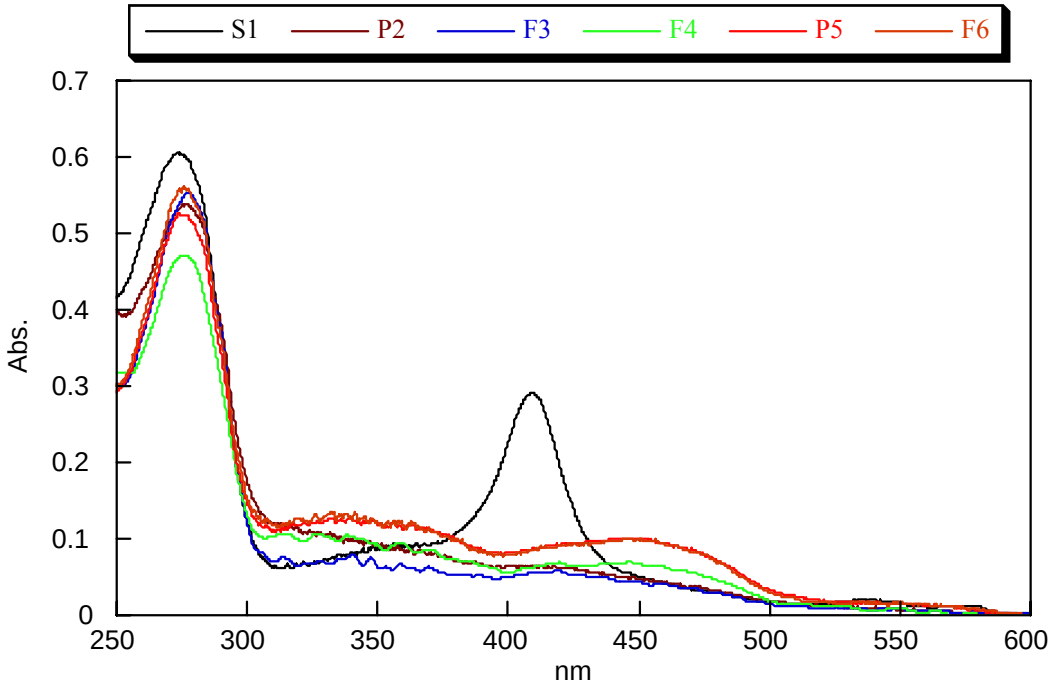

Figure 14. Spectra characters of protein samples from each purification steps. Each fraction is colored as indicated on the top of figure. All fractions protein concentration were adjusted to about 0.5 mg/ml. The UV-2410PC recording spectrophotometer from Shimadzu was used.

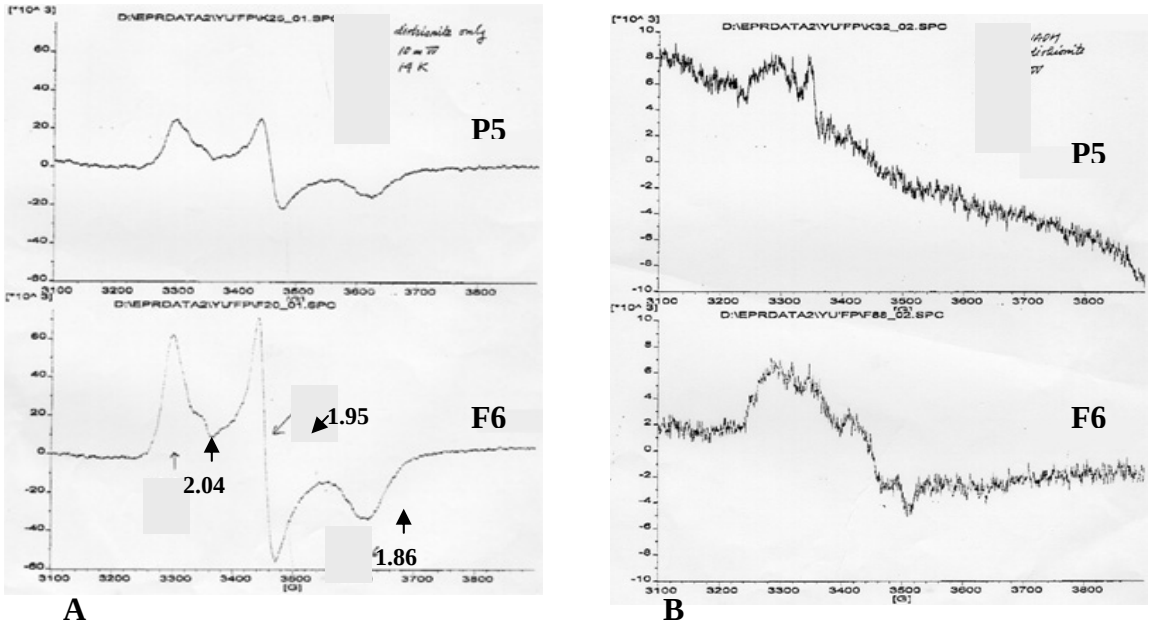

Figure 15. EPR spectra of NADH dehydrogenase. EPR spectra of fractions P5 and F6 have been taken under the condition: A) 5 mM dithionite, 10 mW, and 10 K; B) 1 mM NADH, 5 mM dithionite, 5 mW, and 50 K. In part A, both samples are showing the [4Fe-4S] (N3) clusters reducible by dithionite. In part B, both samples are showing the [2Fe-2S] (N1b) clusters reducible by dithionite, but with much lower content compared with part A.

time. CcO was added at a ratio of 0.002 mg per mg of protein and DTT was added to a final concentration of 5 mM. When CcO was added, cytochrome *c* (0.0005 mg/mg protein), and NaAsc (final concentration of 10 mM) were also added at the same time. An anaerobic condition was achieved by preparing and storing sample under argon atmosphere. As shown in Figure 16, even with addition of DTT (■), P5 lost 90% of its activity within 24 hours when exposed to air. Within anaerobic condition, and added with DTT (■), P5 lasted 48 hours before it lost 90% of its activity. With the addition of both CcO and DTT (■), P5 lasted for 72 hours even though the sample was exposed to air. Finally, with the same condition but under anaerobic condition (■), P5 still had 25% of its activity after 145 hours. In conclusion, NADH dehydrogenase was easily to be oxidized when exposed to air, which results in the loss of its activity. In order to maintain enzyme activity, additions of DTT, along with CcO (addition of cytochrome *c* and NaAsc), and under anaerobic condition are essentials.

Screening for Crystal Growth Conditions

The crystal growth of NADH dehydrogenase was first carried out by testing the conditions in which similar type of proteins, such as iron-sulfur proteins and dehydrogenase, has been successfully crystallized. The following summarizes the various conditions for crystallization we have used:

- Salt: NaCl, (NH4)2SO4,, MgCl2, MgSO4, **KCl**, None;
- Buffer: Tris-Cl, HEPES, MOPS, **K/K pi**;
- pH: 4.6, 5.6, 6.5, **7.5**, **8.0**, 8.5;

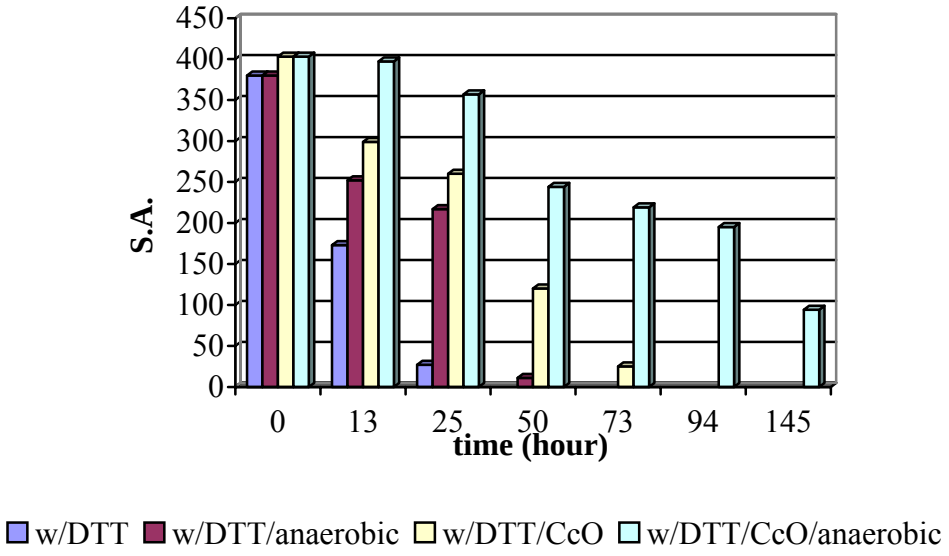

Figure 16. Stability test of fraction P5. Samples were treated under different conditions as indictated with different colored columns. The stability is represented by specific activity (S.A.).

- Precipitant: $(NH_4)_2SO_4$, PEG: 400, **3350, 4000, 6000**, $(NH_4)H_2PO_4$, MgSO4, NaCl;
- Temperature: **4ºC**, 13ºC, 25ºC;
- Others: ethanol, **EDTA, anaerobic, glycerol**.

The conditions, which helped the growth of crystals, are underlined and in bold letters. In short, the most desirable condition for crystallize NADH dehydrogenase so far was dissolving it (to a final protein concentration of 10-12 mg/mL) in a pH 7.5-8.0 K/K phosphate buffer with ~100 mM of KCl, and addition of CcO and DTT as described earlier. The best precipitant was PEG 3350, with a final concentration between 6.5% to 7.2%. An anaerobic condition was required and temperature of 4°C was essential. As shown in Figure 17, small protein crystals were obtained from P5 under the above conditions. Crystallization was performed in capillary tubes.

The commercial available crystallization kit, which contains various buffer conditions, with varying pH, precipitant, and buffer system was also used to obtain suitable conditions for crystal growth. As shown in Figure 18, P5 and F6 stability was described as the amount of precipitation in each condition for every 24 hours during a seven-day observation by using a five-point scoring system. From 5 to 0, the protein and buffer mixture is from clear to total precipitation. The X-axis of this figure represents the reagent sequence of MembFac Kit purchased from Hampton Research. The detailed list of reagent formulation is attached at the end of this chapter. The Y-axis represents the total score of this seven-day observation. The conditions with low score would be considered less stable. The volume ratio of protein to reservoir solution is 3 μL to 2 μL,

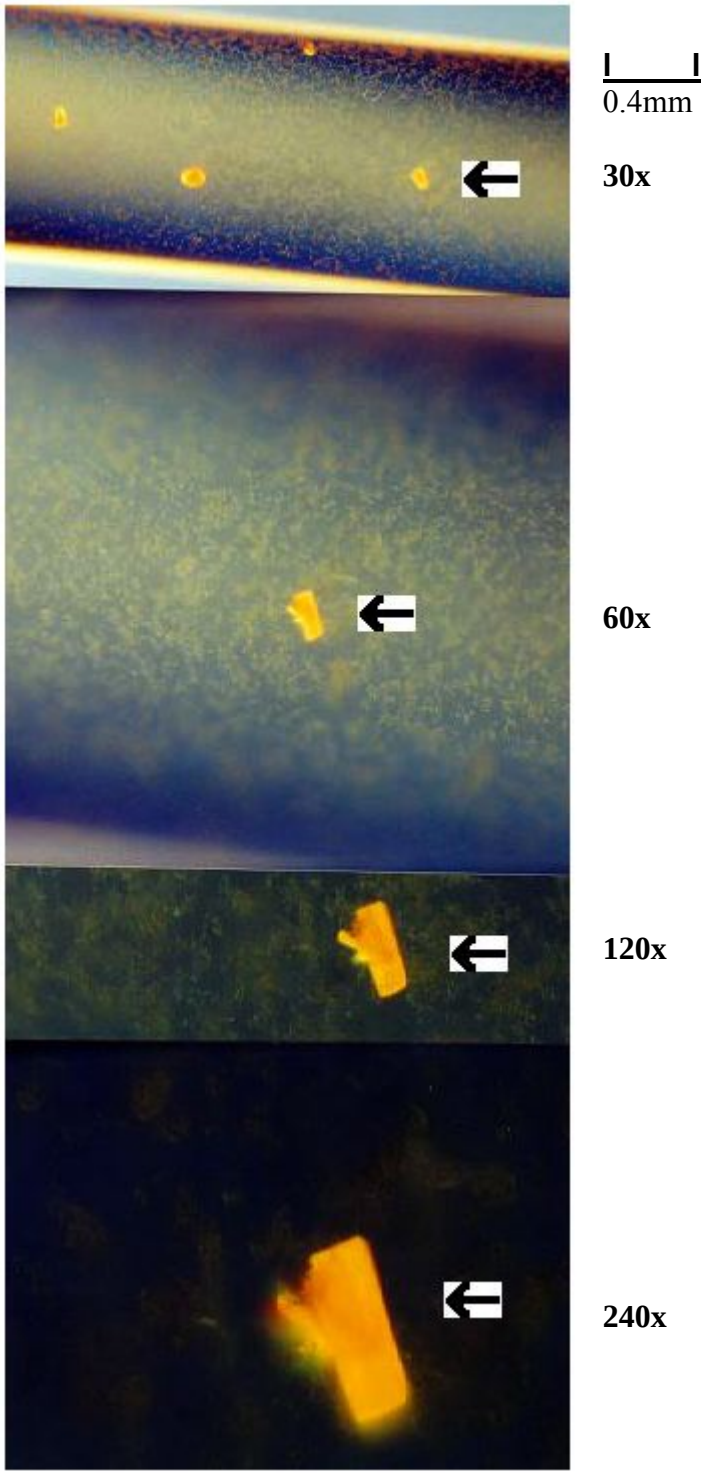

Figure 17. Protein crystals of P5 in capillary tubes. The magnification amplitudes are indicated at the right side of the figure.

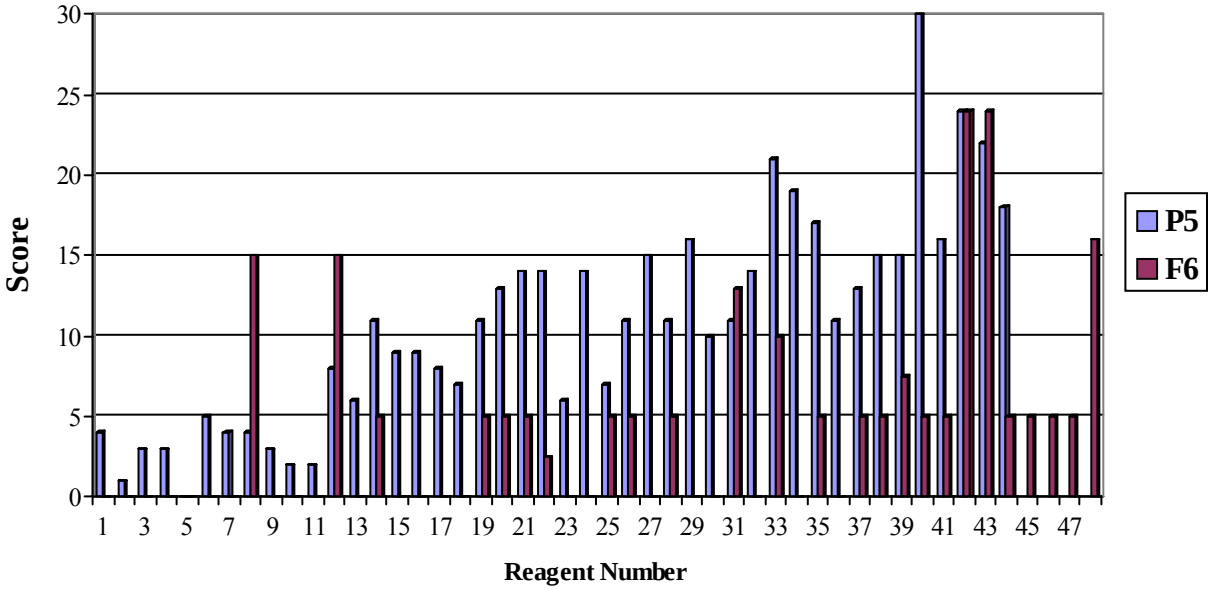

Figure 18. Screening tests for crystal growth. Crystallization of fractions P5 and F6 are scored as the amount of precipitation in each condition for every 24 hours during a seven-day observation by using a five-point scoring system. From 5 to 0, the protein and buffer mixture is from clear to total precipitation. The X-axis of this figure represents the reagent sequence of MembFac Kit purchased from Hampton Research. The Y-axis represents the total score of this seven-day observation.

with a 3 μL to 3 μL exception of 41 to 48 in F6 tests. The protein concentration before mixture was at ~20 mg/mL. A reservoir solution of 300 mL was added in each well during the hanging drop preparation of P5. In the case of F6, 200 μL was added instead of 300 μL. All crystallizations were performed under argon atmosphere to achieve anaerobic condition.

In the tests of P5 crystallization, reagent no. 45 (0.1 M potassium sodium tartrate tetrahydrate, 0.1 M Tris hydrochloride pH 8.5, and 0.4 M magnesium sulfate hydrate) showed small salt crystals the moment protein was mixed with the reagent. From reagent number 45 to 48, phase separation was observed the moment protein was mixed with the reagents. P5 was scored the highest at reagent number 40 (0.1 M lithium sulfate monohydrate, 0.1 M Tris hydrochloride pH 8.5, 12% v/v 2-methyl-2,4-pentanediol), but F6 precipitated within 24 hours in the same condition. With condition number 42 (0.1 M Tris hydrochloride pH 8.5 and 0.1 M sodium acetate trihydrate) and number 43 (0.1 M Tris hydrochloride pH 8.5 and 0.1 M sodium chloride), both P5 and F6 were scored high. Overall, none of the reagent formulas were found helpful for NADH dehydrogenase crystallization.

As a side note, the scoring system can be improved to a more detailed and précised description by adopting the following system which was developed by Hampton Research. 1 Clear Drop; 2 Phase Separation; 3 Regular Granular Precipitate; 4 Birefringent Precipitate or Microcrystals; 5 Rosettes or Spherulites; 6 Needles (1D Growth); 7 Plates (2D Growth); 8 Single Crystals (3D Growth < 0.2mm); 9 Single Crystals (3D Growth > 0.2mm).

Future Direction

First, the stability of NADH dehydrogenase prepared as described above needs improvement. The biggest obstacle of protein crystallization was the denaturation resulting from oxidation of the sample. Therefore, several methods can be utilized to improve the stability. 1) Adding and changing reducing reagents, i.e. DTT, NADH, etc, to the sample during and after the purification process. 2) Following more strict anaerobic conditions, i.e. starting to utilize anaerobic conditions at an earlier stage of the purification. A Nitrogen Dry Box could enable us to carry on the purification in a highly anaerobic environment. 3) If the first two steps fail to improve the stability of NADH dehydrogenase, an alternative purification protocol for this enzyme would be needed.

Second, the quality of the crystals needs improvement, because the crystals we obtained so far were too small to subject to X-ray diffraction. Attempts should be taken to modify the conditions for crystallizing NADH dehydrogenase by changing the precipitant, buffer system, salt concentration, pH, temperature, and other factors.

References

1. Stiggall, Y. H. a. D. E. (1976) *The Enzyme*, Academic Press
2. Galante, Y. M., and Hatefi, Y. (1979) *Arch Biochem Biophys* **192**, 559-568
3. Mackler, B. (1961) *Biochim Biophys Acta* **50**, 141-146
4. Wilson, D. F., and King, T. E. (1964) *J Biol Chem* **239**, 2683-2690
5. Walker, J. E. (1992) *Q Rev Biophys* **25**, 253-324
6. Doeg, K. A., and Ziegler, D. M. (1962) *Arch Biochem Biophys* **97**, 37-40
7. Howard, T. E. K. a. R. L. (1967). Methods Enzymol., 52
8. Ragan, C. I., Galante, Y. M., Hatefi, Y., and Ohnishi, T. (1982) *Biochemistry* **21**, 590-594

Tube Number	Salt	Buffer †	Precipitant
1.	0.1 M Sodium Chloride	0.1 M Sodium Acetate trihydrate pH 4.6	12% v/v 2-Methyl-2,4-pentanediol
2.	0.1 M Zinc Acetate dihydrate	0.1 M Sodium Acetate trihydrate pH 4.6	12% w/v Polyethylene Glycol 4000
3.	0.2 M Ammonium Sulfate	0.1 M Sodium Acetate trihydrate pH 4.6	10% w/v Polyethylene Glycol 4000
4.	0.1 M Sodium Chloride	0.1 M Sodium Acetate trihydrate pH 4.6	12% v/v Isopropanol
5.	None	0.1 M Sodium Acetate trihydrate pH 4.6	12% w/v Polyethylene Glycol 4000
6.	None	0.1 M Sodium Acetate trihydrate pH 4.6	1.0 M Ammonium Sulfate
7.	None	0.1 M Sodium Acetate trihydrate pH 4.6	1.0 M Magnesium Sulfate heptahydrate
8.	0.1 M Magnesium Chloride hexahydrate	0.1 M Sodium Acetate trihydrate pH 4.6	18% v/v Polyethylene Glycol 400
9.	0.1 M Lithium Sulfate monohydrate	0.1 M Sodium Acetate trihydrate pH 4.6	1.0 M mono-Ammonium dihydrogen Phosphate
10.	0.1 M Sodium Chloride	0.1 M Sodium Acetate trihydrate pH 4.6	12% w/v Polyethylene Glycol 6000
11.	0.1 M Magnesium Chloride hexahydrate	0.1 M Sodium Acetate trihydrate pH 4.6	12% w/v Polyethylene Glycol 6000
12.	0.1 M Sodium Chloride	0.1 M tri-Sodium Citrate dihydrate pH 5.6	18% v/v Polyethylene Glycol 400
13.	0.1 M Lithium Sulfate monohydrate	0.1 M tri-Sodium Citrate dihydrate pH 5.6	12% w/v Polyethylene Glycol 4000
14.	0.1 M tri-Sodium Citrate dihydrate	0.1 M tri-Sodium Citrate dihydrate pH 5.6	10% v/v Isopropanol
15.	0.1 M Sodium Chloride	0.1 M tri-Sodium Citrate dihydrate pH 5.6	12% v/v 2-Methyl-2,4-pentanediol
16.	None	0.1 M tri-Sodium Citrate dihydrate pH 5.6	1.0 M Magnesium Sulfate heptahydrate
17.	0.1 M Sodium Chloride	0.1 M tri-Sodium Citrate dihydrate pH 5.6	12% w/v Polyethylene Glycol 4000
18.	0.1 M Lithium Sulfate monohydrate	0.1 M tri-Sodium Citrate dihydrate pH 5.6	12% w/v Polyethylene Glycol 6000
19.	0.1 M Magnesium Chloride hexahydrate	0.1 M tri-Sodium Citrate dihydrate pH 5.6	4% v/v 2-Methyl-2,4-pentanediol
20.	None	0.1 M tri-Sodium Citrate dihydrate pH 5.6	0.1 M Sodium Chloride
21.	0.1 M Lithium Sulfate monohydrate	0.1 M tri-Sodium Citrate dihydrate pH 5.6	4% v/v Polyethylene Glycol 400
22.	None	0.1 M n-(2-Acetamido)iminodiacetic Acid pH 6.5	1.0 M Ammonium Sulfate
23.	0.1 M Lithium Sulfate monohydrate	0.1 M n-(2-Acetamido)iminodiacetic Acid pH 6.5	12% w/v Polyethylene Glycol 4000, 2% v/v Isopropanol
24.	None	0.1 M n-(2-Acetamido)iminodiacetic Acid pH 6.5	1.0 M di-Ammonium hydrogen Phosphate
25.	0.1 M Magnesium Chloride hexahydrate	0.1 M n-(2-Acetamido)iminodiacetic Acid pH 6.5	12% w/v Polyethylene Glycol 6000
26.	None	0.1 M n-(2-Acetamido)iminodiacetic Acid pH 6.5	12% v/v 2-Methyl-2,4-pentanediol
27.	0.1 M Lithium Sulfate monohydrate	0.1 M n-(2-Acetamido)iminodiacetic Acid pH 6.5	1.0 M Magnesium sulfate hydrate
28.	0.3 M Lithium Sulfate monohydrate	0.1 M n-(2-Acetamido)iminodiacetic Acid pH 6.5	4% v/v Polyethylene Glycol 400
29.	0.1 M Ammonium Sulfate	0.1 M HEPES - Sodium pH 7.5	0.5 M di-Sodium hydrogen Phosphate dihydrate 0.5 M di-Potassium hydrogen Phosphate
30.	0.1 M Sodium Chloride	0.1 M HEPES - Sodium pH 7.5	10% w/v Polyethylene Glycol 4000
31.	0.1 M Magnesium Chloride hexahydrate	0.1 M HEPES - Sodium pH 7.5	18% v/v Polyethylene Glycol 400
32.	None	0.1 M HEPES - Sodium pH 7.5	1.0 M Potassium Sodium Tartrate
33.	0.1 M Ammonium Sulfate	0.1 M HEPES - Sodium pH 7.5	18% v/v Polyethylene Glycol 400
34.	0.1 M Ammonium Sulfate	0.1 M HEPES - Sodium pH 7.5	10% w/v Polyethylene Glycol 4000
35.	0.1 M tri-Sodium Citrate dihydrate	0.1 M HEPES - Sodium pH 7.5	12% v/v 2-Methyl-2,4-pentanediol
36.	None	0.1 M HEPES - Sodium pH 7.5	1.0 M tri-Sodium Citrate dihydrate
37.	0.6 M Magnesium Sulfate hydrate	0.1 M HEPES - Sodium pH 7.5	4% v/v Polyethylene Glycol 400
38.	0.6 M Magnesium Sulfate hydrate	0.1 M HEPES - Sodium pH 7.5	4% v/v 2-Methyl-2,4-pentanediol
39.	0.1 M Lithium Sulfate monohydrate	0.1 M HEPES - Sodium pH 7.5	0.1 M Potassium Sodium Tartrate
40.	0.1 M Lithium Sulfate monohydrate	0.1 M Tris Hydrochloride pH 8.5	12% v/v 2-methyl-2,4-pentanediol
41.	0.1 M di-Ammonium hydrogen Phosphate	0.1 M Tris Hydrochloride pH 8.5	0.5 M di-Sodium hydrogen Phosphate dihydrate 0.5 M di-Potassium hydrogen Phosphate
42.	None	0.1 M Tris Hydrochloride pH 8.5	0.1 M Sodium Acetate trihydrate
43.	None	0.1 M Tris Hydrochloride pH 8.5	0.1 M Sodium Chloride
44.	0.1 M di-Ammonium hydrogen Phosphate	0.1 M Tris Hydrochloride pH 8.5	12% w/v Polyethylene Glycol 6000
45.	0.1 M Potassium Sodium Tartrate tetrahydrate	0.1 M Tris Hydrochloride pH 8.5	0.4 M Magnesium Sulfate hydrate
46.	None	0.1 M Tris Hydrochloride pH 8.5	0.2 M Lithium Sulfate monohydrate
47.	None	0.1 M Tris Hydrochloride pH 8.5	0.5 M Ammonium Sulfate
48.	0.1 M tri-Sodium Citrate dihydrate	0.1 M Tris Hydrochloride pH 8.5	5% v/v Polyethylene Glycol 400

† *Buffer pH is that of a 1.0 M stock prior to dilution with other reagent components. pH with HCl or NaOH.*

MembFac contains forty-eight unique reagents. To determine the formulation of each reagent, simply read across the page.

HAMPTON RESEARCH

Solutions for Crystal Growth

34 Journey
Aliso Viejo, CA 92656-3317 U.S.A.
Tel: (949) 425-1321 • Fax: (949) 425-1611
e-mail: tech@hrmail.com
Website: www.hamptonresearch.com

CHAPTER IV

FAST KINETIC STUDY OF BOVINE HEART MITOCHONDRIA

BC$_1$ COMPLEX

INTRODUCTION

Bovine heart mitochondria bc_1 complex catalyzes the transfer of electrons from ubiquinol to cytochrome *c*. The bifurcation of quinol oxidation at the Qo site and quinone reduction at the Qi site are the key features of the Q-cycle mechanism for electron transfer and proton translocation (1,2). The X-ray crystallographic studies show various positions of [2Fe-2S] in different crystal forms and in the presence of different Qo site inhibitors (3-5), indicating a mobile ISP extramembrane domain. The direct proof of the functional significance of such movement is from molecular genetic manipulation of the bacterial cytochrome bc_1 complex. Decreasing the flexibility of the neck region by introducing proline substitutions or other amino acid deletions, greatly reduced electron transfer activity and increased the activation energy of the reaction (6). Also, formation of a disulfide bond between two engineered cysteines in the neck region near the transmembrane helix drastically reduced the electron transfer activity, while release of the disulfide bond by reduction or alkylation of the regenerated cysteines restored the activity (7).

Because of the difficulty of following the reduction of ISP optically and the relatively long mixing dead time of conventional stopped-flow apparatuses, direct evidence of the early involvement of ISP in ubiquinol oxidation is not available. In this chapter, we analyzed the pre-steady state bc_1 complex reduction by quinol using stopped-flow mixing. Utilizing an ultra-fast microfluidic mixer and a freeze-quenching device (8),

coupled with EPR, we have been able to determine the transient state kinetics of ISP reduction by ubiquinol.

EXPEIMENTAL PROCEDURES

Materials

Dodecyl-β-D-maltoside (DM), and n-octyl-β-D-glucopyranoside (OG) were purchased from Anatrace. 2,3-dimethoxy-5-methyl-6-decyl-1, 4-benzoquinone bromine ($Q_0C_{10}Br$) was synthesized in our laboratory (9). Stigmatellin, myxothiazol, and antimycin A were purchased from Sigma. Other chemicals were of the highest purity commercially available.

Enzyme Preparations and Assays

Bovine heart mitochondrial cytochrome bc_1 complex was prepared as previously reported (10). The purified complex was dissolved in 50 mM Tris–Cl buffer, pH 8.0, containing 0.33 M sucrose and 0.01% of DM to a cytochrome *c* concentration of 150 μM and 3-maleimido-proxyl (proxyl), a spin label, was added to a final concentration of 75 μM (from a 50 mM stock solution in ethanol) as an internal standard before the mixture was frozen at −80 °C until use. The purified bc_1 complex contained 9 nmol of cytochrome *b* and 5.5 nmol of cytochrome c_1 per milligram of protein. The concentrations of cytochromes *b* and c_1 were determined spectrophotometrically using

millimolar extinction coefficients of $\Delta E_{562-575\ nm}$=28.5 cm^{-1} mM^{-1} and $\Delta E_{552-540\ nm}$=17.5 cm^{-1} mM^{-1} for cytochromes *b* and c_1, respectively.

For activity assay, the cytochrome bc_1 complex was diluted with 50 mM phosphate buffer, pH 7.4, containing 1 mM EDTA and 0.01% DM to a protein concentration of 0.1 mg/ml. Diluted enzyme solution (5 μl) was added to 990 μl of an assay mixture containing 50 mM phosphate buffer, pH 7.4, containing 1 mM EDTA and 100 mM cytochrome *c* in the presence or absence of inhibitor. Activity was determined by measuring the reduction of cytochrome *c* after addition of 5 μl of 5 mM $Q_0C_{10}BrH_2$ (QH_2). A millimolar extinction coefficient of 18.5 cm^{-1} mM^{-1} was used to calculate the activity. The bc_1 complex used in these experiments had a specific activity about 20 μmol cytochrome *c* reduced/min/nmol cytochrome *b*.

Stopped-Flow Experiments

For the determination of electron transfer rates between the quinol and heme *b* or heme c_1, the cytochrome bc_1 complex was mixed with various concentrations of quinol at room temperature in an Applied Photophysics stopped-flow reaction analyzer SX.18MV (Leatherhead, England). The complex was diluted in the same storage buffer to a cytochrome c_1 concentration of 100 μM. Quinol was diluted in 0.2% DM and 0.2% OG to various concentrations. Reductions of cytochrome *b* and cytochrome c_1 were monitored by the increase of absorption at 559 nm and 550 nm, respectively, and photodiode array scan between 600-500 nm as well. A set of observed rate constants was measured as a function of the concentration of quinol, 1.7-, 3.34-, 6.66-, and 10-fold greater than that of the concentration of cytochrome c_1. When an inhibitor was used, the

cytochrome bc_1 complex was treated with 5-fold molar excess of the inhibitor over heme c_1 for 15 minutes prior to the experiment.

Freeze-Quenching Experiments

The cytochrome bc_1 complex was diluted in the same storage buffer to a cytochrome c_1 concentration of 100 μM and mixed at 1:1 ratio with 666 μM QH_2 in 0.2% DM and 0.2% OG inside the Ultrafast Microfluidic Mixer (Figure 19B). Various time points of the mixture, from 100 μs to 5 ms, were freeze quenched at liquid nitrogen temperature and packed into EPR tubes (Figure 19A). All EPR tubes were stored in liquid nitrogen temperature before analysis (8).

EPR Experiments

The redox state of the ISP, cytochrome *b*, and c_1 were determined by EPR (11), using a Bruker EMX Spectrometer at temperature of about 6 K. The instrument settings were as follows: microwave frequency, 9.45 GHz; microwave power, 2.15 mW; modulation amplitude, 19.57 G; time constant, 0.655 s, and modulation frequency, 100 KHz. Previous experiments indicated that the air trapped inside the sample causes a distorted base line, especially in the heme b/c_1 region of the EPR spectrum. To achieve high signal sensitive, the air remaining within the sample was eliminated by first dipping the EPR tubes containing the freeze-quenched samples into a mixture of isopentane and liquid nitrogen. This solution is at a temperature of about -160 °C. Then the EPR tubes were subjected to vacuum for 30 seconds before being put into the EPR spectrometer. The amount of reduction of ISP was calculated based on the total intensity value of peak

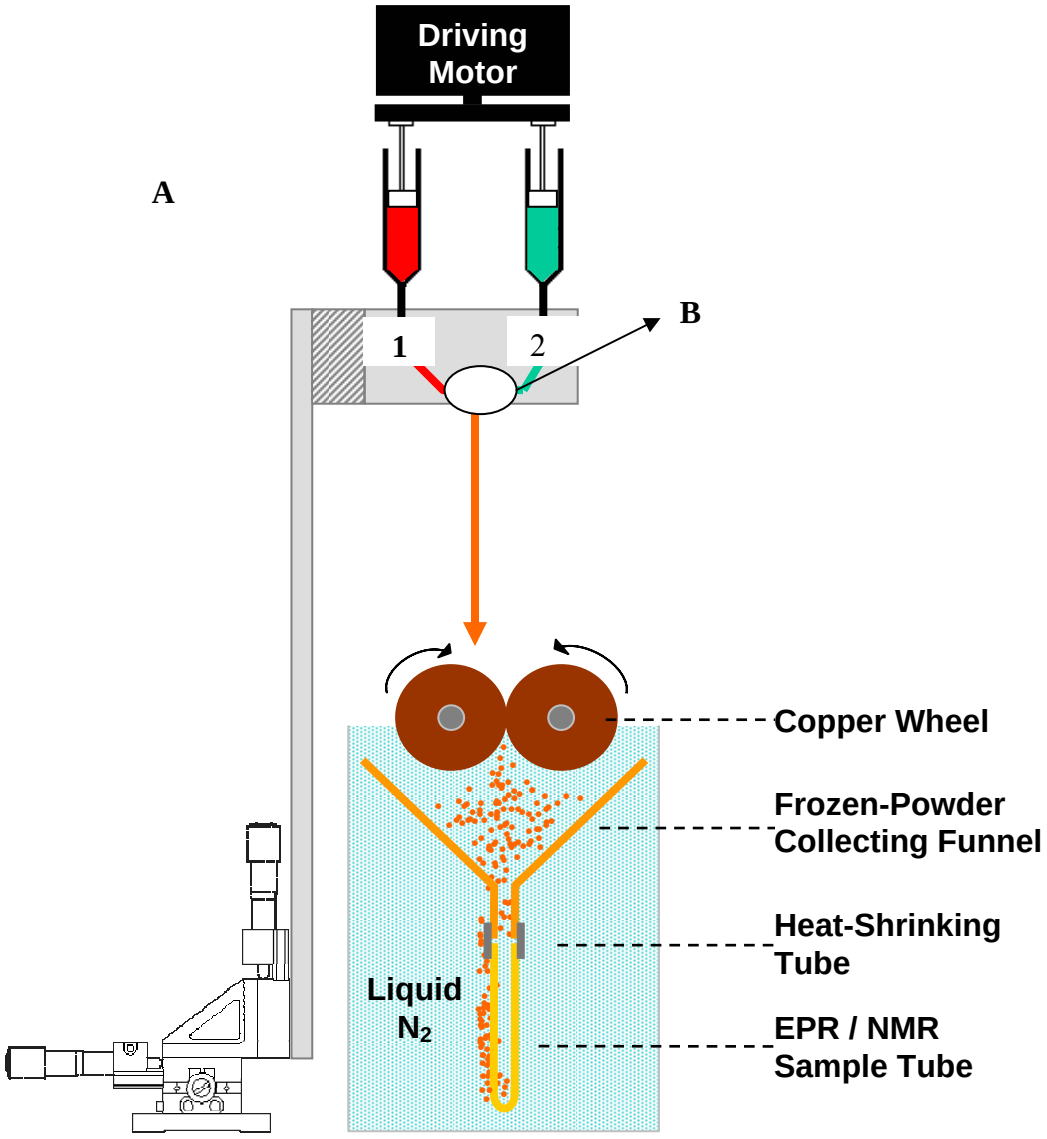
Driving Motor
A
B
1
2
Copper Wheel
Frozen-Powder Collecting Funnel
Heat-Shrinking Tube
Liquid N_2
EPR / NMR Sample Tube

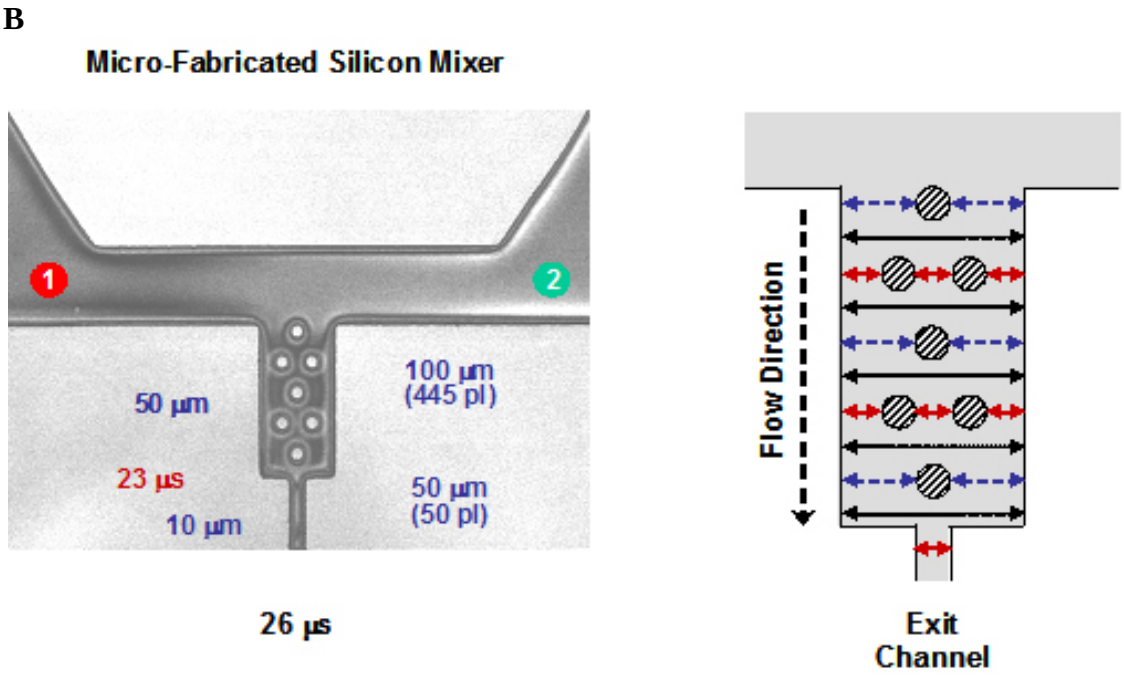

Figure 19. Ultrafast microfluidic mixer and freeze-quenching device for *bc*$_1$ complex reduction by QH$_2$. The cytochrome *bc*$_1$ complex was diluted in the same storage buffer to a cytochrome *c*$_1$ concentration of 100 µM and mixed at 1:1 ratio with 666 µM QH$_2$ in 0.2% DM and 0.2% OG inside the Ultrafast Microfluidic Mixer. Various time points of the mixture, from 100 µs to 5 ms, were freeze quenched at liquid nitrogen temperature and packed into EPR tubes.

to valley around g=1.89 (g_y), and the amount of reduction of b_L was calculated based on the integrated peak area at g=3.77. As described in enzyme preparations and assays, proxyl was added in as an internal standard. In order to normalize the reduction between different time points, both values were divided by the spin label intensity at g=1.98 before comparison with other samples.

RESULTS AND DISCUSSION

Observed Rate Constants Between the Quinol and Heme *b* or Heme c_1

By using stopped-flow mixing, reductions of cytochrome *b* and cytochrome c_1 in bc_1 complex by QH_2 were monitored by the increase of absorption at 559 nm and 550 nm, respectively. With varying concentration of QH_2, 1.7-, 3.34-, 6.66-, and 10-fold greater than that of the concentration of heme c_1, a set of observed rate constants were obtained for reductions of both heme *b* and heme c_1 (Figure 20A, B, Table IV). As shown in Figure 20A, heme *b* reduction was followed by a slower reoxidation assigned as electron transfer from the heme *b* to ubiquinone at the Qi site of the enzyme. A 50% increase of [QH_2] from 333 μM to 500 μM only yielded a 6% increase in the rate constant of heme *b*, from 407 s^{-1} to 432 s^{-1}. Similar results were for the rate constants of heme c_1 reduction as well (Figure 20B), a 50% increase of [QH_2] from 333 mM to 500 mM only gave a 12% increase for the rate constants, from 167 s^{-1} to 187 s^{-1}. These results indicated that the reaction was close to its maximum rate due to the limited quinol accessibility to the bc_1 complex, which results from the low solubility of QH_2 in aqueous

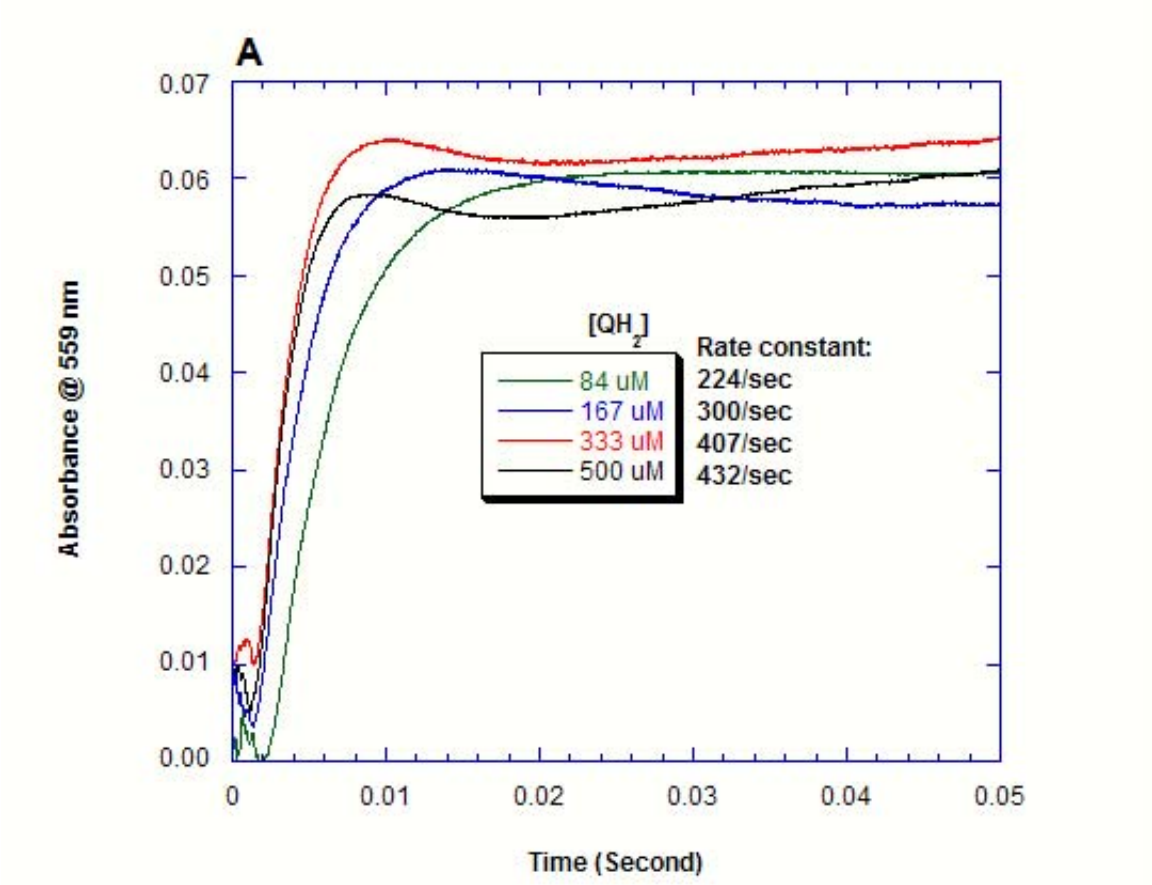
A
Absorbance @ 559 nm
0.07
0.06
0.05
0.04
0.03
0.02
0.01
0.00
0
0.01
0.02
0.03
0.04
0.05
Time (Second)
[QH2]
Rate constant:
84 uM
224/sec
167 uM
300/sec
333 uM
407/sec
500 uM
432/sec

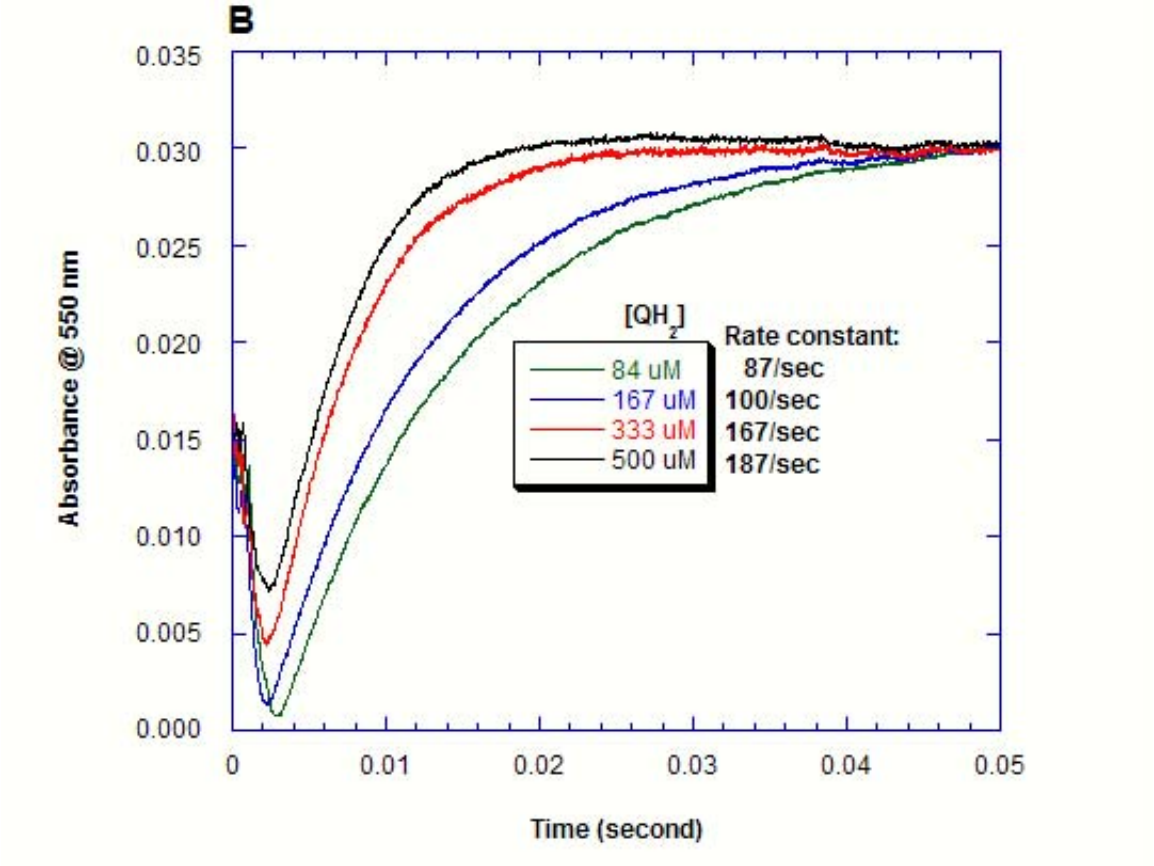

Figure 20. Electron transfer rates between the quinol and heme *b* or heme c_1. Fully oxidized cytochrome bc_1 complex was diluted in 50 mM Tris-Cl, pH 8.0, containing 0.01% DM and 0.33 M sucrose to a concentration of cytochrome c_1 of 100 μM. QH_2 was diluted in 0.2% DM and 0.2% OG to 167 μM, 333 μM, 667 μM, and 1 mM. The complex and QH_2 were mixed 1:1 in stopped-flow apparatus, which gives a final concentration of cytochrome c_1 of 50 μM and QH_2 of 84, 167, 333, and 500 μM. Reductions of cytochrome *b* (A) and cytochrome c_1 (B) were followed by measuring the increase of absorption at 559 nm and 550 nm, respectively.

Table IV. Electron transfer rate constants between QH_2 and cytochrome *b*/c_1.

Rate Constant / $[QH_2]$	QH_2 → cyt. *b*	QH_2 → cyt. c_1
84 μM	**224/sec**	**87/sec**
167 μM	**300/sec**	**100/sec**
333 μM	**407/sec**	**167/sec**
500 μM	**432/sec**	**187/sec**

solution. The $t_{1/2}$=1.6 ms was calculated with the maximum observed rate constant of 432 s^{-1} for heme b reduction, or electron transfer from QH_2 to heme *b* at the Qo site. Also $t_{1/2}$=3.7 ms was calculated with the maximum observed rate constant of 187 s^{-1} for heme c_1 reduction, or electron transfer from QH_2 to heme c_1.

Figure 21 shows the photodiode array scanning of bc_1 complex reduction by QH_2. Fully oxidized cytochrome bc_1 complex was diluted in 50 mM Tris-Cl, pH 8.0, containing 0.01% DM and 0.33 M sucrose to a concentration of cytochrome c_1 of 100 μM. QH_2 was diluted in 0.2% DM and 0.2% OG to 667 μM. The complex and QH_2 were mixed 1:1 in stopped-flow apparatus, which gave a final concentration of cytochrome c_1 of 50 μM and QH_2 of 333 μM. The reaction was followed by photodiode array scanning for 10 seconds. The final after mixing concentration of heme c_1 was 50 μM, and QH_2 was 333 μM. The reaction showed the early reduction of heme *b*, started before 1 ms and followed by the reduction of heme c_1, which started after 3 ms. This was consistent with the measurement of rate constants, which showed the electrons transfer from QH_2 to heme *b* was nearly 2.5 fold (407 s^{-1}/167 s^{-1}) faster than from QH_2 to heme c_1 under the same mixing condition and QH_2 concentration.

When Qi site inhibitor antimycin A was added to the bc_1 complex prior to the stopped-flow experiments (Figure 22), an initial rise in absorbance corresponding to heme *b* reduction was followed by much slower reduction of heme c_1 when comparing with the reaction without antimycin A. Antimycin A blocks the electron transfer from heme b_H to quinone or semiquinone at the Qi site. During the transient state of the reaction, the accumulation of reduced heme *b* slowed down the electron transfer from ISP

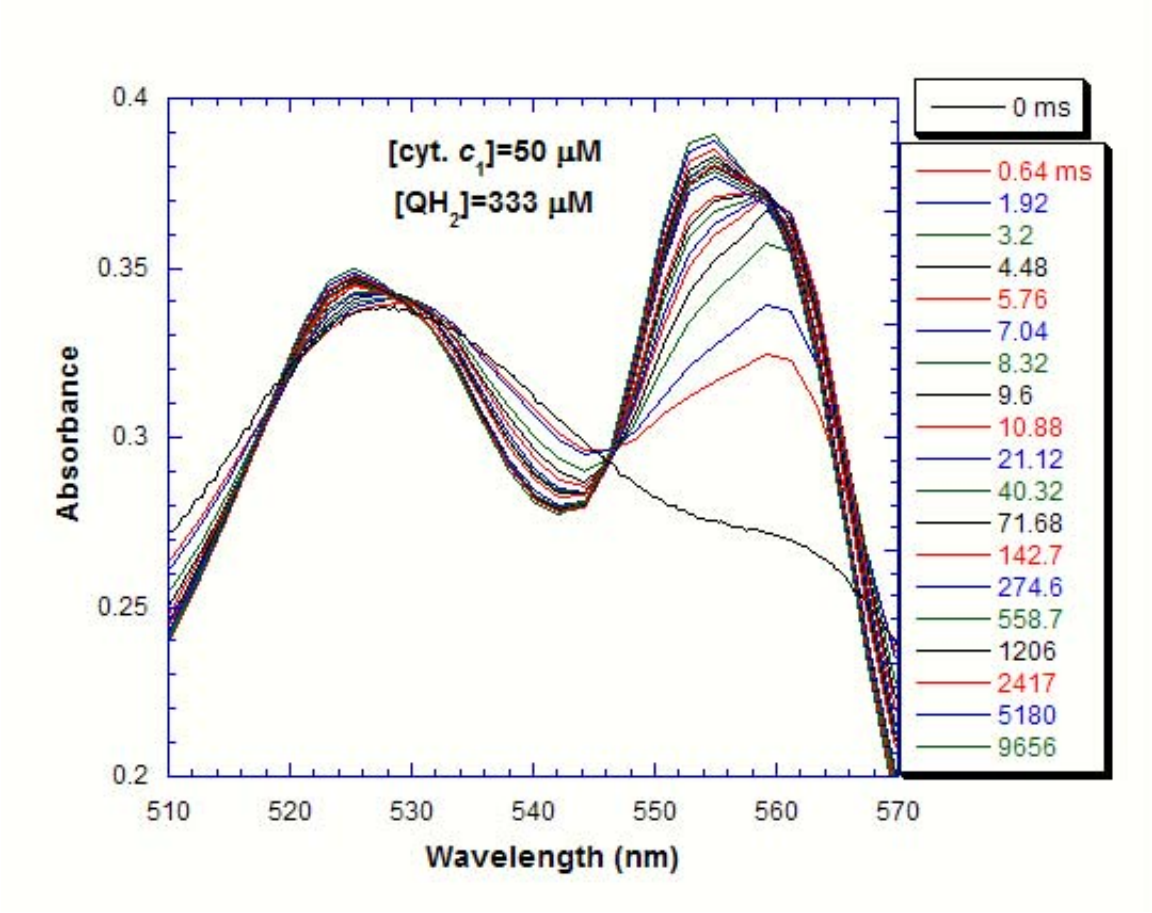

Figure 21. Transient state electron transfer between the quinol and bc_1 complex. Fully oxidized cytochrome bc_1 complex was diluted in 50 mM Tris-Cl, pH 8.0, containing 0.01% DM and 0.33 M sucrose to a concentration of cytochrome c_1 of 100 μM. QH_2 was diluted in 0.2% DM and 0.2% OG to 667 μM. The complex and QH_2 were mixed 1:1 in stopped-flow apparatus, which gives a final concentration of cytochrome c_1 of 50 μM and QH_2 of 333 μM. The reaction was followed by photodiode array scanning for 10 seconds.

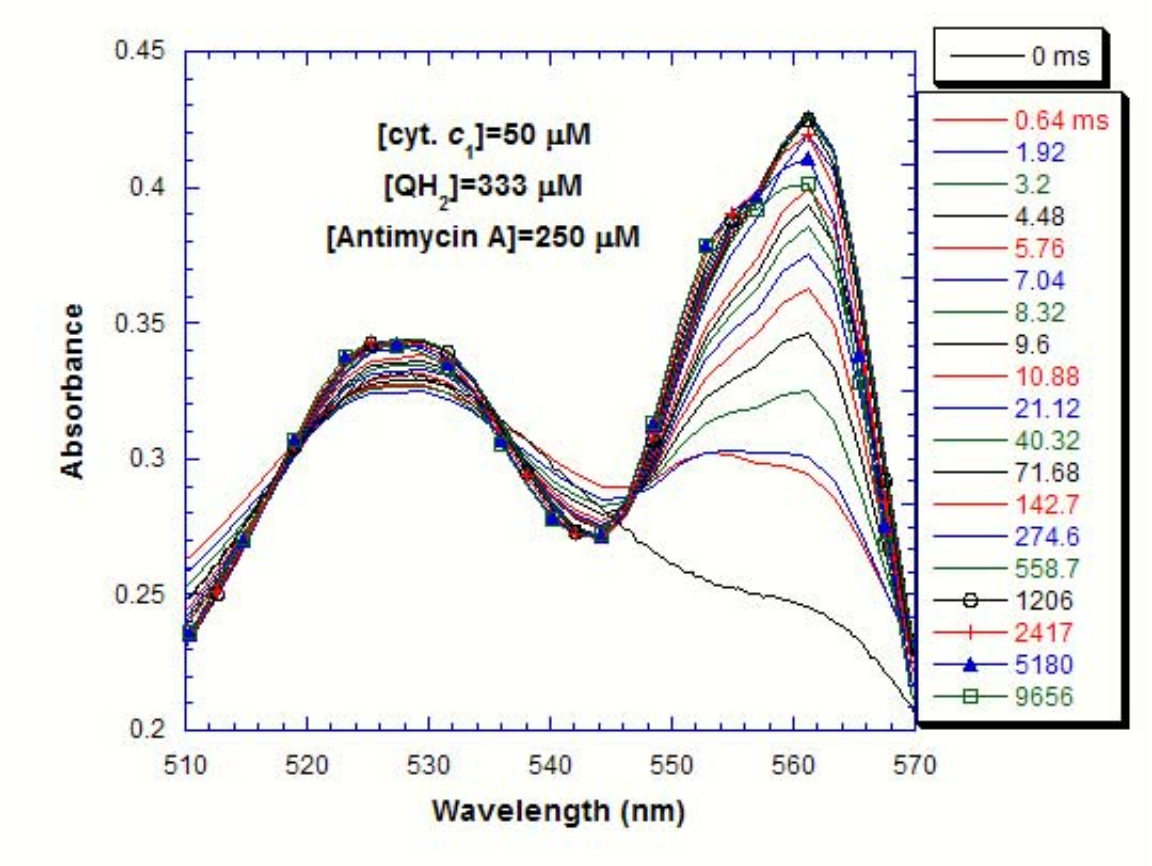

Figure 22. Transient state electron transfer between the quinol and bc_1 complex in the presence of antimycin A. Fully oxidized cytochrome bc_1 complex was diluted in 50 mM Tris-Cl, pH 8.0, containing 0.01% DM and 0.33 M sucrose to a concentration of cytochrome c_1 of 100 µM. QH_2 was diluted in 0.2% DM and 0.2% OG to 667 µM. Antimycin A was added to the bc_1 complex to a final concentration of 500 µM, and incubated for 10 minutes. The complex and QH_2 were mixed 1:1 in stopped-flow apparatus, which gives a final concentration of cytochrome c_1 of 50 µM and QH_2 of 333 µM. The reaction was followed by diode array scanning for 10 seconds.

to heme c_1 at the Qo site which implies the possible requirement of an electron equilibrium between the two heme *b* (b_L and b_H) and the quinone in order to facilitate the movement of reduced [2Fe-2S] towards heme c_1. A study of the effects of antimycin on the pre-steady state reduction kinetics of the bc_1 complex, in the presence or absence of endogenous ubiquinone, shown similar results. In the presence of quinone, antimycin slowed the rate of heme c_1 reduction by ~10 fold, while a slower heme c_1 reduction was also observed in the absence of endogenous quinone, similar to that in the presence of quinone plus antimycin. This suggests that both the low potential and high potential redox components control quinol oxidation at the Qo site (12).

In the presence of stigmatellin, a Qo site inhibitor, which allows reduction of the ISP and locks the ISP in the conformation close to cytochrome *b* (4,13), total inhibition of heme c_1 reduction occurred (Figure 23), while the reduction of heme *b* continued through the electron transfer between heme b_H and quinol or semiquinone at the Qi site. When both stigmatellin and antimycin A were added to the bc_1 complex together (Figure 24), which blocks both electron transfer at Qo and Qi sites, an almost total inhibition of heme *b* and heme c_1 reduction was observed.

Freeze-Quenching of bc_1 Complex Reduced by QH_2

As shown in Figure 19, the bc_1 complex was diluted in the same storage buffer to a cytochrome c_1 concentration of 100 μM and mixed at 1:1 ratio with 666 μM QH_2 in 0.2% DM and 0.2% OG inside the mixer. At various time points of the mixture, from 100 μs to 5 ms, were freeze quenched and ground to powder by the two copper wheels at liquid nitrogen temperature and packed into EPR tubes (8).

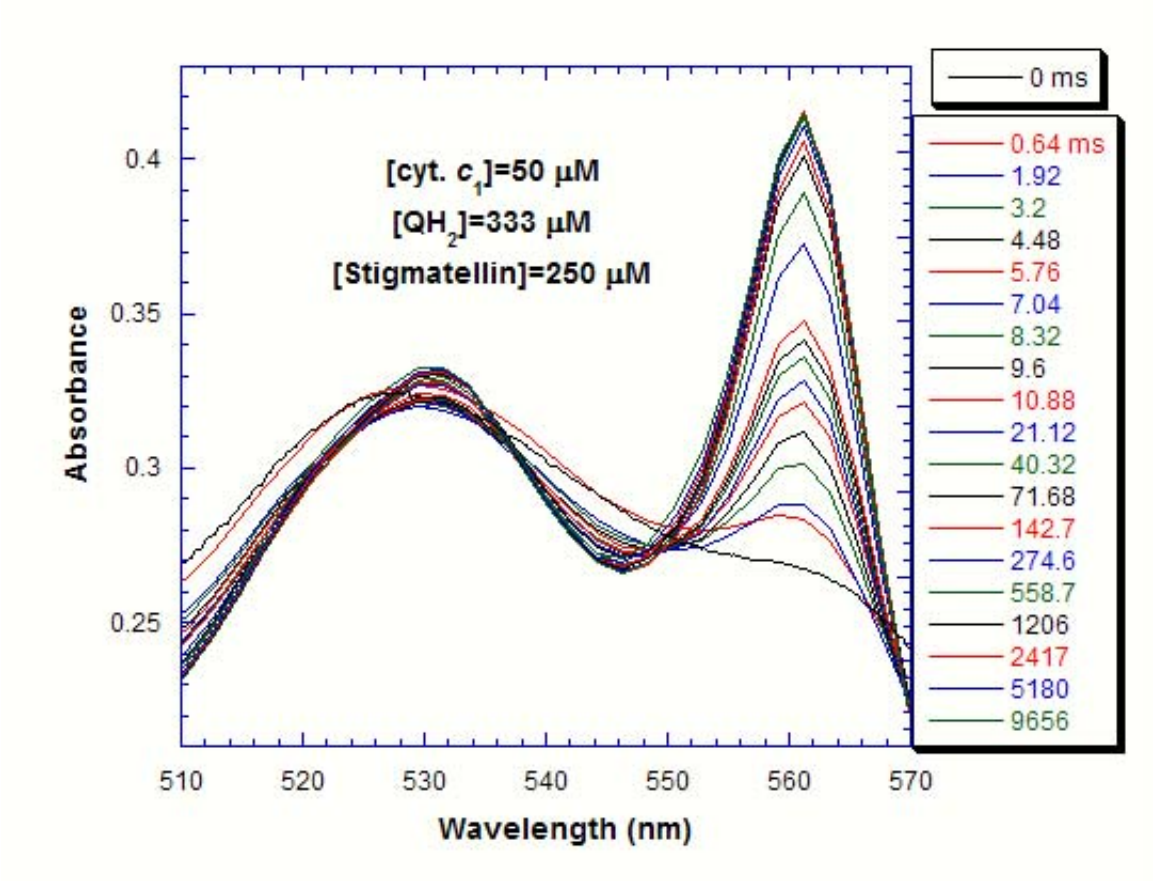

Figure 23. Transient state electron transfer between the quinol and bc_1 complex in the presence of stigmatellin. Fully oxidized cytochrome bc_1 complex was diluted in 50 mM Tris-Cl, pH 8.0, containing 0.01% DM and 0.33 M sucrose to a concentration of cytochrome c_1 of 100 µM. QH_2 was diluted in 0.2% DM and 0.2% OG to 667 µM. Stigmatellin was added to the bc_1 complex to a final concentration of 500 µM, and incubated for 10 minutes. The complex and QH_2 were mixed 1:1 in stopped-flow apparatus, which gives a final concentration of cytochrome c_1 of 50 µM and QH_2 of 333 µM. The reaction was followed by diode array scanning for 10 seconds.

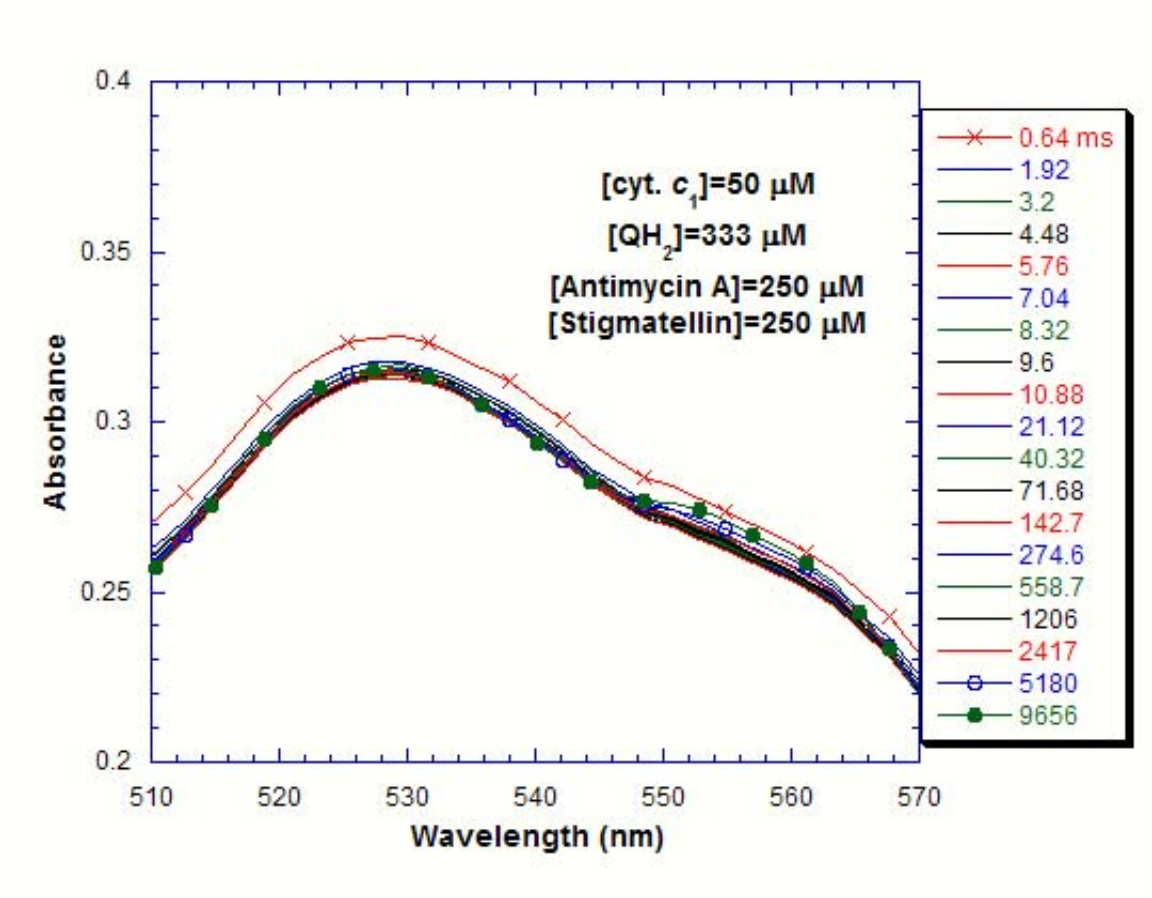

Figure 24. Transient state electron transfer between the quinol and bc_1 complex in the presence of both antimycin A and stigmatellin. Fully oxidized cytochrome bc_1 complex was diluted in 50 mM Tris-Cl, pH 8.0, containing 0.01% DM and 0.33 M sucrose to a concentration of cytochrome c_1 of 100 µM. QH_2 was diluted in 0.2% DM and 0.2% OG to 667 µM. Antimycin A and stigmatellin were added to the bc_1 complex to a final concentration of 500 µM each, and incubated for 10 minutes. The complex and QH_2 were mixed 1:1 in stopped-flow apparatus, which gives a final concentration of cytochrome c_1 of 50 µM and QH_2 of 333 µM. The reaction was followed by diode array scanning for 10 seconds.

Measurements of ISP and Heme b/c_1 Reduction by EPR

As shown in Figure 25, a fully oxidized bc_1 complex EPR spectrum (A) shows the signal of heme b_L (g=3.76) and heme b_H/c_1 (g=3.49), while a fully reduced bc_1 complex EPR spectrum (B) shows characteristic features of ISP with g_x=1.80, g_y=1.89, and g_z=2.02. In Figure 26A, a partially reduced bc_1 complex EPR spectrum shows characteristic features of ISP in the presence of proxyl, with signal of $g_{x, y, z}$=1.98, 2.00, and 2.02 are all from the proxyl. A fully oxidized ISP spectrum under the same condition shows a flat line at the g_y=1.89 position. Figure 26B shows the EPR spectrum with only proxyl under the same buffer condition, which is identical to a fully oxidize bc_1 complex spectrum.

The amount of ISP reduction was calculated based on the absolute value of peak to valley intensity around g=1.89, then divided by the absolute value of the "dip" amplitude of g=1.98 from proxyl in order to normalize the value between different time points samples. By comparing with the fully reduced ISP sample, whose reduction of ISP was calculated the same way, we were be able to calculate the percentage reduction of ISP at different time points.

A similar approach was adopted for calculating the percentage reduction of heme b_L by using the absolute value of the peak high at g=3.76, then normalized by the absolute value of the "dip" amplitude at g=1.98 from proxyl. By comparing with the fully oxidized bc_1 sample, the reduction percentage of heme b_L was established.

A

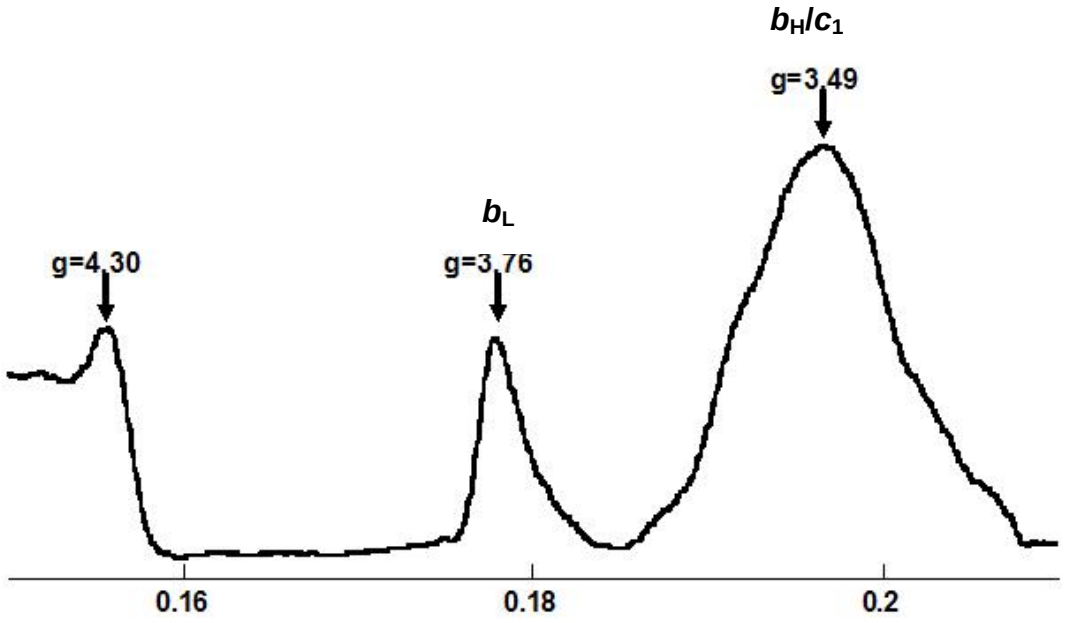
b_H/c_1
g=3.49
b_L
g=3.76
g=4.30
0.16
0.18
0.2

B

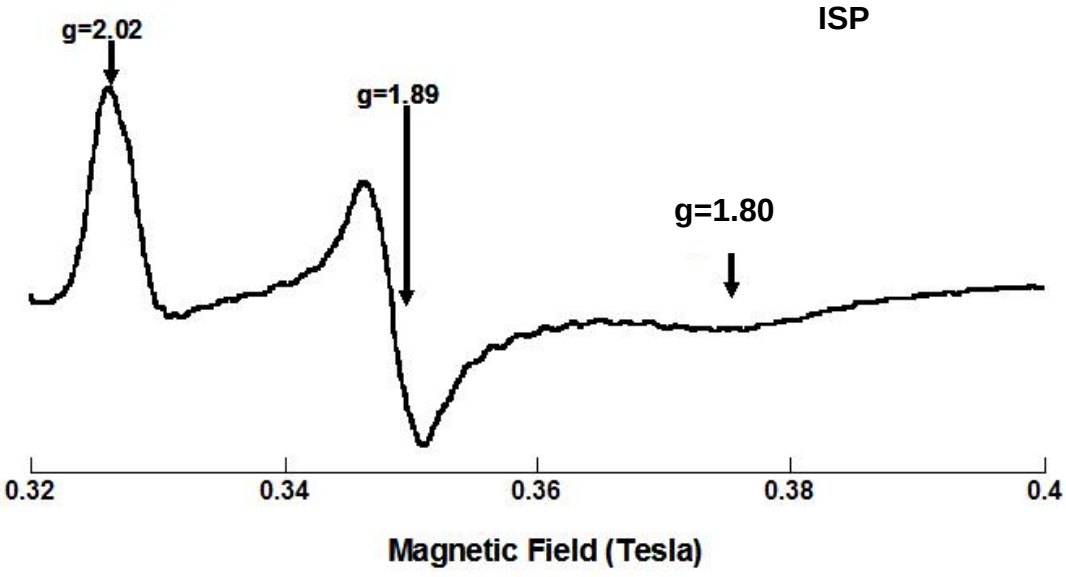
ISP
g=2.02
g=1.89
g=1.80
0.32
0.34
0.36
0.38
0.4
Magnetic Field (Tesla)

Figure 25. EPR spectra of cytochrome b_L, cytochrome b_H/c_1 (A) and ISP (B) and their g values. The instrument settings were as follows: microwave frequency, 9.45 GHz; microwave power, 2.15 mW; modulation amplitude, 19.57 G; time constant, 0.655 s, and modulation frequency, 100 KHz.

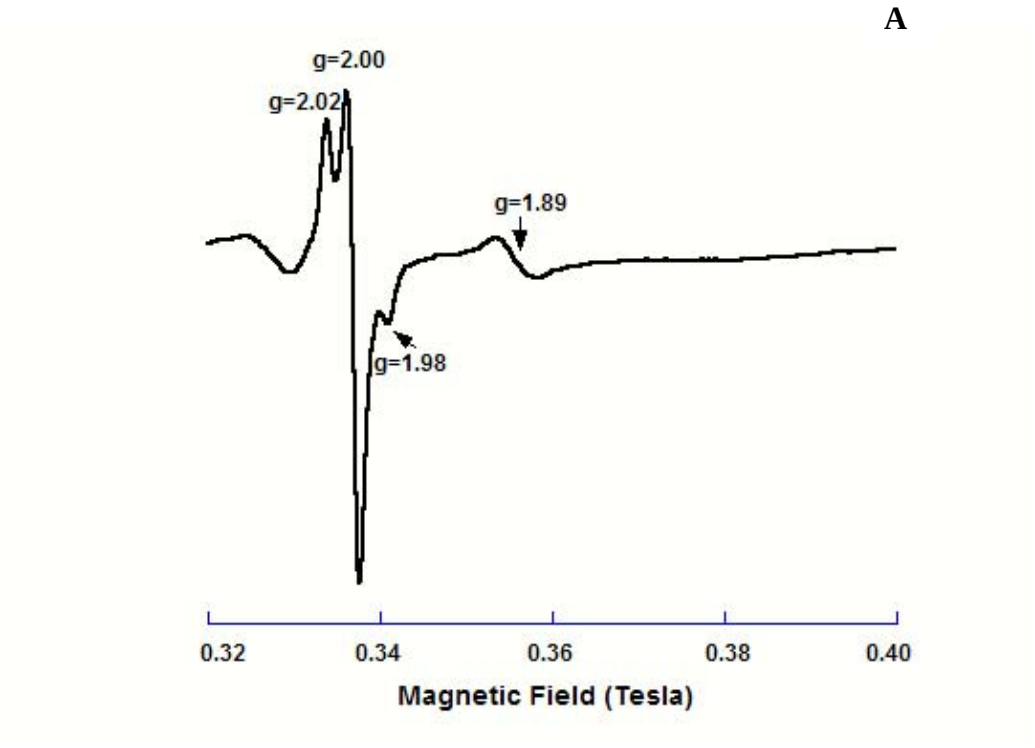
A
g=2.00
g=2.02
g=1.89
g=1.98
0.32
0.34
0.36
0.38
0.40
Magnetic Field (Tesla)

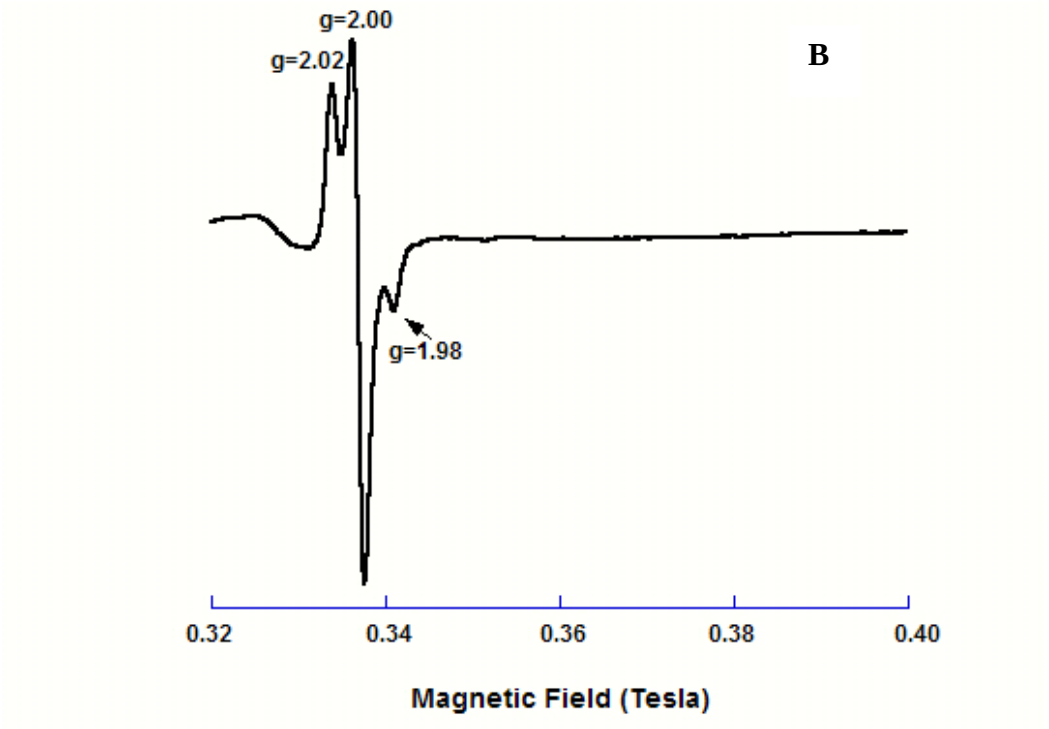
B
g=2.00
g=2.02
g=1.98
0.32
0.34
0.36
0.38
0.40
Magnetic Field (Tesla)

Figure 26. EPR spectra of ISP with spin label (proxyl). A) A partially reduced bc_1 complex EPR spectrum. B) A EPR spectrum with only proxyl under the same buffer condition, which is identical to a fully oxidize bc_1 complex EPR spectrum. The instrument settings were as follows: microwave frequency, 9.45 GHz; microwave power, 2.15 mW; modulation amplitude, 19.57 G; time constant, 0.655 s, and modulation frequency, 100 KHz.

In Figure 27, the ISP and heme b_L reduction percentage are colored in red (circle) and blue (dot), respectively, and plotted as functions of time in a double y axes manner. Notice the zero time point was based on a control sample prepared under the same condition in the absence of QH_2. The reduction of both redox centers reached around 11-12% within 1 ms. The first phase reduction of ISP started at between 100 to 200 μs with $t_{1/2}$ of 250 μs, while reduction of heme b_L starts around the same time with $t_{1/2}$ of 300 μs. The rate constant for electron transfer from quinol to ISP at Qo site was calculated at 2772 s^{-1}, and 2310 s^{-1} for electron transfer from quinol to heme b_L.

Because the rate constants are so large, kinetic characterization of the electron transfer reactions involving bc_1 complex has proven to be difficult. Using a light flash to initiate the electron transfer cycle, a 1650 s^{-1} rate constant was reported for electron transfer from quinol to ISP at the Qo site in *R. capsulatus* bc_1 complex (14). A rate constant of 1200 s^{-1} was found by using a binuclear ruthenium complex to rapidly photooxidize cytochrome c_1 in *R. sphaeroides* bc_1 complex (15). Also using the same technique of rapid photoreduce/photooxidize cytochrome c_1 with ruthenium dimer (Ru_2D), oxidant-induced reduction of cytochrome b_H was observed at a rate constant of 250 s^{-1} in the presence of antimycin A with bovine bc_1 complex, and 1000 s^{-1} with *R. sphaeroides* bc_1 complex (15). The rate constant for electron to transfer from quinol to heme *b*s was found to be 270 s^{-1} using a photoreleasable quinol substrate with mitochondrial cytochrome bc_1 (16).

Thus, the rate constants found in this study are significantly higher than in the previous work. The slightly slower rate constant for electron transfer from quinol to heme

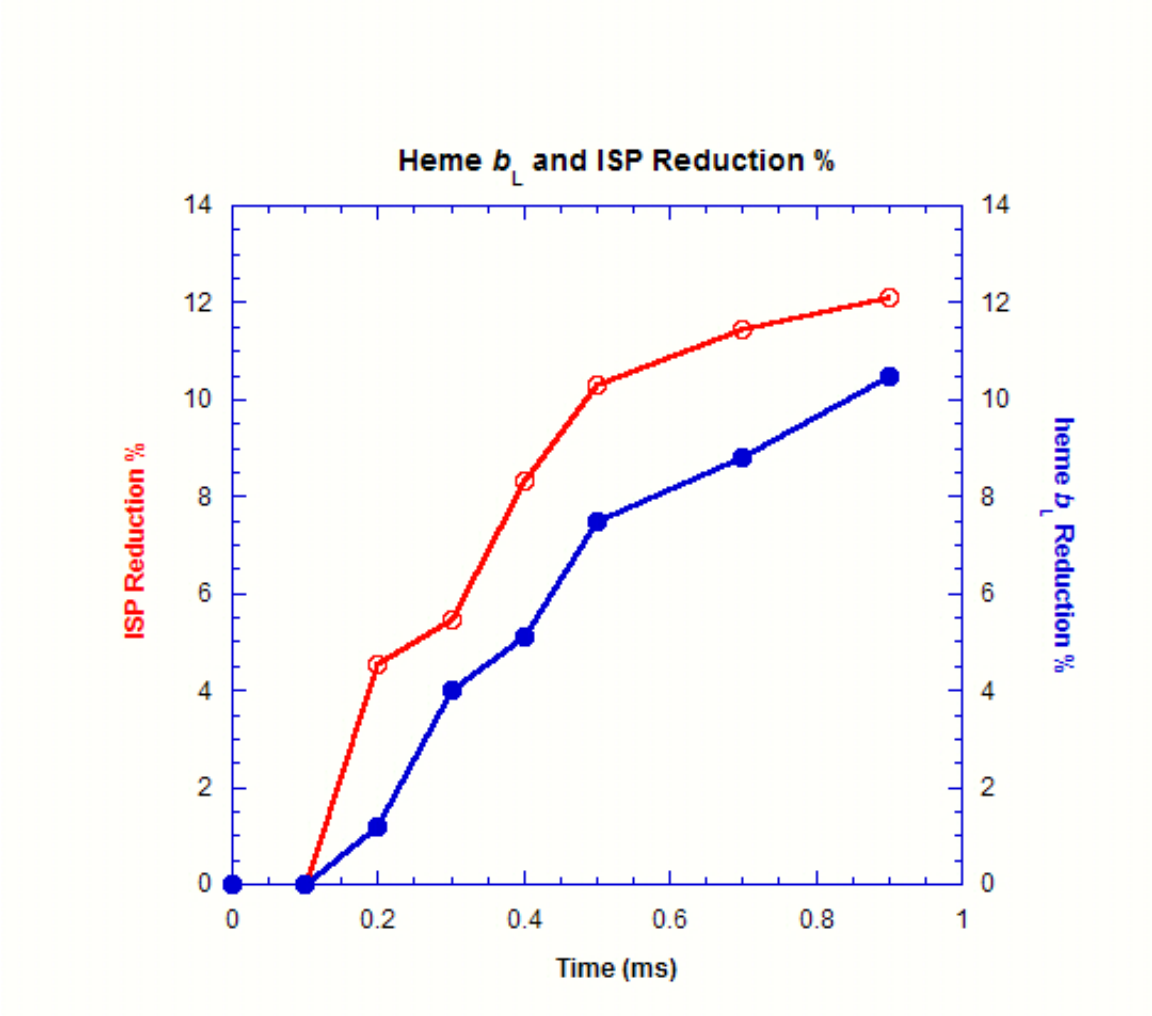

Figure 27. ISP (in red circle) and heme b_L (in blue dot) reduction percentage by QH_2, calculated from EPR spectra, at time points between r 0 to 1 ms.

b_L than that to ISP, indicates the first electron is transferred to the thermodynamically favored ISP, then the second electron is transfer to heme b_L, which is consistent with the Q-cycle mechanism. Also the observation of nearly simultaneous reduction of both ISP and cytochrome b_L strongly supports the electron transfer bifurcation at the Qo site, which is the heart to the operation of the Q-cycle mechanism.

Possible Detection of Semiquinone Radical at the Qo Site

After the first electron transfer from quinol to ISP at the Qo site, a semiquinone is formed, which carries a negative charge and an unpaired electron detectable by EPR. Due to its subsequent fast electron transfer to heme b_L, measurement of semiquinone at the Qo site in a steady state reaction can't be successful. Attempts were made to detect the semiquinone at Qo site under the condition of oxidant-induced reduction of heme *b* in the presence of antimycin A, in which both heme *b* are reduced and cytochrome c_1 is oxidized (17). A semiquinone signal was found that was sensitive to BAL (an inactivator of the iron-sulfur center (18)) and which was hence considered to a semiquinone in the Q_o site. Later though, the signal was proven to be due to semiquinones of complexes I and II (19).

Using this ultrafast freeze-quenching technique, it is possible for us to detect the existent of semiquinone in the Qo site as the observation of the reduction of both ISP and heme *b* starts after 100 μs, which is longer than the dead time of the instrument, which is 75 μs.

As the semiquinone give a single peak at g=2.00 in EPR spectrum, it will overlap with the g_y peak of proxyl as well. A sharp increase of the ratio between the intensity of g=2.00 and g=1.98 would indicate the presence of the semiquinone. As shown in Figure 28, the percentage increase of such value is plotted against time. The time points at 400 μs and 700 μs show 20% and 17% increase of the g=2.00 intensity, while the rest of the samples show a increase average about 6%. This might suggest the possible detection of semiquinone in the Qo site. Further experiments will be necessary to carry out by testing samples at the same time points, and at the absence of proxyl to minimize the effect from spin label.

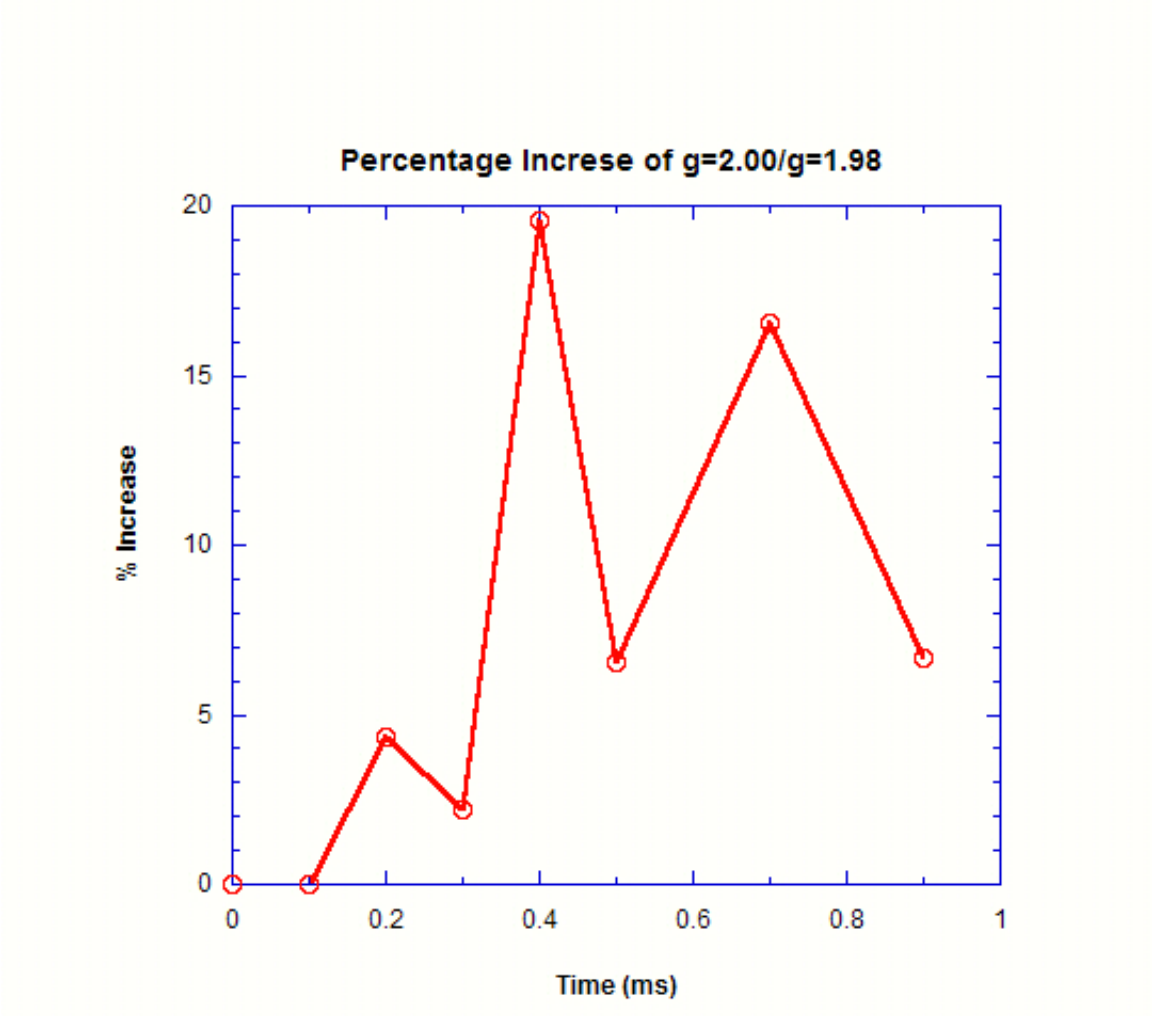

Figure 28. Percentage increase of the ratio between the intensity of g=2.00 and g=1.98 from EPR spectra.

REFERENCE

1. Mitchell, P. (1976) *J Theor Biol* **62**, 327-367
2. Trumpower, B. L. (1990) *J Biol Chem* **265**, 11409-11412
3. Xia, D., Yu, C. A., Kim, H., Xia, J. Z., Kachurin, A. M., Zhang, L., Yu, L., and Deisenhofer, J. (1997) *Science* **277**, 60-66
4. Zhang, Z., Huang, L., Shulmeister, V. M., Chi, Y. I., Kim, K. K., Hung, L. W., Crofts, A. R., Berry, E. A., and Kim, S. H. (1998) *Nature* **392**, 677-684
5. Iwata, S., Lee, J. W., Okada, K., Lee, J. K., Iwata, M., Rasmussen, B., Link, T. A., Ramaswamy, S., and Jap, B. K. (1998) *Science* **281**, 64-71
6. Tian, H., Yu, L., Mather, M. W., and Yu, C. A. (1998) *J Biol Chem* **273**, 27953-27959
7. Tian, H., White, S., Yu, L., and Yu, C. A. (1999) *J Biol Chem* **274**, 7146-7152
8. Lin, Y., Gerfen, G. J., Rousseau, D. L., and Yeh, S. R. (2003) *Anal Chem* **75**, 5381-5386
9. Yu, C. A., and Yu, L. (1982) *Biochemistry* **21**, 4096-4101
10. Yu, C. A., and Yu, L. (1980) *Biochim Biophys Acta* **591**, 409-420
11. McCurley, J. P., Miki, T., Yu, L., and Yu, C. A. (1990) *Biochim Biophys Acta* **1020**, 176-186
12. Snyder, C. H., Gutierrez-Cirlos, E. B., and Trumpower, B. L. (2000) *J Biol Chem* **275**, 13535-13541
13. Hunte, C., Koepke, J., Lange, C., Rossmanith, T., and Michel, H. (2000) *Structure Fold Des* **8**, 669-684
14. Crofts, A. R., and Wang, Z. (1989) *Photosynth. Res.* **22**, 69-87
15. Sadoski, R. C., Engstrom, G., Tian, H., Zhang, L., Yu, C. A., Yu, L., Durham, B., and Millett, F. (2000) *Biochemistry* **39**, 4231-4236
16. Hansen, K. C., Schultz, B. E., Wang, G., and Chan, S. I. (2000) *Biochim Biophys Acta* **1456**, 121-137
17. de Vries, S., Albracht, S. P., Berden, J. A., and Slater, E. C. (1981) *J Biol Chem* **256**, 11996-11998
18. Slater, E. C., and de Vries, S. (1980) *Nature* **288**, 717-718
19. Junemann, S., Heathcote, P., and Rich, P. R. (1998) *J Biol Chem* **273**, 21603-21607

VITA

JIAN ZHU

Candidate for Degree of

Doctor of Philosophy

Thesis: STRUCTURE-FUNCTION STUDIES OF ELECTRON TRANSFER COMPLEXES IN BOVINE HEART MITOCHONDRIA

Major Field: Biochemistry and Molecular Biology

Biographical:

Personal Data: Born in Wuhan, Hubei Province, People's Republic of China, 1971, the son of Lingpin Shen and Weiwen Zhu.

Education: Graduated from Guangzhou No. 6 Middle School, Guangzhou, Guangdong, P. R. China in June 1990; received Bachelor of Science degree from Zhongshan (Sun Yat-Sen) University, Guangzhou, Guangdong, P. R. China in June1994. Completed the requirements for the Doctor of Philosophy degree with a major in Biochemistry and Molecular Biology at Oklahoma State University in December, 2004.

Abstracts Presented at Meetings: Identification of Heme-Ligating Residues in the Largest Membrane-Anchoring Subunit (QPs1) of Bovine Heart Mitochondrial Succinate:Ubiquinone Reductase. (2001) *Biophysical Journal*, 188, B 44. Fast Kinetic Studies of Mitochondrial Cytochrome bc_1 Complex. (2005) *Biophysical Journal*.

Publications: Reconstitution of Cytochrome *b*-560 (QPs1) of Bovine Heart Mitochondrial Succinate-Ubiquinone Reductase. *Biochim. Biophys. Acta*, **1363**, 35-46. Expression of GST-EGF Fusion Protein in *E. coli* and Its Purification. *Acta Scientiarum Naturalium University Sunyatsen*, **37** (3), 13-16. A Mathematical Model for the Transport of Drug Infused in Subcutaneous Tissue. The Fouth China-Japan-USA-Singapore Conference on Biomechanics, 211-213.

Professional Memberships: Biophysical Society; American Association for the Advancement of Science; Oklahoma Academy of Science.

Name: Jian Zhu Date of Degree: December, 2004

Institution: Oklahoma State University Location: Stillwater, Oklahoma

Title of Study: STRUCTURE-FUNCTION STUDIES OF ELECTRON TRANSFER COMPLEXES IN BOVINE HEART MITOCHONDRIA

Page in Study: 107 Candidate for the Degree of Doctor of Philosophy

Major Field: Biochemistry and Molecular Biology

Various complexes within the bovine heart mitochondrial electron transfer chain were studied. The QPs1 subunit of Succinate:Ubiquinone Reductase was over expressed in *Escherichia coli* DH5α cells as a glutathione S-transferase fusion protein (GST-QPs1) using the expression vector, pGEX/QPs1. Recombinant QPs1 contains little cytochrome b_{560} heme. However, addition of hemin chloride reconstitutes the spectral characteristics of cytochrome b_{560}. Reconstituted cytochrome b_{560} in recombinant QPs1 shows a EPR signal at g=2.91. Histidine residues at positions 98 and 120 are responsible for the heme ligation because the H98D or H120D-reconstituted QPs1 fail to restore cytochrome b_{560} upon addition of hemin chloride.

A purification procedure for NADH dehydrogenase of NADH:Ubiquinone Reductase was developed. This procedure involves acid extraction in the presence of organic solvent followed by ammonium sulfate fractionation, and DEAE column chromatography. Purified NADH dehydrogenase contains 3 protein subunits with apparent molecular weight of 51, 24, and 10 kD. It catalyzes oxidation of NADH by artificial electron acceptor, ferricyanide, with specific activity of 471 μmol $Fe(CN)_6^{3-}$ reduced/min/mg protein. The purified NADH dehydrogenase contains one FMN, five irons, and two EPR detectable iron sulfur clusters, one [4Fe-4S] and one [2Fe-2S]. Preliminary results of crystallization have been discussed.

Using ultra-fast microfluidic mixer and freeze-quenching device, coupled with EPR, the pre-steady state kinetic of ISP reduction by ubiquinol was determined. The complex was mixed with reduced $Q_0C_{10}Br$ (QH_2) to a final concentration of 50 μM of cytochrome c_1, and 333 μM of QH_2 in the ultrafast microfluidic mixer and freeze-quenching at various time points, ranging from 100 μs to 5 ms. The first phase reduction of ISP starts between 100 to200 μs with $t_{1/2}$ of 250 μs. A similar reduction kinetic is also observed for cytochrome b_L with $t_{1/2}$ μs of 350 μs indicating an almost simultaneously reduction of both ISP and b_L. Possible detection of semiquinone radical at Qo site is also discussed.

Advisor's Approval: _____